POLITECNICO DI TORINO
Repository ISTITUZIONALE

Recent Developments and Perspectives for Memristive Devices Based on Metal Oxide Nanowires

(Article begins on next page)

22 September 2024

REVIEW

Nanowire Memristors

ADVANCED
ELECTRONIC
MATERIALS
www.advelectronicmat.de

Recent Developments and Perspectives for Memristive Devices Based on Metal Oxide Nanowires

Gianluca Milano, Samuele Porro, Ilia Valov,* and Carlo Ricciardi*

Memristive devices are considered one of the most promising candidates to overcome technological limitations for realizing next-generation memories, logic applications, and neuromorphic systems in the modern nanoelectronics and information technology. Despite the continuous efforts, understanding the resistive switching mechanism underlying memristive/neuromorphic behavior still represents a challenge. Metal oxide nanowire-based memristors appear suitable model systems for a deeper understanding of the involved physical/chemical phenomena due the possibility for localizing and investigating the switching mechanism. In practical aspects, nanowire-based devices can be grown using a bottom-up approach, thus being considered reliable candidates for going beyond the current scaling limitations of the top-down approach by the standard lithography. In addition, taking into advantage of the high surface-to-volume ratio of these nanostructures, new device functionalities can be achieved by exploiting surface effects. In the literature, a variety of nanowire-based devices such as single nanowires, nanowire arrays, and networks are reported to exhibit memristive behavior, explained by different switching mechanisms. This work provides a comparative review and a comprehensive analysis of device performances and physical phenomena responsible for memristive and neuromorphic behavior in such nanostructures. The analysis of the state-of-art of memristor devices based on nanowires and nanorods represent a milestone toward the development of nanowire-based artificial neural networks.

1. Introduction

In the last years, the enormous growth of digital data increased the need of next-generation electronic devices able to be scaled beyond the Moore's law. One of the most promising candidates for a new memory concept is the memristor (abbreviation for memory resistor). Theorized in 1971 by Chua[1] from symmetry arguments, memresistance was experimentally observed in 2008 Strukov et al.[2] in nanoscale systems. Even though memristive behavior was observed in many fields such as biology, chemistry, and physics, solid state electronics memristors are usually two terminal devices that exhibit resistive switching properties.[3] In these devices, the internal resistance state depends on the history of applied electrical stimuli, such as applied voltage and/ or current. It should be noticed that the roots of resistive switching phenomena date back to the end of the 19th century where the resistivity variations of metallic powder were studied by Calzecchi-Onesti,[4] while resistive switching devices were proposed as a new generation of nonvolatile memories even before the experimental evidence of memristor, as reviewed by Waser and Aono[5] in 2007.

However, the interest in resistive switching devices dramatically increased in recent years after being associated to the concept of memristor.[2,3] Indeed, memristors promise to be disruptive in electronics for the high speed, high scalability, low power consumption, and compatibility with complementary metal-oxide semiconductor (CMOS). For these reasons, they can be exploited for the realization of a new generation of memories that can store and process information, for digital and logic applications, for analog circuits, and for neuromorphic applications where the memristor can emulate synaptic dynamics and is the key element for the realization of artificial neural networks.[6–20] Indeed, a wide range of synaptic functionalities including long-term plasticity (LTP), short-term plasticity (STP), spike time-dependent plasticity (STDP), spike rate-dependent plasticity (SRDP), potentiation, and depression were reported in memristive systems.[21]

Conventional memristors are capacitor-like devices realized with a top-down approach where an active material is sandwiched in between two electron conductors, thus realizing a

G. Milano, Dr. S. Porro, Prof. C. Ricciardi
Department of Applied Science and Technology
Politecnico di Torino
C.so Duca degli Abruzzi 24, 10129 Torino, Italy
E-mail: carlo.ricciardi@polito.it
G. Milano
Center for Sustainable Future Technologies
Istituto Italiano di Tecnologia
Corso Trento 21, 10129 Torino, Italy
Dr. I. Valov
JARA—Fundamentals for Future Information Technology
52425 Jülich, Germany
E-mail: i.valov@fz-juelich.de
Dr. I. Valov
Peter-Grünberg-Institut (PGI 7)
Forschungszentrum Jülich
Wilhelm-Johnen-Straße, 52425 Jülich, Germany

The ORCID identification number(s) for the author(s) of this article can be found under https://doi.org/10.1002/aelm.201800909.

**ADVANCED
SCIENCE NEWS**
www.advancedsciencenews.com

**ADVANCED
ELECTRONIC
MATERIALS**
www.advelectronicmat.de

metal–insulator–metal (MIM) structure.[22–26] Even if various physical mechanisms can be exploited to realize this class of devices, one of the most studied resistive switching mechanisms are the redox based resistive switching memories based on the valence change memory effect (VCM), electrochemical metallization effect (ECM) and thermochemical thermo-chemical memory effect (TCM).[22] Both ECM and VCM cells are nanoscale electrochemical systems that couple ionic and electronic transport mechanisms.[5,27] In case of ECM mechanism, the variation of the internal resistance of the device is a consequence of the electromigration of metal cations through a solid electrolyte, while in VCM system resistive switching is triggered by the migration of oxygen anions (and is commonly described by the motion of the corresponding oxygen vacancies).[22,28] Instead, in case of TCM mechanism, electrochemical processes underlying resistive switching are driven by current-induced Joule heating effects.[29] Despite memristive behavior was observed in a wide range of materials, such as amorphous and polycrystalline transition metal-oxide,[24–26] perovskite oxides and chalcogenides,[24,30] 2D materials-based structures,[31–35] and organic materials;[36,37] the resistive switching mechanisms are far from being completely understood and dominated.

In this scenario, memristor devices based on quasi-1D structures represent a unique platform for the investigation of the physical mechanism of switching at the nanoscale, taking advantage of the high spatial localization of the switching events. Among 1D structures that exhibit memristive properties, metal-oxide nanowires (NWs) and nanorods (NRs) are the most studied. Since the first experimental observation of resistive switching properties in single metal-oxide NWs by Kim et al.[38] in 2008, the growing interest of NW-based resistive switching devices has also to be ascribed to the high device scalability, since these nanostructures can be grown by self-assembling using a bottom-up approach. Indeed, the bottom-up paradigm allows to highly control the wire dimensions directly during the growth process with a precision that is not achievable by the conventional top-down approach of lithography.[39] Moreover, the high surface-to-volume ratio can be exploited for the realization of new classes of devices where the memristive properties can be modulated and/or induced by surface treatments and functionalization or by applying light stimuli, thus paving the way for the realization of memristive sensors.

In this work, memristive properties of metal-oxide NWs are reviewed with a particular focus on the physical mechanism underlying the resistive switching events. After a brief description of NWs and NRs synthesis techniques in Section 2, the fabrication of the most common NW-based resistive switching devices is discussed in Section 3. Then, resistive switching mechanisms in single isolated nanowires are analyzed and compared in Section 4. Single crystal, polycrystalline, and heterostructured NWs are considered, discussing the impact of the chemical composition as well as the structural properties of these nanostructures on memristive characteristics and performances. Instead, resistive switching devices based on NWs and NRs arrays and networks are discussed in Sections 5 and 6, respectively. The aim of Section 7 is to give an overview of how memristive

Gianluca Milano is a PhD student in physics at Politecnico di Torino and Italian Institute of Technology (IIT). He received his bachelor's and master's degrees in physics from University of Torino in 2013 and 2015, respectively, working on the growth and characterization of graphene. His current research interests focus on the realization of memristive systems based on nanostructures, from material synthesis to device characterization and neuromorphic computing.

Ilia Valov is the Principle Investigator at the Forschungszetrum Jülich, Germany and holds lectures on nanoelectrochemistry at the RWTH-Aachen University. His main research interests are on nanoscale phenomena and processes in electrochemical systems, with focus on memristive devices for memory, selector and neuromorphic applications, energy conversion, and electrocatalysis.

Carlo Ricciardi is an associate professor in Physics of Condensed Matter at Politecnico di Torino, Italy, where he serves as reference faculty for the international master degree in "Micro and Nano technology for Integrated Systems". His main research interests are i) memristor based neuromorphic systems; ii) synthesis and characterization of nanostructured materials; iii) nanomechanical devices for innovative biological and chemical sensors.

properties of these nanostructures with high surface-to-volume ratio can be modulated by means of surface treatments and functionalization, by using nanocomposites or by light stimuli. Moreover, the application of these devices as sensors is discussed. Finally, future perspectives of NW-based memristive devices and architectures are discussed in Section 8.

**ADVANCED
SCIENCE NEWS**

www.advancedsciencenews.com

**ADVANCED
ELECTRONIC
MATERIALS**

www.advelectronicmat.de

2. Synthesis of Metal Oxide Nanowires and Nanorods

A large variety of methods for the synthesis of metal oxide NWs were reported in literature. Depending on the growth process, different morphologies as well as crystallographic and chemical qualities can be achieved. All these aspects can strongly influence the resistive switching behavior. Several previous review articles have described in detail the methods for synthesis of metal oxide NWs.[40–43] This paragraph is intended to give a short summary.

Generally, the synthesis of NW can be achieved following two different approaches, namely top-down and bottom-up technologies, as schematized in **Figure 1**. The first approach is based on standard CMOS microfabrication methods involving deposition of materials on flat substrates and etching and/or ion beam milling, electron and focused-ion beam, lithography techniques, nanoimprinting, and scanning probe microscopy techniques used to selectively remove and pattern the layers.[44–47] The bottom-up approaches, based on the assembly of molecular building blocks or chemical synthesis, are much more interesting due to improved purity, dimensional control, low cost, and the possibility of doping and surface functionalization. Bottom-up approaches can be subdivided into two categories: vapor or solution phase growth.

Vapor phase growth or chemical vapor deposition (CVD) regroup a number of different techniques that are generally (but not always) performed at low pressure (LP-CVD) in a vacuum chamber with controllable temperature under gas flow. CVD techniques are particularly versatile in order to tailor the deposition of NWs or other types of nanostructures, like

nanobelts, nanosprings, nanorings, nanoribbons, nanosheets, nanotetrapods, etc.[48,49] This type of deposition can be obtained also at atmospheric pressure (AP-CVD), without need of vacuum equipment.[50] CVD generally involves the use of a precursor material (typically metal or metal oxide[51]) that is evaporated and transported by a carrier gas toward a substrate, where it nucleates, sometimes in presence of a catalyst. The use of metal oxide precursors is typically associated with the presence of a carbon containing solid, like graphite, to be mixed with the precursor powder in order to lower the process temperature (generally in the order of 1000 °C), in vapor phase transport processes.[52–59] Vapor–liquid–solid (VLS) and vapor–solid (VS) processes are usually performed in a tubular furnace with a temperature gradient between the precursor and the substrate, allowing condensation and nucleation of nanostructures downstream the gas flow.[60–64] VLS mechanisms involve a vapor phase precursor and a liquid catalyst droplet over a substrate, producing solid crystalline nanostructures.[65–68] On the other hand, VS mechanisms follow a similar route without the use of a catalyst, crystallizing nanostructures directly on the substrate, after nucleation of seed nanocrystals.[69–76] In some processes, a seeding layer of nanocrystals is deposited previously to CVD by various methods, e.g., spin coating and annealing a solution of a salt containing the corresponding metal,[75,76] or by sputtering a thin layer of the corresponding oxide.[56,77] VLS and VS processes are usually performed using a horizontal tubular furnace, with substrates and precursors loaded inside a quartz tube in regions that can be held at different temperatures, depending on the process.[63] Deposition temperatures vary depending on processes and materials, and typically range between 500 and 900 °C. A
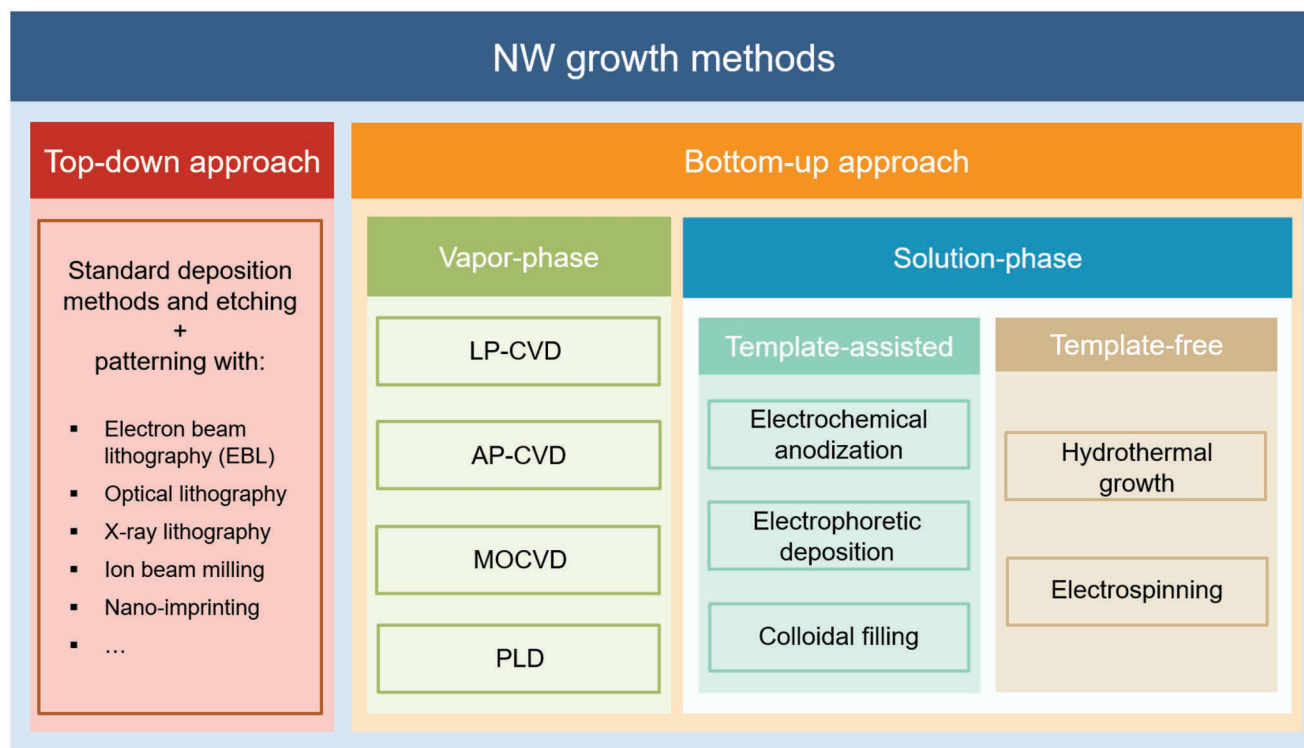

Figure 1. Growth methods employed for the synthesis of nanowires.

**ADVANCED
SCIENCE NEWS**
www.advancedsciencenews.com

**ADVANCED
ELECTRONIC
MATERIALS**
www.advelectronicmat.de

particular class of CVD techniques, named metal organic CVD (MOCVD), uses metal organic precursors that are vaporized at relatively low temperatures (100–200 °C), and transported by a carrier gas toward the substrates, which are held at deposition temperatures of about 500–600 °C.[78] MOCVD provides the advantages of precise control of the gas precursors, the possibility of doping, the large substrate area, and the industrial scalability.[79] Finally, also the pulsed laser deposition (PLD) technique should be mentioned, as besides being a well-established technique for the production of various thin film materials,[79] it was recently proposed also for the fabrication of metal oxide NWs in high pressure processes using inert gas instead of reactive oxygen.[80–83]

The second category of bottom-up approaches for deposition of metal oxide NWs relates to solution phase growth techniques. The main advantage of this family of processes is the low temperature required for crystallization, which contributes to considerably reduce the cost and complexity of equipment. Moreover, processes are typically repeatable and compatible with CMOS technology. The growth mechanism is similar to VLS, as solution phase growth usually involves the presence of a nanosized metallic droplet (or crystalline seed) that catalyzes the decomposition of (typically) organic precursors promoting crystallization of NWs, either on a substrate or directly in solution.[44] Solution phase growth can be classified depending on the presence of a template during deposition: electrochemical anodization, electrophoretic deposition, and colloidal filling are typically used as template-assisted methods,[43] while hydrothermal approaches and electrospinning are template-free.[41,84–86]

Electrochemical anodization is commonly used in industry to produce metallic coatings, and it is based on the application of electric bias to a solution containing charged reactive species that diffuse and react at the surface of a counter-electrode substrate, leading to deposition of thin layers. This procedure, applied to a template of porous membranes made of various materials, such as anodized alumina or polycarbonate, leads to the formation of NW (or nanotube) structures whose size depends on the porosity of the template, which is removed after deposition.[87–90] The NWs morphology and dimensions, aspect ratio and area density, as well as their ordering, can be tailored by the anodization process parameters (voltage) and the choice of template characteristics.[91,92] A slightly different approach, named electrophoretic deposition, was also reported as template-assisted process. In this approach, colloidal dispersions of nanosized charged particles are set into an oriented motion by the application of an external electric field. This motion is used to grow films by enriching the solid particles from the colloidal dispersion onto the surface of an electrode.[43] Polycrystalline oxides are typically obtained by electrophoretic deposition,[93–95] although the possibility of growing single-crystal nanostructures with processes assisted by mild annealing was also demonstrated.[96] Finally, direct template filling with colloidal dispersion of liquid precursors and subsequent solidification was also reported as a method for achieving deposition of NWs and nanotubes.[97–99] Template-assisted methods typically produce polycrystalline oxides, and often present the drawback of poor structural and mechanical resistance of high aspect ratio NWs after template removal.[44]

The deposition of metal oxide NWs in liquid environment is very often achieved using template-free methods.[41] Template-free solution phase growth techniques employ a surfactant to promote anisotropic crystal growth directly in a solution (typically aqueous) of metal oxide precursors, over a substrate that in some cases can be pretreated by sol–gel techniques in order to generate nanosized crystalline seeds.[75,100–104] In hydrothermal techniques, the aqueous solution of a precursor metal salt is placed in an autoclave at temperatures usually between 100 and 300 °C and relatively high pressures. Ultrasonic stirring or microwave heating can assist the process.[105] Hydrothermal techniques were widely used to produce a large variety of metal oxide nanostructures, like oxides of Ti,[106–109] V,[110–115] Cd,[116,117] Zn,[75,118–123] Fe,[124–126] Mn,[127,128] Mo,[129,130] Co.[131] On the other hand, electrospinning techniques are characterized by the formation of nanosized fibers induced by the application of high voltages to precursor solutions that are jetted over a substrate.[132] Very thin fibers (nm-scale diameter) can thus be achieved exploiting the instability of the jetted electrified solution and the concurrent evaporation of the solvent.[133–135] The use of electrospinning was demonstrated for the production of Co,[136] Mn,[137] Fe,[138] In,[139] Ti,[140] Zr,[141] Ni,[142] and Zn[143] oxide NWs.

3. Device Fabrication

Memristor are two terminal devices where an insulator material is sandwiched in between two metal electrodes in MIM configuration, as schematized in **Figure 2**a. As reviewed by Lanza et al.,[144] several device configurations based on thin films can be exploited for the realization of these devices such as common bottom electrode structures, cross-point junctions, and cross-bar arrays. However, the realization of memristors based on NWs requires new fabrication paradigms, as discussed in the following.

The MIM structure based on single NWs is usually realized by contacting single isolated nanostructures by means of metal electrodes in a planar structure, as schematized in Figure 2b. The first fabrication step requires the deposition of isolated nanostructures on a target substrate. This can be done by dispersing NWs in a solution and then by dip dropping or spin coating. As an alternative, a "dry" approach avoiding interaction of the nanostructures with solvents consists in a mechanical transfer of NWs with the help of a wire or a mounted hair. Then, contact geometries can be defined through optical and/or electron beam lithography. It is important to notice that lithographic processes necessarily imply the interaction of nanostructures with chemicals such as resist polymers and/or solvents. In some cases, this interaction can be detrimental for the nanostructures causing corrosion and degradation, as for example reported in case of ZnO NWs.[145] In general, the effect of the interaction between nanostructures and chemical compounds employed during lithographic steps has to be carefully evaluated. In order to avoid the use of resist polymers, contacts can be defined through direct writing techniques such as ion/electron beam induced deposition or, alternatively, by directly dispersing nanostructures on prepatterned electrodes. In addition, electrical characterization of these nanostructures can be
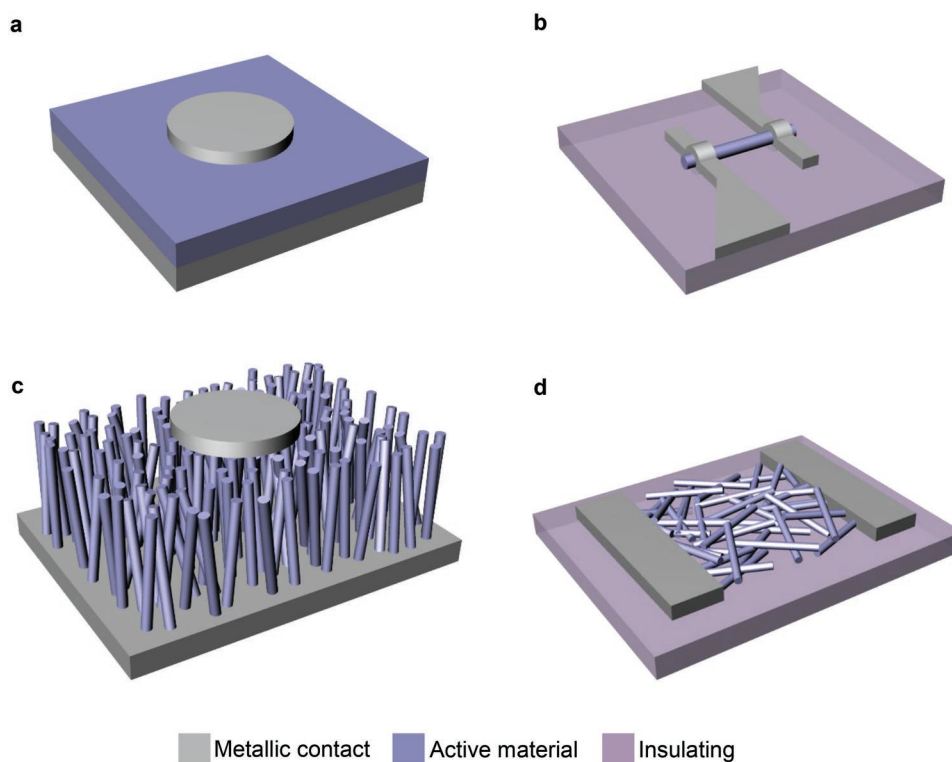
Figure 2. Schematic representation of NW-based resistive switching devices. a) Conventional thin-film based MIM structure, b) single NW device, c) NW array device, and d) NW network device.

achieved by in situ micromanipulation or by conductive atomic force microscopy (C-AFM). A detailed discussion concerning methods used for contacting single nanowires can be found in the review of Rojo et al.[146] Note that the choice of the target substrate results to be crucial, since it must provide i) considerably higher electrical resistance with respect to the NW in order to avoid leakage currents, and ii) low mobility of ions on its surface in order to ensure no influence on the resistive switching mechanism. In this configuration, a control experiment realizing only electrodes without the NW is usually necessary to exclude any influence of the substrate on the resistive switching performances. Despite complicating the fabrication process, all these issues can be solved by considering suspended nanostructures. In addition, it is important to underline that the realization of device architectures where the functionalities are enclosed in single NWs is complicated by the required manipulation and assembly of these structures at the nanoscale, in order to realize ordered arrays of NW-based devices. For this purpose, several techniques were proposed to align and assemble NWs such as magnetic field alignment,[147,148] fluidic alignment,[149] AC electric fields,[150] holographic optical traps,[151] dielectrophoresis,[152,153] and Langmuir–Blodgett technique.[154]

An easy approach to fabricate NW-based resistive switching devices consists in using as grown NW arrays. Indeed, in this case the device fabrication does not imply the NW dispersion with subsequent lithographic steps. In this device configuration, as grown NW arrays are sandwiched in between a bottom electrode (usually the growth substrate of NWs) and a top electrode, as schematized in Figure 2c.

A different approach consists in the fabrication of resistive switching devices based on networks realized with randomly oriented NWs. In this case, alignment and assembly of nanostructures are not required, since the devices functionalities are enclosed in the randomic interconnection in between nanowires. It is possible to distinguish two types of resistive switching devices based on nanowire networks depending on the device structure: stacked and planar devices. In case of stacked devices, the NW network is sandwiched in between two metal electrodes, similarly to NW array devices. Instead, planar devices are realized by spreading nanowires on an insulating substrate and then depositing lateral electrodes, as schematized in Figure 2d. Random network of nanowires can be simply realized by dispersing NWs in a solution and by subsequent drop-casting, spin-coating, or spray-coating.

Thus, different device configurations based on nanowires were proposed for the realization of resistive switching devices. As discussed in the following sections, different device configurations resulted not only in different device performances but also on different resistive switching mechanisms.

4. Resistive Switching in Single Isolated Nanowires

Single metal-oxide NWs can provide a unique platform for understanding the switching event at the nanoscale, since the high localization of the switching phenomena allows direct investigation of the physical mechanism. In these structures,

**ADVANCED
SCIENCE NEWS**
www.advancedsciencenews.com

**ADVANCED
ELECTRONIC
MATERIALS**
www.advelectronicmat.de

the switching mechanism can strongly depend on the NW material, microstructure, metal/NW interface, and metal contacts. In this section, resistive switching mechanisms in single NWs were classified into valence change mechanism, electrochemical metallization mechanism, and phase change mechanism, while resistive switching performances of these nanostructures are summarized in **Table 1**.

4.1. Valence Change Switching Mechanism

Defects in metal oxide materials play a crucial role for resistive switching. Indeed, it is widely accepted that in several memristive systems the switching mechanism can mainly be attributed to the motion of oxygen-related ionic defects that are generally much more mobile with respect to transition metal cations.[22–24] Initially, the electroforming process creates an abundance of oxygen vacancies near the cathode (–) as a consequence of the migration of oxygen ions toward the anode (+), according to the oxygen exchange reaction[22]

$$O_O \leftrightharpoons V_O^{\bullet\bullet} + 2e' + \tfrac{1}{2}O_2(g) \tag{1}$$

Where O_O denotes oxygen ions in regular lattice sites while $V_O^{\bullet\bullet}$ denotes oxygen vacancies, according to the Kröger–Vink notation. It is important to notice that the equilibrium of oxygen vacancies in the active layer is affected by oxygen partial pressure in the environment that can thus influence the memristive behavior. Under the action of the applied electric field, these point defects can migrate toward the opposite electrode forming a conductive path of reduced metal-oxide phase that decreases the overall resistance of the NW, since oxygen vacancies act as donors (i.e., in presence of oxygen vacancies the metal-oxide becomes n-type doped). As a consequence, the device is turned into a low resistance state (LRS). When an opposite polarity is applied, migration of oxygen-related species in the opposite direction is responsible for a RESET process that turns back the device to the high resistance state (HRS). In this framework, it is important to underline that a redistribution of oxygen vacancies in the metal-oxide involves also the modification of the Schottky barrier height at the metal/semiconductor interface that regulates electronic conduction.[22,155] It should be noticed that, since oxygen vacancies are not considered chemical species, their migration is the result of the movement of negatively charged oxygen ions in the opposite direction. This mechanism is usually called VCM.[22] Even if resistive switching phenomena are usually attributed exclusively to the migration of oxygen ions, it has been reported that in metal-oxide systems the migration of metal cation defects can also play an active role during switching.[156] In some cases, the defect-related conductive path formation/rupture is dominated by thermal effects induced by Joule heating. In these conditions, thermochemical redox processes prevail over electrochemical processes and unipolar resistive switching is observed. Differently from the bipolar switching in which the formation and annihilation of the conductive channel occur at opposite voltage polarities, the conductive path dynamics are controlled by imposing the same voltage polarity to the device. When temperature dominates the switching behavior, we refer

to a TCM.[22,157] Moreover, depending on the spatial localization, filamentary or area distributed resistive switching mechanisms can be distinguished.[24]

4.1.1. Single Crystalline NWs

The high localization of the switching event allows an in situ analysis of chemical composition and morphological changes during resistive switching in single crystal NWs.[158–160] In this way, it was possible to correlate the electrical properties and the spatial distribution of defects (i.e., the local metal-oxide stoichiometry) in the NW. Direct evidences of oxygen ion migration and structure evolution during the SET process were reported by Huang et al.[158] in single crystalline ZnO NWs grown by VLS method. During the forming process, morphological analyses by in situ transmission electron microscopy (TEM) spectroscopy analyzed the real-time growth of a protrusion near the anode, as can be seen from the series of TEM images in **Figure 3**a–d. The formation of these protrusions was ascribed to the migration of oxygen ions that were restricted to the electrode, as confirmed by energy dispersive X-ray spectroscopy (EDS) reported in Figure 3e–h. As a consequence of oxygen ions motion, the created oxygen vacancies in the NW are responsible for the formation of a conductive path along the NW in the LRS. Instead, the RESET occurred as a consequence of Joule heating that breaks conductive filaments, giving rise to a unipolar behavior. In a similar manner, Fan et al.[159,160] observed the migration of oxygen vacancies by electron energy loss spectroscopy (EELS) during bipolar resistive switching in single CuO NWs contacted by nanorobotic manipulators. Interestingly, in this work, the forming process was performed by exposing part of the CuO NW to a TEM electron beam. In this fashion, an abundance of oxygen vacancies was created in part of the NW by electron beam irradiation that expelled part of O atoms from the lattice. By using this procedure, it was possible to avoid an electrical electroforming that can eventually cause the breakdown of the NW.

The migration of oxygen vacancies was responsible for resistive switching also in single crystalline TiO_2 NWs contacted by Au electrodes, as reported by O'Kelly et al. in 2014.[161] Since the memristor demonstration by Strukov et al.[2] in 2008, TiO_2 has attracted great attention for the realization of memristive devices and several physical mechanisms of switching were reported in TiO_2 films.[162] In case of TiO_2 NWs, O'Kelly et al.[161] proposed that the switching mechanism is based on the modification of the Schottky barrier height at the TiO_2/Au interface due to the local change of stoichiometry in the dielectric layer. In the pristine state (initial state), the Schottky barrier dominates the electronic conduction, as depicted in **Figure 4**a. During electroforming, oxygen vacancies are created at the interface of the positively biased Au contact by redox processes, according to the reaction (1). The high concentration of oxygen vacancies, which act as n-type donors, decreases the height and width of the Schottky barrier, as depicted in Figure 4b. This resulted in an increased charge injection and an overall decrease of NW resistance in the developed state. Instead, during the RESET process the reverse reaction occurred, and the HRS was restored. It is worth noticing that the mechanism here reported is an interfacial resistive switching, in which oxygen vacancies

ADVANCED
SCIENCE NEWS
www.advancedsciencenews.com

ADVANCED
ELECTRONIC
MATERIALS
www.advelectronicmat.de

Table 1. Overview of the works reported in literature concerning single isolated nanowires with memristive properties. Most relevant device characteristics as well as electrical performances are reported.

Ref.	Year	NW material	NW diameter	Electrodes material	Electrodes spacing	$\lvert V_{FORMING} \rvert$	$\lvert V_{SET} \rvert$	$\lvert V_{RESET} \rvert$	Endurance (# of cycles)	Retention (s)	OFF/ON ratio	Switching behavior
[38]	2008	NiO	70 nm	Ti/Au[b]	1 μm	≈2.5 V	1.2 V	0.52 V	N.A.	N.A.	≈10^3	VCM, Unipolar
[213]	2009	Au/NiO/Au	≈250 nm	Pt	≈900 nm[d]	Forming-free	≈5.2 V	≈6 V	N.A.	N.A.	≈10^4	VCM, Bipolar
[194]	2009	MgO/NiO	10 + 10 nm[a]	Pt and Ir/Pt C-AFM tip	≈1 μm	N.A.	≈10 V	≈10 V	6	10^4	≈10^2	VCM, Bipolar
[196]	2010	MgO/Co$_3$O$_4$	10 + 5 nm[a]	Pt/Au[b]	≈250 nm	≈30 V	<30 V	<10 V	10^8	10^4	up to 300	VCM, Bipolar
[17]	2011	ZnO	N.A.	Ti	N.A.	≈22 V	≈7 V	≈12 V	100	N.A.	up to 7.7×10^5	VCM, Unipolar
[173]	2011	ZnO	500 nm	Au	N.A.	N.A.	<10 V	N.A.	20	N.A.	≈10^5	VCM, Threshold
[302]	2011	MgO/Co$_3$O$_4$	10 + 5 nm[a]	Pt/Au[b]	≈250 nm	≈35 V	<30 V	<20 V	10^8	10^4	≈10^2	VCM, Bipolar
[204]	2011	Ni/NiO	75 + 4.5 nm[a]	Au	≈3–4 μm	N.A.	≈0.5–3.5 V	≈0.5–3.5 V	25	≈3.5×10^6	≈10^2	VCM, Threshold/Unipolar
[217]	2011	ZnO	≈150 nm	Cu–Pd[c]	<~1 μm	N.A.	≈3 V	≈1.6 V	7	2×10^6 s	>10^5	ECM, Bipolar
[198]	2012	MgO/TiO$_2$	10 + 5 nm[a]	Pt	N.A.	N.A.	<30 V	<10 V	N.A.	10^4	≈10^2	VCM, Bipolar
[205]	2012	Au/Ga$_2$O$_3$	40 + 40 nm[a]	Ti/Au[b]	Up to 2.44 μm	14.3 V	≈5 V	≈8.5 V	100	3×10^4	>10^3	VCM, Bipolar
[219]	2012	Zn$_2$SnO$_4$	≈150 nm	Cu–Pd[c]	<~1 μm	N.A.	≈1.6 V	≈1V	14	5 months	>10^5	ECM, Bipolar
[160]	2013	CuO	30/50 nm	Au/W (nano manipulators)	≈3 μm	e-beam induced forming	<1 V	<1 V	N.A.	N.A.	N.A.	VCM, Bipolar
[158]	2013	ZnO	100 nm	Ti/Au[b]	500 nm	>40 V	<40V	<40 V	N.A.	N.A.	>10^2	VCM, Unipolar
[167]	2013	WO$_3$	≈80 nm	Au	≈1 μm	>10^6 V m^{-1}	<5	<5	N.A.	N.A.	N.A.	VCM, Bipolar
[174]	2013	ZnO	≈150 nm	Pt	2–3 μm	Forming-free	0.5 V	0.2 V	25	N.A.	≈1.5	Unipolar
[239]	2013	VO$_2$	≈160 nm	Ag	≈30 μm	–	≈0.34 V	<0.1 V	N.A.	N.A.	≈10^4	PCM, Unipolar
[212]	2013	ZnO/Zn$_2$SnO$_4$	N.A.	Ag	N.A.	N.A.	≈1.5 V	N.A.	≈6	N.A.	≈5	Bipolar
[220]	2013	Na-doped ZnO	≈300 nm	Ag	≈2.5 μm	N.A.	<40V	<40 V	10^3	10^5 s	>10^3	ECM, Bipolar
[161]	2014	TiO$_2$	50/100 nm	Au	2 μm	10 V[e]	<10 V	<10 V	100[h]	N.A.	N.A.	VCM, Unipolar

Table 1. Continued.

Ref.	Year	NW material	NW diameter	Electrodes material	Electrodes spacing	$|V_{FORMING}|$	$|V_{SET}|$	$|V_{RESET}|$	Endurance (# of cycles)	Retention (s)	OFF/ON ratio	Switching behavior
[188]	2014	CuO	≈50 nm	Ni	2 µm	Forming-free	0.875–2.25 V	0.43–0.78 V	50	N.A.	>10³	VCM, Bipolar/Unipolar
[189]	2014	ZnO	≈20 µm	Ag	≈1 mm	1.5 V[e]	0.19–0.4 V	0.62–0.8 V	100	N.A.	up to 10³	VCM, Unipolar
[183]	2014	ZnO–TiO₂	≈80 nm	Pt–Ti/Pt[c]	N.A.	N.A.	–5 V	9 V	N.A.	N.A.	≈10²	VCM, Bipolar
[175]	2015	ZnO	≈50 nm	Ti	≈3 µm	N.A.	N.A.	N.A.	100	4 × 10³	up to ≈10³	VCM, Bipolar
[225]	2015	ZnO	≈50 nm	Ag	≈1 µm	≈–35 V	≈22 V	≈30 V	300	N.A.	≈10³	ECM, Bipolar
		Ga-doped ZnO	≈100 nm			≈–35 V	≈–25 V	≈40 V	500	N.A.	≈10²	
		Sb-doped ZnO	≈100 nm			≈40 V	≈40 V	≈–40 V	>2000	N.A.	≈10³	
[164]	2016	TiO₂	100/200 nm	Au	4 µm	Forming-free	<8 V	<8 V	10	N.A.	N.A.	VCM, Bipolar
[176]	2016	ZnO	≈100 nm	Ti	≈3 µm	N.A.	0.5/8 V[f]	–1.5/–10 V[f]	100	10⁴	≈10³	VCM, Bipolar
[177]	2016	ZnO	50/150 nm	Au	N.A.	N.A.	<10 V	<10 V	N.A.	N.A.	N.A.	VCM, Bipolar
[179]	2016	ZnO	50/100 nm	Ti/Au[b]	500 nm	N.A.	<40 V[g]	N.A.	N.A.	2 × 10³	>10³	VCM, Bipolar
[214]	2016	Ni–CuOₓ–Ni	≈70 nm	Pt	≈3 µm[d]	N.A.	≈5.2–7.2 V	≈4–4.5 V	N.A.	7200 (2 h)	≈10	VCM, Bipolar
[230]	2016	Cu/SiO₂	≈150 + 15 nm[a]	Cu–Au[c]	N.A.	≈7 V	≈2.3 V	≈1.2 V	10⁴	≈10⁶ s	≈10⁶	ECM, Bipolar
[170]	2017	NaₓWO₃	300 nm	Au	≈4 µm	N.A.	<4 V	<4 V	N.A.	N.A.	N.A.	ECM, Bipolar
[178]	2017	ZnO	100 nm	Ti/Au[b]	500 nm	N.A.	≈21 V	≈30 V	N.A.	2 × 10³	>10³	VCM, Bipolar
[206]	2017	ITO/HfO₂	80–250 + 5/10 nm[a]	Ti/Au[b]	≈2 µm	≈1.1 V	≈0.6	≈0.65	10³	10⁴	≈10	VCM, Bipolar
[232]	2017	Ag/TiO₂	≈63 + ≈15 nm[a]	Ag/Al or (Au/Al)	≈2.4 µm	N.A.	≈0.4 V	≈–0.1 V	150 / 15	Up to 10³ / >10⁶ s	Up to 10⁵ / 10⁷	ECM, Bipolar/Unipolar
[211]	2018	HfO₂/NiO/Ni	55 + ≈10 + 20 nm[a]	Ti/Au[b]	≈2.8 µm	N.A.	1–3 V	1–2 V	205	Up to 10⁷	10⁴	VCM, Unipolar
[226]	2018	ZnO	104 nm	Ag–Pt[c]	≈180 nm/400nm	Down to ≈2 V	<4 V	<1 V	300	>10³	Up to >10²	ECM, Bipolar/Threshold

a)NW diameter + shell layer(s) thickness; b)First layer in contact with the NW (adhesion layer)/metallic overlayer; c)Asymmetric electrodes; d)Thickness of the oxide layer in a multisegmented NW; e)Device formed with a fixed steady-state constant bias voltage; f)Results after surface treatment; g)ISET voltage decreased to <10 V under illumination; h)Cycle is referred to a set of pulses.

ADVANCED
SCIENCE NEWS
www.advancedsciencenews.com

ADVANCED
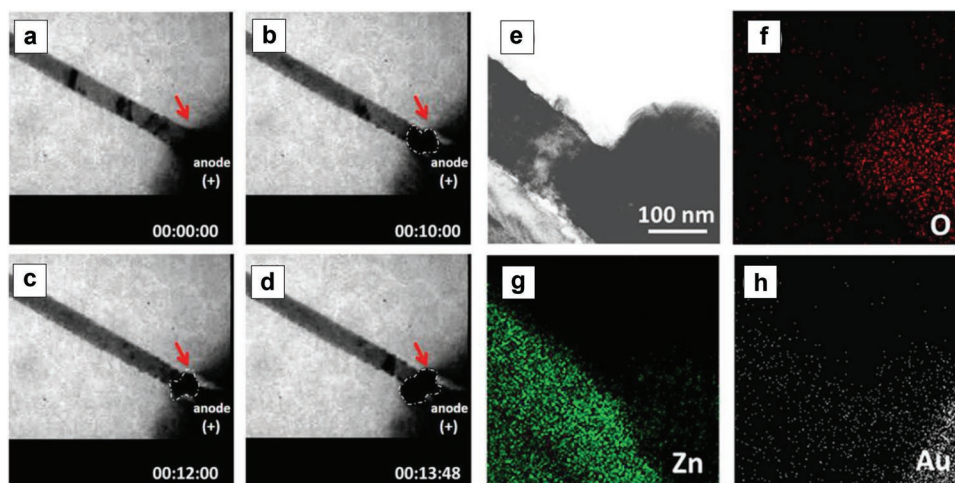**ELECTRONIC**
MATERIALS
www.advelectronicmat.de

Figure 3. Series of in situ TEM images from the real time video during the SET process reporting a) the pristine state, b,c) the protrusion evolution (indicated by the red arrow), and d) the formed protrusion when the NW turned into the LRS; e) TEM image and corresponding EDS mapping of f) oxygen, g) zinc, and h) gold near the protrusion in the LRS, evidencing the accumulation of oxygen ions near the anode. All panels adapted with permission.[158] Copyright 2013, American Chemical Society.

are distributed along the interface that controls the device conductivity, differently from the filamentary model, where oxygen vacancies are organized into a strongly localized filament across the two electrodes.[163] For this reason, by manipulating the amount of oxygen vacancies at the interface, it is possible to achieve multiple resistance states. Indeed, experimental results showed that it was possible to gradually increase the NW conductance via successive voltage pulses application, as shown in Figure 4c. Lin et al.,[164] considering similar Au/TiO_2 NW/Au devices, proposed that plasmonic-enhanced optical absorption at the TiO_2/Au interface induced by femtosecond laser irradiation can enhance the mechanical and electrical properties of contacts, allowing an engineering of the local concentration of charged defects in TiO_2 NW near the interface. Thanks to this treatment, the electroforming process can be avoided, and the stability of the multilevel memory was improved.

The analogic behavior characterized by the possibility of tuning the device in a wide range of resistance states is the fundamental prerequisite for the emulation of synaptic plasticity of biological systems. In this case, the synaptic weight (device conductivity) can be regulated by input stimuli such as voltage spikes. By exploiting this principle, Hong et al.[165] emulated synaptic plasticity processes and learning rules such as STDP and Hebb's rule in a single TiO_x NW. The schematization of the implementation of the spike timing rules is presented in **Figure 5**a. In case of STDP, the device conductance was regulated by means of the time in between preneuron and postneuron spikes (Figure 5b), while the Hebb's law was obtained by determining the synaptic weight through photocurrent (Figure 5c). Note that the performances of these devices are limited by the very high operating voltages (up to 200 V) and by the long pulse time length (in the order of seconds). Interestingly, it was shown that neuromorphic-like devices based on TiO_2 nanowires can be sensitive to heterogeneous physical stimuli, as shown by O'Kelly et al.[166] that reported associative memory with time-dependent correlation in between voltage and optical pulse stimuli.

The drift of oxygen vacancies was considered responsible for memristive properties with hysteretic $I–V$ characteristics also in hexagonal WO_3 NWs, as observed by He et al.[167] Moreover, it
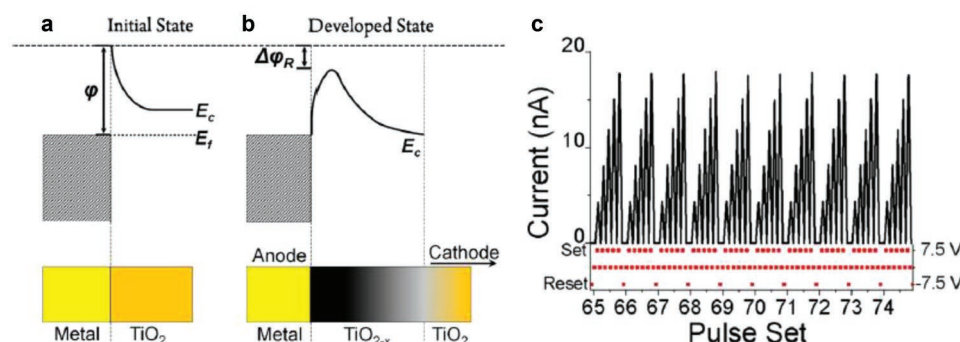

Figure 4. Schematic representation of the interfacial switching mechanism in TiO_2 nanowires; a) initial state where the Schottky barrier dominates the conduction mechanism and b) after forming where the Schottky barrier height and width were decreased; c) successive voltage pulses (7.5 V) gradually decrease the TiO_2 NW conductance. A reset pulse was applied to restore the HRS. All panels adapted with permission.[161] Copyright 2014, American Chemical Society.

ADVANCED
SCIENCE NEWS
www.advancedsciencenews.com

ADVANCED
ELECTRONIC
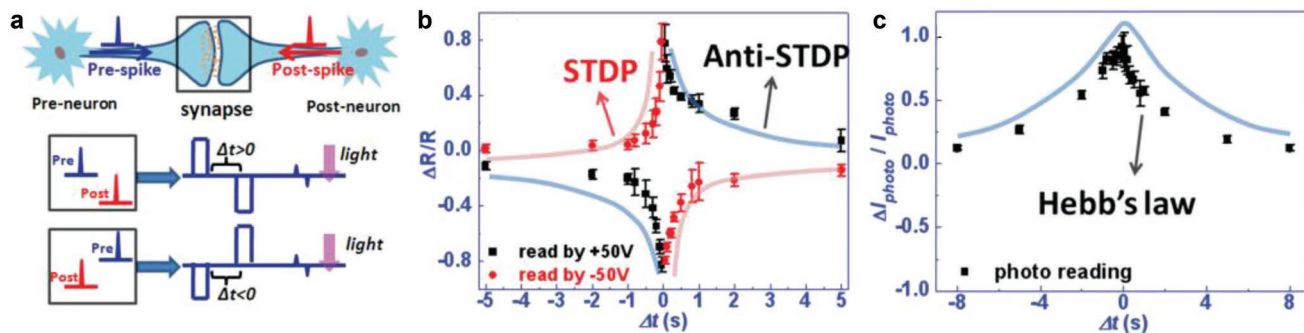**MATERIALS**
www.advelectronicmat.de

Figure 5. Schematic representation of synaptic plasticity implemented by means of regulating the time in between preneuron and postneuron spikes in a single TiO$_x$ nanowire. b) Spike time dependent plasticity (STDP) and c) Hebb's learning rules implemented in the nanowire. All panels adapted with permission.[165] Copyright 2016, Wiley-VCH.

was shown that resistive switching properties of WO$_3$ NWs can be influenced by water molecule adsorption.[168,169] It is worth noticing that new features of resistive switching can be observed in Na$_x$WO$_3$ (sodium tungsten bronze) NWs as observed in a later work by Lei et al.,[170] where the switching was proposed to be controlled by the migration of Na$^+$ ions along the NW and can be thus attributed to a metallization memory effect.

Among all single crystal NWs, isolated single crystalline ZnO NWs are the most extensively studied nanostructures that exhibited resistive switching properties.[171–179] Even if resistive switching was previously observed in ZnO thin films grown by different techniques,[180–182] resistive switching in single crystalline ZnO nanowires with wurtzite structure grown by VLS technique was reported for the first time in 2011 by Chiang et al.[171] In this case, the Ti/ZnO NW/Ti devices exhibited two well defined resistance states with high performances in terms of HRS/LRS ratio that was reported to be as high as 7.7×10^5 with an endurance of 100 cycles. Despite this, high forming voltage ($\approx$22 V) and SET and RESET voltages ($\approx$7 and $\approx$12 V) were observed. By considering similar devices based on single ZnO NW with Ti/Au electrodes, Zhang et al.[179] showed the influence of the substrate layer on the resistive switching performances. By realizing a suspended NW-based device, they observed a reduction of switching voltages and an increase of the LRS current that were attributed to the improved thermal insulation of the device. However, as revealed by TEM measurements by Chiang et al.,[171] in these devices a TiO$_2$ interfacial layer is present at the Ti/ZnO interface because of the higher affinity of Ti compared to Zn with O (enthalpies for TiO$_2$ formation is –933 kJ mol^{-1} while for ZnO is -350 kJ mol^{-1}). Thus, in this case the switching mechanism can be dominated by the oxygen vacancies exchange at the ZnO–TiO$_2$ interface, as reported by Huang et al.[183] in case of ZnO/TiO$_2$ multisegmented NWs (see Section 4.1.3.).

It has to be noticed that a large variety of metal oxide NWs presented a high concentration of oxygen vacancies directly after the growth process, since a deficit in oxygen is more energetically favored with respect to stoichiometric oxide.[167] The initial amount of oxygen vacancies and defects resulting from the synthesis can strongly impact the switching parameters and performances, thus the growth conditions play a crucial role for the realization of NW-based resistive switching devices. However, the concentration of defects in NWs can be modified

by proper treatments even after the growth process. By using this approach, few works reported an increase of the device performances of single crystalline NWs by surface treatments that can modify the amount of oxygen vacancies in the NW,[173,175,176] or can introduce an amorphous layer at the metal–oxide/electrode interface.[177] These aspects will be further discussed in Section 7.1.

Despite the switching mechanism based on the migration of oxygen-related defects is widely accepted, not only for NWs, but in a wide range of metal-oxide resistive switching devices,[22] it was proposed that resistive switching in ZnO NW can be purely electronic, without involving defect migration. Indeed, considering Pt/ZnO NW/Pt devices, Karthik et al.[174] proposed a switching mechanism based on the screening model of polar charges that are present at the two wire's ends, as previously reported by Song et al.[172] in case of Pt/ZnO NW/Au devices. The peculiar spontaneous polarization of ZnO surfaces arises from the non-centrosymmetric crystal structure, with Zn and O atoms tetrahedrally bonded and stacked along the [0001] direction. As a result, a spontaneous polarization is present in charged (0001) ZnO surfaces.[184] In these devices, it was proposed that part of the electrons that are injected from metal contacts can be trapped by polar charges at the interface. When a threshold voltage value is reached, electrons have enough energy to be detrapped from polar charges with a consequent dramatic increase of current. Thus, the LRS is reached. Instead, decreasing the voltage, a RESET process occurs when electrons no longer have enough energy to be detrapped from polar charges. As observed by Karthik et al.,[174] SET and RESET occurred at different voltages (around 0.5 and 0.2 V, respectively) and this behavior was attributed to Joule heating effects that provide more power to electrons for escaping traps during the reverse voltage scan. However, the key limitation of these devices is the poor OFF/ON ratio that is about 1.5 in case of unipolar Pt/ZnO nanowire/Pt resistive switching devices.[174]

4.1.2. Polycrystalline NWs

Resistive switching can be strongly influenced by the material microstructure and thus the physical mechanism of switching in polycrystalline materials can be different with respect to single crystals. Indeed, in polycrystalline materials the grain

**ADVANCED
SCIENCE NEWS**

www.advancedsciencenews.com

**ADVANCED
ELECTRONIC
MATERIALS**

www.advelectronicmat.de

center is generally not involved in the switching mechanism that is likely to be located in the highly defective grain boundaries, as recently reported for NiO and ZnO polycrystalline films and MoS$_2$ monolayers.[31,185,186]

Kim et al.[38] reported for the first time in 2008 resistive switching in NWs, by considering polycrystalline NiO NWs contacted by Ti/Au electrodes. The synthesized NWs were polycrystalline with grain size that is comparable to the NiO NW diameter, as can be seen in **Figure 6**a. The NiO nanowire device, with electrodes spacing of 1 μm, exhibited a forming voltage of about 2.5 V and a unipolar resistive switching behavior with V_{RESET} of 0.52 V and V_{SET} of 1.2 V (Figure 6b). It should be noticed that the electric field needed to form the NW-based device ($\approx 2.5 \times 10^6$ V m^{-1}) was about one order of magnitude lower with respect to polycrystalline NiO film devices.[187] Authors proposed that the low voltages observed for electroforming in NiO NW-based devices compared to NiO thin films can be ascribed to the peculiar microstructure of NWs that are characterized by a diameter that is smaller or comparable to the grain size and/or to the presence of Ni defects. However, this aspect still needs to be clarified. Using a similar growth technique based on metal deposition in an AAO template and subsequent oxidation, Liang et al.[188] investigated resistive switching in polycrystalline CuO NWs contacted by Ni electrodes. After the growth process, NWs resulted to be partially oxidized with the presence of three different phases that resulted in CuO, Cu$_2$O, and Cu nanograins embedded into the NW, as demonstrated by X-ray diffraction (XRD), TEM, and EELS characterizations. Interestingly, a forming-free behavior was observed and low electric field of ≈ 6.8 kV cm^{-1} was necessary to turn the device to the LRS state (V_{SET} = 1.375 V). The forming-free behavior was ascribed to the high density of defects due to the coexistence of different copper and copper oxide phases that facilitate the creation of a conductive path in between the two electrodes. The switching mechanism was proposed to be triggered by oxygen vacancies. During the SET process, oxygen vacancies diffuse from anode to cathode under the action of the electric field and form a conductive filament. The ionic migration is promoted also by Joule heating induced by electron injection, while additional oxygen vacancies can be generated at the CuO$_x$/anode interface. Instead, it was proposed that the RESET process in these nonpolar devices (with the coexistence of bipolar and unipolar switching) has to be mainly attributed to Joule heating. Even if oxygen vacancies are considered to be responsible for the resistance transition as in

the case of single crystal CuO NWs, in this case Cu nanograins inside the material play a crucial role locally enhancing the electric field and thus the diffusion of oxygen vacancies. Endurance of 50 cycles was obtained in bipolar conditions, which was discussed to be more stable with respect to unipolar switching because of the localization of the filament rupture near the grounded electrode.

Resistive switching was observed also in ZnO polycrystalline microwires grown by vapor phase transport method, as reported by Huang et al.[189] Despite the huge electrode spacing of about 1 mm in an Ag/ZnO MW/Ag device, electroforming occurred applying a stress voltage of 1.5 V, while SET and RESET voltages were reported to be less than 1 V. A HRS/LRS ratio of 10^3–10^4 and an endurance of 100 cycles was observed. While in HRS the conduction mechanism was dominated by space-charge-limited-current (SCLC) mechanism, an ohmic conduction was observed in LRS suggesting that resistive switching is consistent with the formation of metallic conductive filaments. It was proposed that the unipolar resistive switching is linked with the abundant dislocations and stacking defects that were present in the wire, as revealed by TEM images. It should be noticed that, even if electrochemically active electrodes of Ag were used, the switching mechanism is unlikely to be attributed to ECM because of the large electrode spacing and the low electric fields involved. In addition, a comparison of these results with previously discussed results for single crystalline ZnO nanowires evidenced that in case of polycrystalline wires the electric field needed to form a conductive path is dramatically reduced, from $\approx 8 \times 10^8$ V m^{-1} in case of single crystalline NW[158] to $\approx 1.5 \times 10^3$ V m^{-1} in case of a polycrystalline microwire.[189] These observations clearly evidenced that the NW microstructure and defectivity play a crucial role during the switching events.

4.1.3. Heterostructured NWs

Recently, a wide range of heterostructured nanowire structures have been synthesized for different purposes. Indeed, by controlling the composition at the nanoscale of these heterostructures and by combining different materials with specific functions, it is possible to realize different kinds of devices, such as efficient photovoltaic cells,[190] flexible supercapacitors with high performances,[191] high capacity electrodes for ion batteries,[192] and high performances field effect transistors.[193] In 2009, Oka et al.[194] reported nonvolatile resistive switching in core–shell nanowires composed of a MgO core and a single crystalline NiO shell layer. In this case, MgO NWs were grown by a VLS method and the single crystalline NiO shell layer was realized using the laser molecular beam epitaxy technique. Interestingly, resistive switching was observed by means of C-AFM measurements. Indeed, only one Pt electrode was deposited on the NW while a conductive Ir/Pt coated Si cantilever was placed at a distance of about 1 μm on the NW, acting as a second electrode. Bipolar resistive switching was attributed to the NiO shell layer, since no resistive switching was observed on the bare MgO nanowire. However, the stability of these devices was strongly influenced by the instability of the C-AFM tip. The switching mechanism in these core–shell
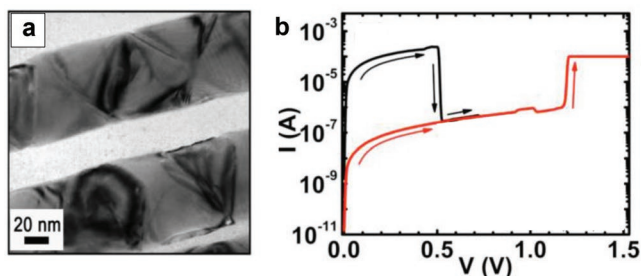

Figure 6. a) TEM image of the polycrystalline NiO NWs; b) I–V characteristics showing unipolar resistive switching of the device. All panels adapted with permission.[38] Copyright 2008, American Institute of Physics.
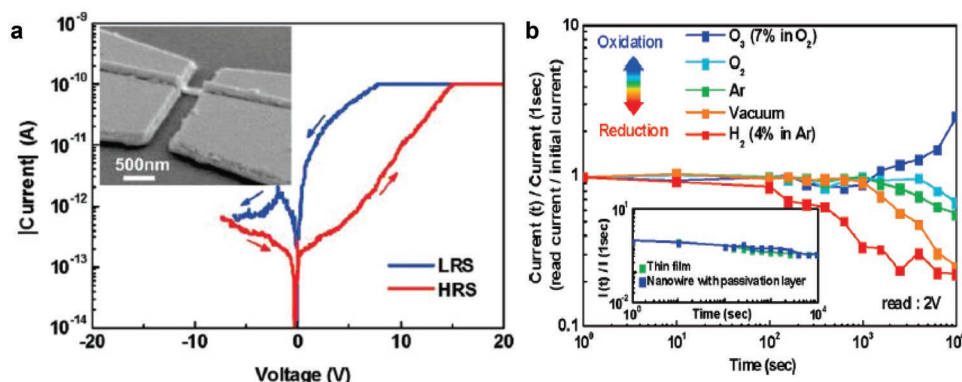
ADVANCED
SCIENCE NEWS
www.advancedsciencenews.com

ADVANCED
ELECTRONIC
MATERIALS
www.advelectronicmat.de

Figure 7. a) *I–V* characteristics of a single MgO/NiO core–shell single NW. The inset shows an SEM image of the fabricated devices; b) retention data in the LRS of the NW exposed to different atmosphere gases; the inset shows a comparison of the retention of a device with a passivation layer compared to a thin-film based device. All panels adapted with permission.[195] Copyright 2010, American Chemical Society.

NWs was further discussed using conventional symmetric Pt/Au electrodes in a following work by Oka et al.,[195] evidencing bipolar resistive switching (see **Figure 7**a) with an endurance up to 10^6 cycles. In this case, authors observed that the electric field intensities ($\approx 10^7$ V m^{-1}) involved in the switching mechanism were comparable to those in sandwich devices where NiO thin films act as the active material. However, the planar NW based device turned out to be a good platform for examining the switching mechanism by investigating the chemical reaction with the surroundings. Indeed, performing retention measurements in the LRS in different atmospheres (Figure 7b), Oka et al. revealed that the current tends to decrease if the atmosphere is chemically reduced while increases in an oxidizing environment, suggesting that redox events dominate the switching mechanism. Note that the effect of surroundings can be mitigated by inserting a passivation layer to the NW device, as shown in the inset of Figure 7b, where the retention of a NW with passivation layer is compared to that of a thin-film device. The physical mechanism of switching was attributed to the creation of a conductive path due to the migration of cation vacancies induced by the electric field.

A multistate capability was observed in similar devices by Nagashima et al.[196] where MgO NWs were covered by 5 nm Co_3O_4 shell layer. It was shown that the LRS can be tuned in a wide range of values (from $\approx 10^9$ Ω to $\approx 10^{11}$ Ω) by varying the compliance current (CC) value during the SET transition,

without affecting the HRS value. These devices exhibited high endurance (10^8 cycles) and high retention (10^4 s). The bipolar switching behavior was driven by the electric field rather than current (a relationship between SET and RESET voltage was observed while no correlation between SET current and RESET current was observed) and the resistive switching mechanism was attributed to electrochemical redox events with a conductive path formed by oxygen rich phases along the p-type Co_3O_4 semiconductor shell. However, the switching mechanism was deeply investigated in a subsequent work by Nagashima et al.[197] using three different approaches based on atmosphere controlled measurements for investigating interaction with surroundings (similarly to the approach previously used by Oka et al.[195]), field effect measurements in a NW field effect transistor (NW-FET) configuration to identify the carrier type of the conductive paths and multiprobe measurements to understand the switching location. The strategy is depicted in **Figure 8**. The proposed switching mechanism based on experimental results was ascribed to the formation of p-type conductive paths with cation vacancies from anode to cathode, as revealed by atmosphere-controlled measurements. Furthermore, FET measurements confirmed that conduction mechanism in LRS is dominated by holes while the switching location was observed to be located near the cathode side by means of multiprobe measurements. It is worth noticing that the strategy adopted by Nagashima et al.[197] is promising to investigate the

Figure 8. Schematic illustration of the strategy for investigating resistive switching mechanism in core–shell NWs by means of atmosphere-controlled measurements, field effect measurements in NW-FET configuration and multi-probe measurements. Adapted with permission.[197] Copyright 2011, American Chemical Society.

**ADVANCED
SCIENCE NEWS**

www.advancedsciencenews.com

**ADVANCED
ELECTRONIC
MATERIALS**

www.advelectronicmat.de

switching mechanism in different oxides by changing the active shell layer material. For example, electrical measurements in different atmospheres allowed to unveil the n-type conductive path responsible resistive switching in MgO core–TiO$_2$ shell nanowires.[198] The modulation of the conduction properties in different environments can be exploited for the realization of resistive switching sensors, as discussed in Section 7.4. It is important to remark that this strategy can be adopted only in planar devices and not in widely studied capacitor-like devices where the switching mechanism is hidden in stacked sandwich structures: for these reasons, nanowires can be considered a good platform to investigate the resistive switching mechanism in a wide range of materials. In particular, planar type devices can enhance the capability of understanding the role of surroundings during resistive switching[199] that can have a strong impact on resistive switching properties and device reliability. As recently observed in thin film-based devices, the incorporation of moisture and/or oxygen from the environment can affect electrochemical properties of the memristive cells, impacting the forming process as well as resistive switching properties and parameters.[200–203]

Using a completely different approach, resistive switching was observed also considering conductive nanowires covered by an oxidized shell layer, in which the switching occurs along the radial direction of the NW. Differently from the previous cases in which the NW core was highly insulating and acted merely as a support, in this case the conductive NW core acts as an electrode. He et al.[204] reported resistive switching in Ni nanowires covered by a NiO shell layer. First, Ni NWs were grown by electrodeposition of Ni using AAO templates and then dispersed on an insulating substrate of SiO$_2$. Au electrodes were then patterned on isolated NWs. Then the NWs were oxidized by a self-limited oxidation in air for 3 days except from the surface regions covered by Au electrodes and, at the end, a new Au electrode was fabricated on the NiO layer. A schematic representation of the device is reported in **Figure 9**a where the current path through the core Ni NW and across the NiO shell layer is evidenced. Electrical characterization revealed the coexistence of both threshold resistive switching (volatile) and memory resistive switching depending on the current compliance values

adopted during the voltage sweep (Figure 9b). According to theoretical calculation, memory resistive switching was attributed to the formation of a conductive filament across the NiO layer based on oxygen vacancies interactions, while threshold switching was attributed to electric field driven transition phenomena without the formation of a conductive path. Authors underlined that NiO–Ni nanojunctions minimize the size of the device and provide a good platform to reveal the resistive switching mechanism. However, strictly speaking, resistive switching in these nanowire-based devices is buried on a sandwich structure in the metal/nanowire interface that is similar to conventional capacitor-like devices.

By similarly using a metallic inner core and an insulative shell layer, Hsu and Chou[205] realized Au/Ga$_2$O$_3$ core–shell NWs. However, in this case electrodes were all deposited on the Ga$_2$O$_3$ insulating shell layer without direct access to the Au inner core. Resistive switching was attributed to the formation/rupture of oxygen vacancies filaments in the Ga$_2$O$_3$ layer, in between the metal electrode and the Au inner core of the NW. Since in this case the switching events are located in the shell layer along the axial direction of the NW, while the inner conductive core acts only as a conductor channel, the electrode spacing is not a crucial parameter for resistive switching behavior. For this reason, Hsu and Chou[205] observed invariant V_{SET} and V_{RESET} when considering different electrode spacings (from 900 nm up to 2.44 µm). This property can be exploited to realize multiple electrodes on a single NW, thus realizing a multitude of resistive switching cells with comparable characteristics on the same NW. A similar mechanism of switching along the axial direction was proposed by Huang et al.[206] by considering conductive indium tin oxide (ITO) single crystal NWs covered with an HfO$_2$ shell layer. Interestingly, the amorphous shell layer was here realized by means of atomic layer deposition (ALD). This technique, that is widely employed for the realization of metal oxide thin films for memristive applications,[207–209] results to be particularly promising for the realization of amorphous shell layers on self-assembled NWs, since it allows conformal coatings on high aspect ratio nanostructures with very high control of the shell thickness down to few nanometers.[210] In ITO core–HfO$_2$ shell NWs, authors

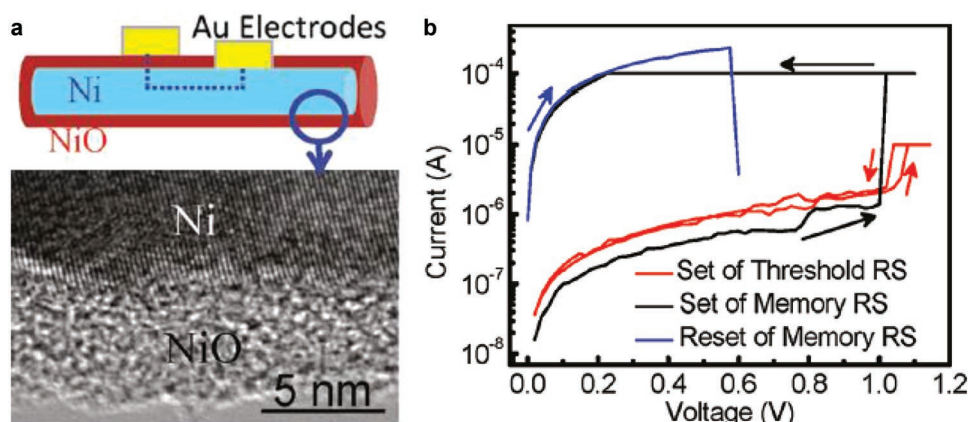**Figure 9.** a) Schematic representation of the NiO/Ni core–shell nanowire device and TEM image of the amorphous NiO shell layer; b) I–V characteristics of the device that exhibited threshold and memory resistive switching. All panels adapted with permission.[204] Copyright 2011, American Chemical Society.
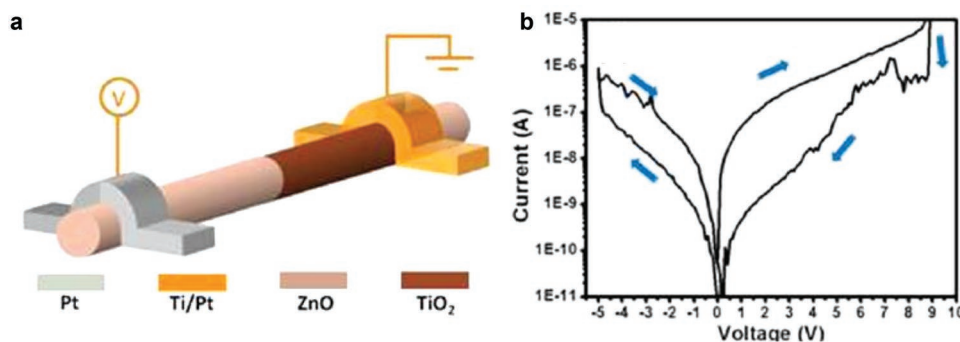
**ADVANCED
SCIENCE NEWS**
www.advancedsciencenews.com

**ADVANCED
ELECTRONIC
MATERIALS**
www.advelectronicmat.de

Figure 10. a) Schematic representation of a resistive switching device based on a ZnO/TiO$_2$ multisegmented NW and b) bipolar resistive switching characteristic of the device. All panels adapted with permission.[183] Copyright 2014, American Chemical Society.

pointed out that the square shape of the NW creates local field enhancement near the NW edges where the filament formation is thus favored. These observations open the way to geometry architecture engineering of NW-based devices in order to reduce the operating voltages and the randomness of filament formation that can be a source of switching instability and irreproducibility. It should be noticed that the use of ALD can open the way to the investigation of memristive behavior in multishell NWs, as proposed by Huang et al.[211] that reported improved resistive switching performances of NiO/Ni NWs by adding ALD deposited shell layers to form a multishell NW structure.

Resistive switching devices can be realized also by exploiting interface effects between the shell layer and the inner core, as observed by Cheng et al.[212] in ZnO/Zn$_2$SnO$_4$ core–shell NWs. It was proposed that in this case the switching mechanism is dominated by interface states that are the result of the lattice mismatch at the ZnO/Zn$_2$SnO$_4$ interface. Authors proposed that the acceptor-type interfacial states can be filled or emptied by injected electrons, depending on the applied voltage polarity. This resulted in an elimination or creation of an interface potential barrier that turned the device to the LRS or HRS, respectively.

Also multisegmented NWs composed of different materials along the NW length were exploited for the realization of resistive switching devices. Huang et al.[183] reported resistive switching behavior in devices based on single multisegmented ZnO/TiO$_2$ NWs (see **Figure 10**a). The multisegmentation was realized transforming ZnO to TiO$_2$ in part of the NW by means of solid to solid cationic exchange reaction, as revealed by real time TEM observations. The multilayered NW exhibited resistive switching behavior as reported in Figure 10b that authors ascribed to the oxygen exchange (i.e., oxygen vacancy exchange) between ZnO and TiO$_2$ segments under the action of the applied electric field, as confirmed by EDS measurements after SET and RESET processes. The presence of a TiO$_2$ segment on one hand acts as an oxygen reservoir and on the other hand limits the current load when the device is in the ON state, thus increasing the reliability of the device.

Resistive switching was observed also in case of metal–oxide–metal (MOM) segmented nanowires. Indeed, in 2009 Herderick et al.[213] observed resistive switching in individual Au/NiO/Au segmented NWs contacted by Pt electrodes, where the NiO acts as the active layer. Authors pointed out that the

MOM structure provided high quality contacts and a fine control of the oxide thickness. Afterward Park et al.[214] observed resistive switching also in Ni/CuO/Ni multisegmented NWs, where the CuO segment acts as the active switching layer. It is particularly interesting the case of NiO/Pt multilayered NWs that can be exploited for the realization of multilevel memories when arrays are considered, as discussed by Huang et al.[215] (see Section 5).

4.2. Electrochemical Metallization Switching Mechanism

ECM is based on electrochemical dissolution and subsequent deposition of an active electrode that is responsible for the formation of a conductive bridge in the solid electrolyte under the action of the applied electric field.[28,216] In electrochemical metallization cells (ECM cells), also called programmable metallization cells or conductive bridge random access memory, the active material is usually sandwiched in between an electrochemical active material (usually Ag or Cu) and an electrochemically inert electrode. When a bias voltage is applied to the cell, resistive switching can occur in three steps[28]

1) Anodic dissolution of the active metal electrode through the reaction

$$M \rightarrow M^{n+} + ne^- \qquad (2)$$

2) Drift of metal ions toward the counter electrode across the solid electrolyte under the action of the high electric field.
3) Reduction and deposition of metal ions (as pure metal) on the surface of the inert counter electrode according to the reaction

$$M^{n+} + ne^- \rightarrow M \qquad (3)$$

The deposition of metal ions through electrocrystallization allows the creation of a metallic filament in between the two electrodes, switching the device to the LRS. When an opposite polarity is applied, electrochemical dissolution of the metallic filament occurs, and the device is turned back to the HRS. Even if many efforts have been made to study the ECM mechanism in conventional stacked MIM structures using different solid electrolyte materials and electrodes,[28] only few works concerning the ECM mechanism in NW-based devices are reported in literature.

**ADVANCED
SCIENCE NEWS**
www.advancedsciencenews.com

**ADVANCED
ELECTRONIC
MATERIALS**
www.advelectronicmat.de

4.2.1. Single Crystalline NWs

ECM mechanism was reported in single nanowire-based devices in 2011 by Yang et al.[217] In this case, single crystalline ZnO NWs grown by CVD were contacted by using asymmetric electrodes: an electrochemical active Cu electrode and an electrochemical inert Pd/Au electrode (see inset in **Figure 11**a). The proposed switching mechanism is based on the formation/retraction of a Cu nanoparticle chain on the NW surface. Indeed, when a positive polarity is applied to the copper electrode, oxidization of Cu occurs and Cu^{2+} ions start to migrate along the NW under the applied electric field. When Cu ions reach the counter electrode, reduction occurs, and a metallic bridge is formed in between the two electrodes turning the device into the LRS. Thus, I–V measurements revealed bipolar resistive switching as reported in Figure 11a. In a single filament scenario, authors proposed that the overall resistance in the LRS is ascribable to two different contributions, the resistance of metal islands and tunnel resistances in series, as schematized in Figure 11b. Considering these two contributions, it was possible to explain the mixed metallic and semiconductor behavior observed for the temperature-dependence of resistivity in the LRS. However, the switching mechanism in these devices was theoretically analyzed in details by Raffone et al.[218] that studied the extraction and diffusion of Cu atoms from the electrode to the ZnO NW surface by means of density functional theory (DFT). They proposed a novel switching mechanism that does not imply the formation of a continuous metallic filament on the NW surface. Indeed, when a positive voltage is applied to the Cu electrode, Cu atom extraction occurs and adatoms can spread over the NW surface acting as n-type dopants and decreasing the overall resistance of the NW (LRS is established). When an opposite polarity is applied, Cu ions are moved back eventually joining into nanoparticles. Thus, a region free of doping metal atoms is created and the device turns into the HRS. It should be noticed that in this case the formation of a continuous conductive filament is not needed, according to experimental observations by Yang et al.[217] that do not observe a continuous filament on the NW surface after

switching, as revealed by energy dispersive X-ray spectroscopy. Although the devices reported by Yang et al.[217] exhibited a high OFF/ON ratio ($>10^5$) with good retention (2×10^6 s), the endurance performances are limited (7 cycles are reported) by the NW breakdown due to Joule heating. Considering a similar device structure, the same resistive switching mechanism was observed also considering a single Zn_2SnO_4 NW that exhibited a large HRS/LRS ratio ($>10^5$) and a fast switching speed below 20 ns.[219]

ECM mechanism in single ZnO NWs was observed also considering Ag electrodes, as reported by Qi et al.[220] in 2013. Here, Na-doped single ZnO NWs were contacted by symmetric Ag electrodes and exhibited bipolar resistive switching with endurance of 10^3 cycles and retention of at least 10^5 s. Differently from the case of nondoped ZnO NWs, Na-doped NWs exhibited self-compliance behavior and did not require an external control of the maximum current flowing into the device to avoid the NW breakdown. This behavior was attributed to the Na doping (that is a p-type dopant in ZnO) that acts as a load resistor in series allowing the realization of self-complianced device. In addition, self-rectifying behavior was observed and was ascribed to the formation of a good contact between NW and Ag at the biased side, while at the grounded side conduction is dominated by a Schottky contact. It should be noticed that a self-rectifying behavior is a crucial property in memory arrays in order to avoid misreading due to sneak currents during read operations,[221,222] while self-complianced devices can prevent an irreversible hard breakdown of the devices without any external control, thus reducing the circuit design complexity.[223] However, the limiting parameter of the devices realized by Qi et al.[220] were the high programming voltages (about 40 V for V_{SET} and −40 V for V_{RESET}). The switching mechanism in such devices was ascribed to the formation and annihilation of an Ag nanoisland chain along the NW, similarly to the previously described mechanism of metal ion migration on surfaces reported by Yang et al.[217] and Yang et al.[224] After cycling, Ag nanoislands were observed on the NW as presented in **Figure 12**a,b, with the maximum Ag content on the biased side of the NW (Figure 12c). Even if the ion migration inside the nanowire bulk cannot be a priori
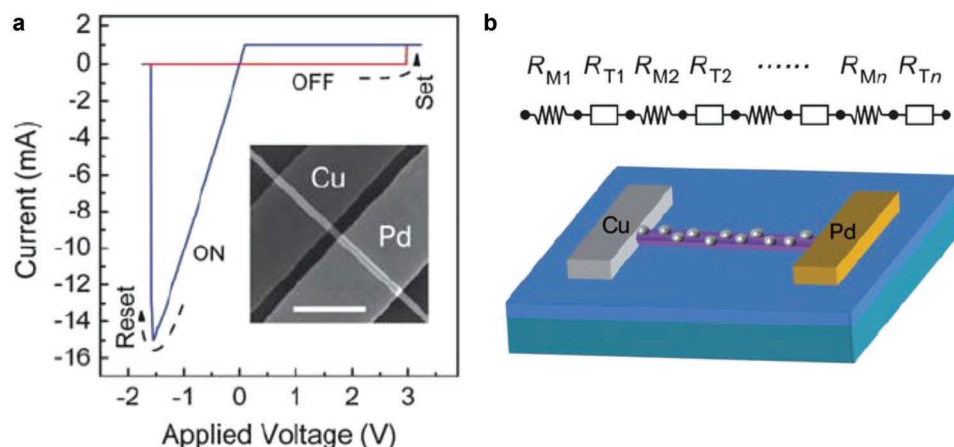

Figure 11. a) Bipolar resistive switching in Cu/ZnO NW/Pd device; the inset shows a SEM top view of the resistive switching device. b) Schematization and equivalent circuit of the switching mechanism based on the formation of a metallic filament on the NW surface. All panels adapted with permission.[217] Copyright 2011, Royal Society of Chemistry.
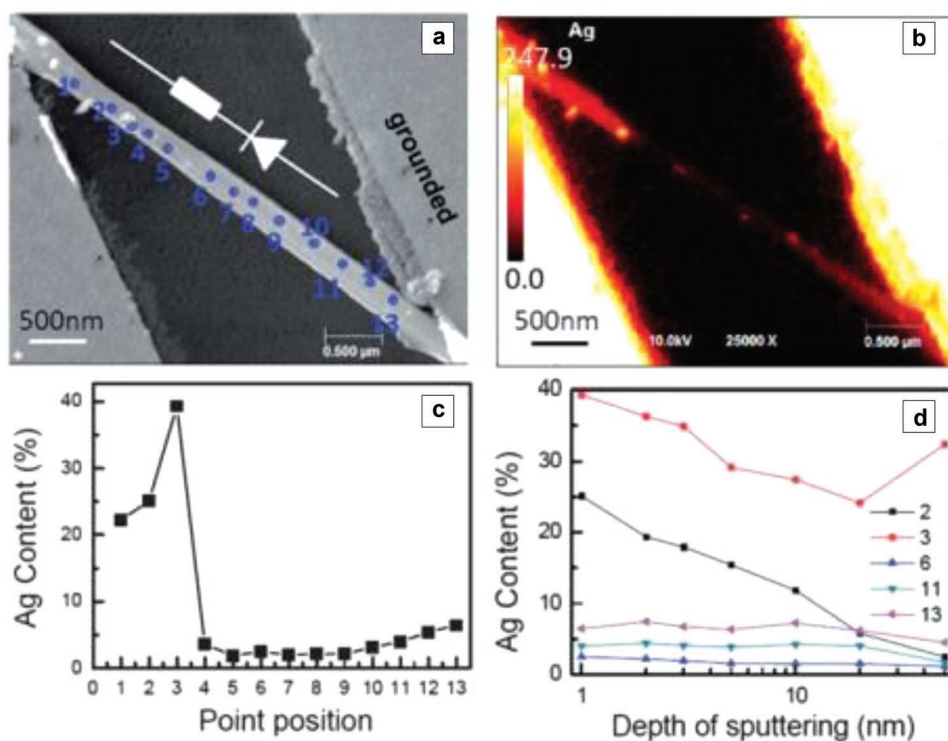
Figure 12. a) SEM image and b) map of Ag of the Ag/Na-doped ZnO NW/Ag device after *I–V* characterization; c) Ag content on the NW surface in different positions revealing that the Ag content is higher at the biased side; d) Ag content after removal of different thicknesses by sputtering revealing that the Ag content is mainly distributed on the NW surface. All panels adapted with permission from.[220] Copyright 2013, Royal Society of Chemistry.

excluded, the filament formation is proposed to occur mainly on the nanowire surface as revealed by Auger electron spectroscopy (AES) analysis after cycling (Figure 12d). Exploiting the same resistive switching mechanism, Wang et al.[225] investigated the effect of Ga and Sb doping on resistive switching of single ZnO NWs. They observed that both Ga- and Sb-doped ZnO nanowires exhibited self-rectifying characteristics, while Sb-doped ZnO exhibited also self-compliance behavior, similarly to the previously reported case of Na-doped ZnO NWs.[220] It was shown that doping can reduce the V_{SET} and V_{RESET} fluctuations and can improve the device endurance that was observed to be over 2000 cycles in case of Sb-doped NWs. However, the role of doping during resistive switching is still to be elucidated. By exploiting Ag dynamics on the NW surface, Milano et al.[226] showed that it is possible to achieve in a single device a wide range of functionalities such as multilevel nonvolatile resistive switching, threshold switching with selector capability, and emulation of synaptic plasticity of biological synapses. All-in-one functionalities together with a detailed understanding of the physical/electrochemical mechanism of switching based on migration of Ag^+ ions on the crystalline ZnO surface make these nanostructures suitable model systems for the investigation of the ECM mechanism of synaptic/resistive switching at the nanoscale.

Considering NWs, the ECM mechanism was observed only considering the migration of Ag and Cu ions. Even if the migration of metal ions and nanoclusters in dielectrics was observed also considering other metals such as Ni and Pt, the electric field required for the dissolution and migration of Ag and Cu ions is considerably lower than other metals, as reported by

Yang et al.[227] For example, Raffone and Cicero[228] proved that the migration of Pt atoms on the ZnO NW surface under the action of an electric field can in principle occur but is impossible in practice, since a high amount of energy is necessary for Pt atoms extraction from the contact. In general, it should be pointed out that the ECM mechanism based on the migration of metal atoms on the NW surface still needs further investigations and can differ from ECM mechanism in conventional thin film devices because of the considerably higher electrode spacing and surface effects that can allow faster ionic percolation. In addition, since metallic atoms are supposed to move on the NW surface, a direct observation and investigation of the switching mechanism in those planar devices is possible. For these reasons, NW-based resistive switching devices are good candidates for investigating the physical mechanism and for studying ionic percolation and dynamics of ECM cells.

4.2.2. Heterostructured NWs

An alternative way of realizing ECM cells based on single NWs is to consider core–shell structures, where only the shell structure acts as the electrolyte and switching events are located along the axial direction of the NW. This approach was first considered by Dong et al.[229] in 2008 considering Si NWs covered by an amorphous Si (a-Si) shell layer and contacted by an Ag electrode. The switching mechanism in these cross-point devices was ascribed to the formation of Ag conductive filaments across the a-Si layer that connected the Ag electrode and
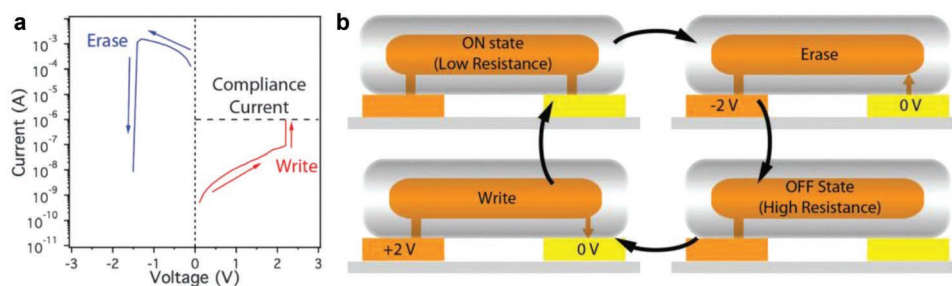
Figure 13. a) Bipolar resistive switching of Cu–SiO$_2$ core–shell NWs; b) schematic representation of the resistive switching mechanism based on the formation/rupture of a Cu filament in the SiO$_2$ shell layer near the Au electrode. All panels adapted with permission.[230] Copyright 2016, Royal Society of Chemistry.

the Si inner core. By using a similar approach, Flowers et al.[230] in 2016 observed resistive switching in Cu–SiO$_2$ core–shell NWs contacted by Au and Cu asymmetric electrodes. Initially, a positive bias voltage of about 7 V was necessary to electrically connect the two electrodes by the formation of Cu filaments in the SiO$_2$ shell (electroforming process). After that a connection between the two electrodes was established, RESET (erase) occurred applying a negative voltage at the Cu electrode that resulted in a retraction of the Cu filament that connected the Cu inner core and the Au electrode. The device was turned in the LRS (write) by applying a positive voltage to the Cu electrode, giving rise to the bipolar resistive switching behavior reported in **Figure 13**a. The resistive switching mechanism is schematized in Figure 13b. These devices exhibited high performances, with an endurance of 10^4 cycles and a write speed that was estimated to be around 50 ns. Cu–core SiO$_2$ shell NWs dispersed in ethylcellulose have been proposed as building blocks for the realization of fully printed memristors.[231] Exploiting the formation/rupture of metallic filaments across the shell layer, resistive switching was observed also in Ag–TiO$_2$ core–shell NWs by Manning et al.[232] In this case, a nonpolar resistive switching was observed as a consequence of the formation/rupture of Ag filaments through the TiO$_2$ shell layer that enabled to connect the Ag electrodes to the Ag core of the NW. The switching mechanism was favored by the highly defective polycrystalline microstructure of TiO$_2$ and by the Ag inclusions in the shell layer due to the growth process. The device exhibited both bipolar and unipolar switching characteristics (nonpolar switching) depending on the applied current compliance.

4.3. Phase Change Switching Mechanism

In phase change memories, the switching mechanism is based on the reversible phase change of a material that possesses at least two phases with different electrical properties.[233] Usually, in phase-change materials the LRS is achieved by crystallization obtained by heating the material above the crystallization temperature (e.g., with Joule heating from an electrical pulse), while the HRS is achieved by melt-quenching that causes the material amorphization.[234,235] This mechanism was exploited for the realization of NW-based memories much earlier than the experimental demonstration of memristors by Strukov et al.[2] in 2008. Indeed, memory effects in phase change NWs were already observed in chalcogenide nanowires such as GeTe NWs[236] and Ge$_2$Sb$_2$Te$_5$ NWs.[237,238] Lee et al.[238] demonstrated that Ge$_2$Sb$_2$Te$_5$ NWs can be used for the realization of nonvolatile memories inducing reversible phase change by Joule heating from crystalline (LRS) to amorphous (HRS). These devices exhibited high performances in terms of data retention (extrapolated to be years) and endurance (>10^5 cycles). However, memristive properties based on phase change in metal-oxide nanowires were reported in 2013 by Bae et al.,[239] where the metal-to-insulator transition in hydrothermally synthesized VO$_2$ nanowire was investigated. In this work, about four orders of magnitude of accessible resistances were achieved by exploiting the phase transition between the insulating monoclinic (VO$_2$(M)) and the metallic rutile (VO$_2$(R)) structures, resulting in the typical hysteresis loop presented in **Figure 14**a. Starting from the insulating phase, at about 0.34 V the resistance decreased
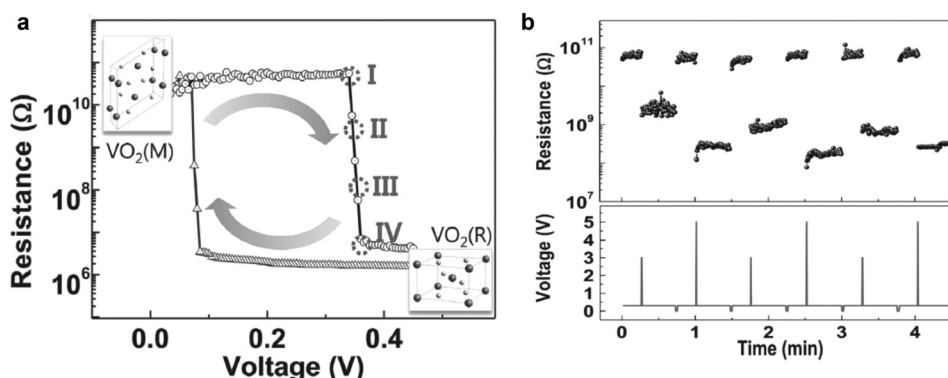

Figure 14. a) Resistance hysteresis loop due to Joule heating driven phase change in VO$_2$ nanowires; the gradual phase change from M to R structure is marked in the loop; b) the device demonstrated the ability of information storage with multilevel capability. All panels adapted with permission.[239] Copyright 2013, Wiley-VCH.

**ADVANCED
SCIENCE NEWS**
www.advancedsciencenews.com

**ADVANCED
ELECTRONIC
MATERIALS**
www.advelectronicmat.de

in correspondence of metal-to-insulator transition (MIT) transition driven by self-Joule heating, while the initial HRS was restored when the applied voltage was decreased. The hysteretic loop arises because of the energy for the M to R transition is larger than the energy for R to M transition, according to differential scanning calorimetry that evidenced a transition from M to R structure and vice versa at about 68 and 59 °C, respectively. Authors showed that the M to R transition is gradual because a mixed state of M and R phases can coexist in the nanowire as a consequence of the percolative nature of the MIT. For this reason, the internal resistance state can be tuned over a wide range of values depending on the metallic-to-insulative phase ratio. Varying the amplitude, the amount, and the number of voltage pulses, authors were able to achieve multiple resistive states. As shown in Figure 14b), a multilevel memory can be realized by using low voltage pulses (3 and 5 V) for writing, while using 0 V for erasing. Despite the high performances of these devices that do not need an external heating source to maintain the temperature near the transition temperature (T_c), the switching characteristics of the NW are preserved by applying a bias voltage (0.3 V) for maintaining the thermally stable state of the nanowire. This means that, if the bias voltage is switched off (0 V), the device does not maintain the internal resistance state. Despite this, the absence of an external heating source and low programming voltages make these devices good candidates for practical applications.

5. Resistive Switching in Nanowire and Nanorod Arrays

Resistive switching devices based on NW arrays represent by far the most investigated device configuration due to the ease of device fabrication, as previously discussed in Section 3. It is worth noticing that memristive devices based on NW arrays where a large number of NWs are contacted in parallel in between a top and a bottom electrode (refer to Figure 2c) have not to be confused with arrays of memristor where each memristive cell can be accessed independently (i.e., cross-bar array). Kim et al.[38] showed that the resistive switching mechanism investigated in single NiO NW can be exploited to realize NW array-based resistive switching devices that consisted in hundreds of vertically aligned NWs embedded in the AAO

membrane and connected in parallel in between an Au bottom electrode and a tungsten probe that acted as the top electrode. In this case, unipolar resistive switching was observed even for high NW length (up to 25 μm) and a lower electric field with respect to NiO thin film was observed for electroforming (about 8 kV cm^{-1}). In order to investigate the switching mechanism in NiO NW arrays, Huang et al.[215] reported a semiconductor type of carrier transport in the ON state, characterized by a resistance increasing with decreasing temperature. For this reason, the conduction mechanism in LRS was attributed to hopping through percolation paths formed by oxygen related defects in the highly defective polycrystalline NiO structure. In a NW array, each vertically aligned NW can be considered a resistive switching device, as shown by Brivio et al.[240,241] in case of Au/NiO/Au and Au/NiO$_x$/Ni/Au heterostructured NWs. By using a C-AFM to combine surface morphology and current maps, authors showed that it is possible to switch a single selected NW in the array. The experimental setup is schematized in **Figure 15**a. Before forming, low current was observed in the considered area of the NW array, as can be seen from Figure 15b. After that, the C-AFM tip was placed on a selected NW and a voltage sweep was applied in order to induce the forming process (see Figure 15c). After forming, a high current spot was observed on the selected NW that underwent electroforming, as can be seen in Figure 15d. Unipolar resistive switching behavior with low power consumption was observed in case of Au/NiO/Au multilayered NW arrays, while bipolar switching was observed in Au/NiO$_x$/Ni/Au NW arrays as a consequence of the asymmetric structure.

By considering NiO NWs, it was observed that the resistive switching performances can be strongly enhanced by realizing multilayered NiO/Pt NW structures.[215] In this case, Pt layers act as intermediate electrodes, reducing the migration length of oxygen ions that resulted in lower and narrow distributed switching voltages. In a subsequent work, Huang et al.[242] showed that multilayer NiO/Pt NW array structures (see **Figure 16**a) can be exploited for the realization of multilevel resistive switching devices. The existence of multistate in NiO/Pt NW arrays was explained in terms of a binary resistor model, as schematized in Figure 16b, and is strictly connected to the structure of the NW that is composed of a large number of NiO segments comprised in between Pt segments. When the device is in the LRS, the application of a voltage pulse resulted
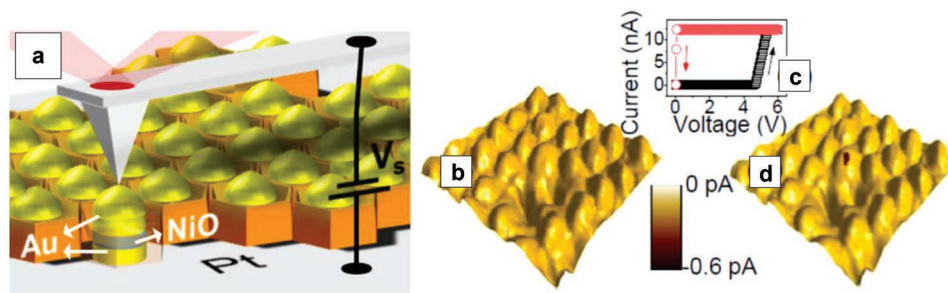

Figure 15. a) Schematization of the experimental setup for C-AFM measurements on NW arrays. b) AFM image evidencing the 3D topography of the Au/NiO/Au NW array. The map color is related to the current map; c) forming process of a selected NW; d) AFM image after the forming process, evidencing a high current spot on the selected NW after the forming process. Adapted with permission.[240] Copyright 2012, American Institute of Physics.
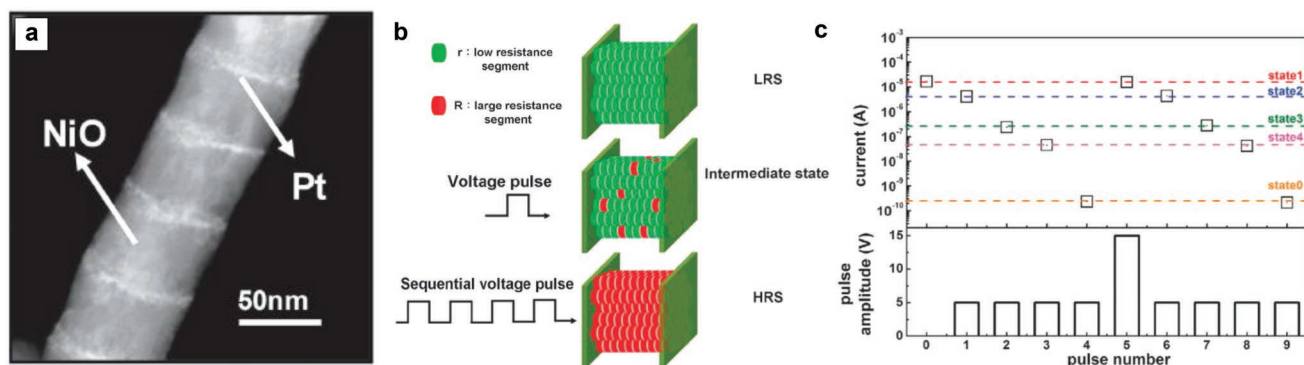
Figure 16. a) TEM image of a multilayered NiO/Pt nanowire; b) schematic diagram of the mechanism underlaying the multilevel memory effect described by the binary-resistor model; c) multilevel states of multilayered NiO/Pt NW array device after the application of different numbers of voltage pulses; current is read at 0.5 V while the pulse width was fixed at 20 ns. All panels reproduced and adapted under the terms of Creative Commons Attribution 3.0 License.[242] Copyright 2014, the authors, published by Springer Nature.

in a probability for a NiO segment to turn to the HRS. In such case, the device exhibited an intermediate resistance state, since not all the segments are turned OFF. By applying a sequence of voltage pulses, the effect is additive and a larger number of NiO segments exhibit high resistances. The HRS of the device is reached when all segments are turned OFF. As can be seen from Figure 16c, the modulation of the resistance state is reproducible and exhibited a large window of accessible resistances (HRS/LRS up to ≈10⁵), making these devices particularly promising for multilevel memory applications.

Among NW and NR arrays, resistive switching in ZnO nanostructures is the most widely investigated[164,186,243–260] because of the relatively easy synthesis of these structures.[261,262] Before the first experimental observation of resistive switching in a single isolated ZnO NW, Chang et al.[243] first reported in 2010 resistive switching behavior in ZnO NR layer. Vertically aligned ZnO NRs were hydrothermally grown on an ITO substrate (see **Figure 17**a) that acted also as the bottom electrode, while a Pt top electrode was realized by sputtering, thus realizing Pt/ZnO NRs/ITO capacitor-like devices. These devices exhibited bipolar resistive switching with multilevel capability depending on the

applied CC, as shown in Figure 17b. Despite the average length of NWs was about 2.9 µm, low SET and RESET voltages were observed (mean values for SET and RESET voltages are 0.72 V and −0.59 V, respectively), making these devices suitable for low voltage electronic applications. In addition, an endurance of 120 cycles and a retention of 10³ s were proved. The switching mechanism was ascribed to the condensation of O vacancies and/or Zn interstitials to form conducting filaments on the NW surface, where higher mobility of defects is expected. Authors proposed that in such structures a superior stability can be achieved with respect to thin films because of geometry, since straight rather than branched filaments can be formed on vertically aligned ZnO NRs. Park et al.[255] proposed that in ZnO NR arrays the 1D geometry of NRs can localize the filament formation because the NR diameter is similar to the conductive filament dimension, allowing reproducibility of resistive switching parameters. As proposed by authors, the strong localization of the conductive filament can be an advantage for the realization of switching devices on flexible substrates, since bending is more prone to change the conductive filament morphology in thin-film devices, thus affecting their stability. Instead, the ZnO
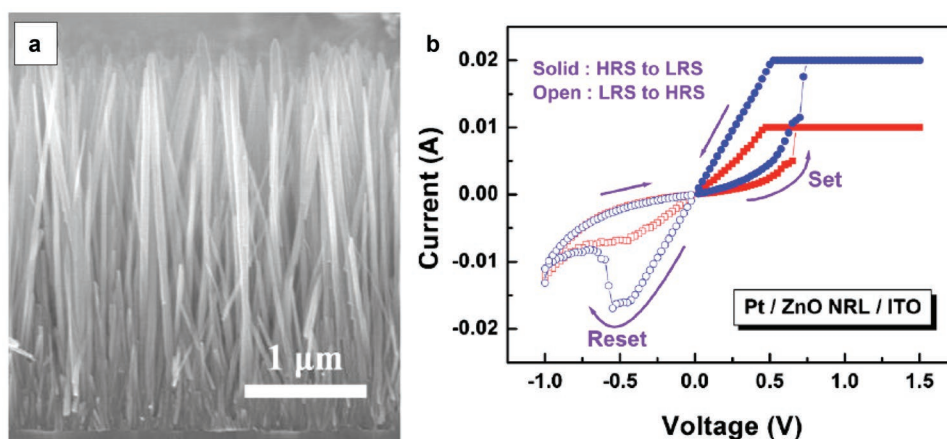

Figure 17. a) Cross-sectional SEM image of an array of vertically aligned ZnO NRs grown on an ITO substrate; b) bipolar resistive switching behavior in a Pt/ZnO NR array/ITO capacitor-like device exhibiting multilevel capability. All panels adapted with permission.[243] Copyright 2010, American Institute of Physics.

NW based device on a flexible substrate exhibited the same *I–V* characteristics even after a bending test performed for 100 times. In addition, it has been demonstrated that the conductivity in ZnO NR array devices can be exploited for the emulation of synaptic functions, since the device conductivity can be progressively modulated by means of voltage spike trains.[263]

Also in case of ZnO NW arrays, each NW can be considered as a switching device as reported by Dugaiczyk et al.[264] In this work, vertically aligned ZnO NWs were grown by CVD on a Cu substrate that acted also as the bottom electrode, while an Au coated AFM tip was used as the top electrode allowing to make a contact to the top of a single NW. In this case, unipolar resistive switching was observed and attributed to a thermochemical mechanism (that is not polar dependent) of formation/rupture of a conductive filament of oxygen vacancies on the NW surface. When a strong electric field is applied, oxygen vacancies are proposed to align together and form a conductive filament between the two electrodes, while the RESET occurs when the conductive path is destroyed by Joule heating. Authors pointed out that the lower electric field to form a conductive path in ZnO NWs ($\approx$30 kV cm^{-1}) compared to previously reported values for bulk ZnO (330 kV cm^{-1} were reported by Chang et al.[265] in case of sputtered ZnO thin films) suggested that the filament forms on the surface rather than in bulk, when higher mobility of defects is expected. Since authors proposed that the filament formation occur on the NW surface, the slight variability in the measured current and voltage considering different NWs (about ±20%) was ascribed to the difference of surface area as a consequence of different NW diameters. Similarly, resistive switching characteristics were observed in

single vertical aligned ZnO NRs grown on a conductive substrate and contacted by means of Pt-coated AFM tips.[266,267]

For practical resistive random access memory (RRAM or ReRAM) applications, Tseng et al.[244] proposed the realization of resistive switching devices based on ZnO NR array/polymethylmethacrylate (PMMA) heterostructures. ZnO NRs were synthetized by means of hydrothermal method and subsequently a PMMA solution was dropped, spin-coated, and dried on the ZnO nanorod, thus embedding NRs in the polymer. In the present case, the ITO substrate acted as the bottom electrode, while the top electrode was realized by Al evaporation. Bipolar resistive switching was observed, with an endurance of 200 cycles. Similarly, ZnO NW arrays embedded in insulating photoresist[248] and in poly 4-vinyl phenol[260] were reported to exhibit resistive switching behavior. In all these works, the polymer embedding was proposed to avoid short circuits between top and bottom electrodes and was supposed not to be actively involved in the resistive switching mechanism that was mainly attributed to the NWs. However, it was shown that the presence of a polymer coating can strongly influence the resistive switching properties and the conduction mechanism of ZnO nanostructures by modifying the surface states[207,250] (see Section 7), and thus these devices cannot be considered good platforms for understanding the physical mechanism of switching in ZnO NW arrays.

A more detailed analysis of the switching mechanism in ZnO NW arrays was proposed by Milano et al.[186] In this work, authors pointed out that a polycrystalline ZnO layer (called in this work base) is present in between the catalyst substrate and the NW after the CVD growth, as can be seen in **Figure 18**a. This layer can have an active role during
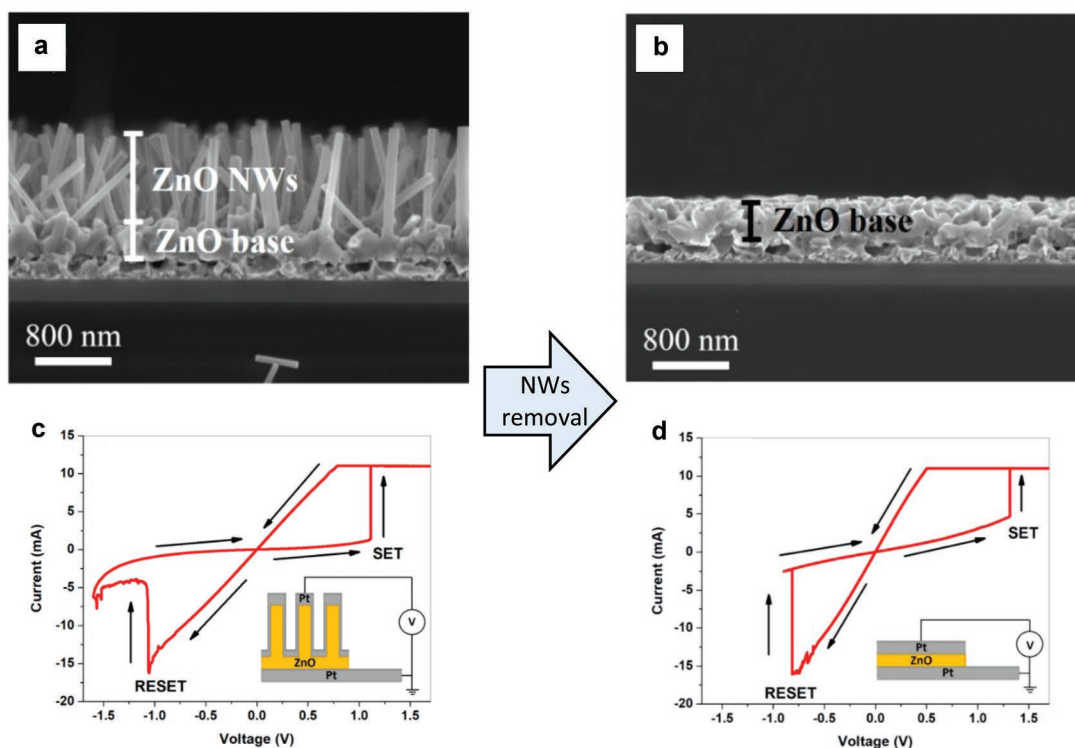

Figure 18. SEM image of a) the ZnO NW array and b) the base layer alone after the mechanical removal of NWs. Bipolar resistive switching of c) Pt/ZnO NW array/Pt and d) Pt/ZnO base/Pt resistive switching devices. All panels adapted with permission.[186] Copyright 2018, American Chemical Society.
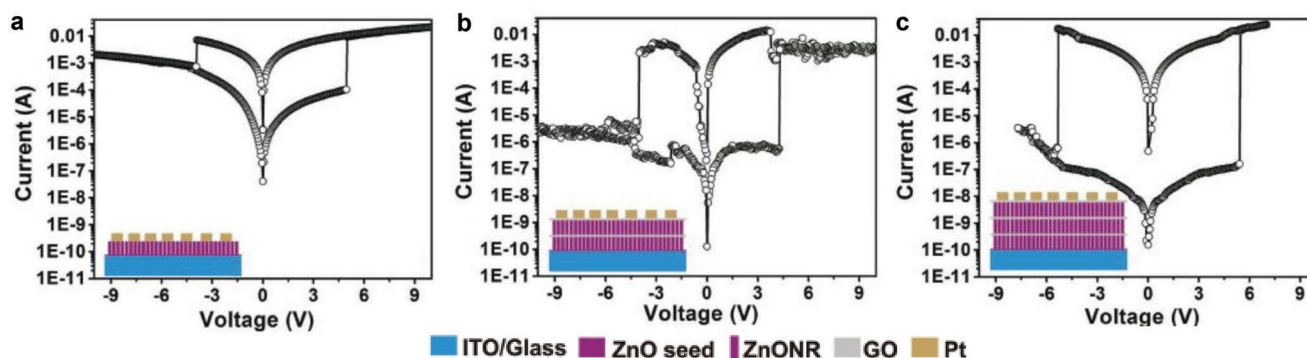
Figure 19. Bipolar resistive switching in a) primary, b) secondary, and c) ternary ZnO NR array/GO multilayer structured devices realized with an ITO bottom electrode and a Pt top electrode. All panels adapted with permission.[251] Copyright 2017, Wiley-VCH.

resistive switching, since the top electrode can penetrate the ZnO NW array down to the base layer, as investigated by cross-sectional EDS measurements. Analyses performed on the base layer after the mechanical removal of NWs (an SEM image of the base layer alone can be seen in Figure 18b) revealed similar structural and chemical properties with respect to NWs. Electrical measurements were performed on the ZnO base layer alone and in presence of NWs, by using symmetric Pt electrodes. $I-V$ characteristics of the NW array and the base alone are shown in Figure 18c,d, respectively. In both cases bipolar resistive switching was observed with similar conduction mechanism in both LRS and HRS and comparable switching parameters (V_{SET}, V_{RESET}, and I_{RESET}). These observations suggested that, even in presence of NWs, the switching mechanism can be located in the ZnO base layer, where the switching mechanism can be ascribed to the formation of oxygen vacancies assisted filaments located at the highly oriented grain boundaries. Since the conduction mechanism is highly localized in filaments in the base layer during the ON state, no significant differences in the LRS were observed with and without NWs, while the removal of NWs resulted in a lower HRS, since the conduction mechanism in the OFF state is more delocalized. It has to be noticed that a switching mechanism located in the base layer cannot be excluded also for hydrothermally grown NWs, where a ZnO thin film is usually used as seed layer for the NW growth and can act as a base layer (e.g., ZnO films of 5–10 nm of thickness were realized by Chang et al.[243] as seed layers for the ZnO NW hydrothermal growth). It is important to notice that this work did not exclude resistive switching in single ZnO NWs but evidenced that the switching mechanism in NW arrays can strongly differ from the case of single isolated NWs. The memristive behavior of ZnO NW and NR arrays can be further enhanced and modified by surface treatments, surface functionalization, or by using nanocomposites,[247,249,250,252] as discussed in Section 7.

An interesting approach to increase the ON/OFF ratio in ZnO NR arrays was proposed by Anoop et al.[251] that realized hybrid ZnO NRs/graphene oxide (GO) structures. GO oxide was deposited on ZnO NRs arrays acting as a seed layer for a subsequent growth of a second layer of ZnO NRs, thus realizing secondary and tertiary multilayer stacking structures. By using an ITO bottom electrode and a Pt top electrode, the resistive switching properties were analyzed as a function of the number of layers. As can be seen from **Figure 19**a–c, it was observed that increasing the number of layers resulted in an increment of the HRS/LRS ratio that was measured to be 3.3×10^5 in case of tertiary multilayer structure, without strongly affecting the SET and RESET voltages. The switching mechanism was ascribed to the formation/rupture of oxygen assisted filaments on the NW sidewalls, observing an Ohmic behavior in the LRS and SCLC behavior in the HRS. The increment of the HRS/LRS ratio was mainly imputed to the increase of the HRS, since no strong variation of the LRS as a function of the number of layers was observed. Indeed, when no localized conduction paths are formed (HRS), the dominating bulk resistance of the ZnO NRs/GO structure increases with the number of layers, thus increasing the ON–OFF window. It is important to notice that these devices exhibited stable resistive switching with an endurance of 1000 cycles and a retention of 5×10^4 s.

Moreover, Huang et al.[245] showed that the growth of ZnO NR arrays on sputtered ZnO thin films can improve and stabilize the resistive switching performances in thin film devices realized with Pt symmetric electrodes. The thin ZnO NR layer (NR length of about 150 nm) was characterized by a higher concentration of oxygen vacancies with respect to the ZnO thin film, as revealed by X-ray photoelectron spectroscopy (XPS) measurements. The asymmetry in the oxygen vacancies concentration gives rise to an asymmetric Schottky barrier that resulted in a rectifying $I–V$ characteristic. The presence of these nanostructures improved resistive switching properties of devices acting as supplementary reservoir of oxygen vacancies, reducing the operation voltage and stabilizing device performances. It was shown that these devices can be potentially used in crossbar arrays, demonstrating the feasibility of a 1D1R configuration connecting two devices back to back in series. Also in case of ZnO-based electrochemical metallization memory cells, resistive switching performances can be improved by the insertion of a nanorod layer on a sputtered ZnO thin film, as reported by Simanjuntak et al.[257] Authors proposed that, by properly adjusting the defect concentration and morphology or NRs, it is possible to increase the switching characteristics of Cu/ZnO NR-ZnO TF/ITO devices in terms of device stability.

In addition, Huang et al.[245] showed that the presence of NRs leads to a hydrophobic surface with self-cleaning properties that can prevent the damage of these devices in real environment. Superhydrophobic properties were observed also
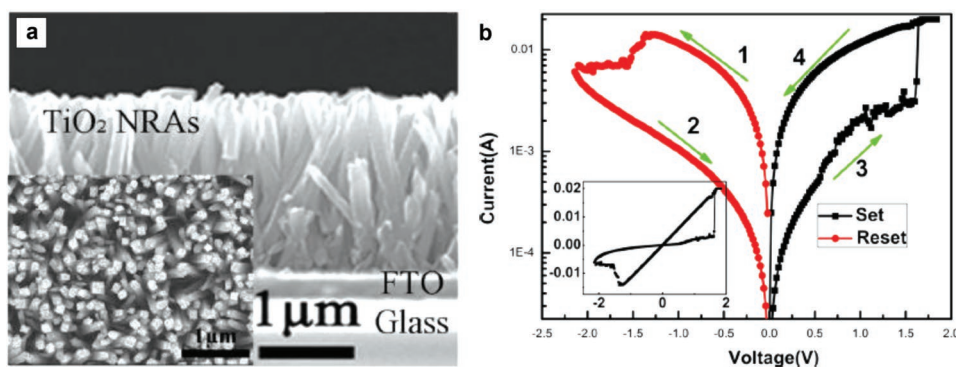
ADVANCED
SCIENCE NEWS
www.advancedsciencenews.com

ADVANCED
ELECTRONIC
MATERIALS
www.advelectronicmat.de

Figure 20. a) Cross-section SEM image of TiO_2 NR arrays; the inset shows a top view SEM image; b) I–V characteristics (in semilogarithm scale) of Pt/TiO_2 NR array/FTO devices that exhibited bipolar behavior; the inset shows I–V characteristics in linear scale. All panels reproduced with permission.[269] Copyright 2011, Electrochemical Society.

in case of tungsten oxide NWs, allowing the realization of waterproof resistive switching devices as demonstrated by Lee et al.[268] After the deposition of an Au top electrode, the observed bipolar resistive switching mechanism was attributed to the valence change mechanism at the interface between the W_{18}/O_{49} NWs and the W bottom electrode. It was shown that after a chemical modification of the NW surface by octadecyltrichlorosilane, the array surface became superhydrophobic and the I–V characteristics were not affected after being submerged in water. In this fashion, it was possible to avoid failures of the device due to water contact. More interestingly, Park et al.[253] showed that it was possible to measure light-induced resistive switching properties of ZnO NWs even directly when they are submerged in water (see Section 7). The superhydrophobicity of ZnO NWs, that was attributed to the combined effects of the rough surface and a chemical treatment with a low-surface-tension perfluorinated liquid, allowed the formation of an air pocket layer on the NR array surface that did not allow water to penetrate the device causing failures of the device.

Resistive switching was observed also in case of hydrothermally grown arrays of TiO_2 NRs in both rutile[269–271] and anatase[272] phases. Considering anatase TiO_2 NR arrays, bipolar resistive switching was observed by Senthilkumar et al.[272] considering Ti/TiO_2 NR/FTO devices that exhibited an endurance of 10^5 cycles and a retention of 5×10^3 s. The proposed switching mechanism in this case can be explained by taking into account the Ti/TiO_2 interface. Here, an interfacial TiO_x layer can be formed during the top electrode deposition because of the Ti oxidable characteristics. During the forming process, oxygen ions are moved toward the FTO positive biased electrode, thus reducing the TiO_x interfacial layer to TiO_{x-y} and increasing the overall current. It was proposed that the formation/rupture of conductive filaments at the interface through the oxidation and reduction of the TiO_x layer is responsible for the observed bipolar resistive switching. However, electrical measurements as a function of electrode area would be suitable to understand if the mechanism is filamentary or interfacial, as proposed by Sassine et al.[163] in case of TiO_2 and HfO_2 thin films.

Before the observation of resistive switching in anatase TiO_2 NR arrays, resistive switching was investigated in TiO_2 NRs

with tetragonal rutile phase by Zhang et al.[269] In this work, capacitor-like devices were realized growing vertically aligned TiO_2 NRs on a fluorinated tin oxide substrate (FTO) (see **Figure 20**a) and depositing a Pt top electrode. As presented in Figure 20b, these devices exhibited bipolar resistive switching behavior, characterized by an endurance of 100 cycles and a retention of 3×10^5 s. In these devices, during the HRS the Schottky barrier between the Pt/TiO_2 NRs dominated the conduction mechanism. When a positive voltage is applied at the Pt top electrode, it was proposed that oxygen vacancies can drift and accumulate at the cathode and, when the electroforming voltage is reached, conductive filaments of oxygen vacancies can penetrate the Schottky barrier turning the device to the LRS. The formation/rupture of these filaments gives rise to bipolar resistive switching. Authors noticed that, despite lower electric fields are involved in NRs with respect to TiO_2 thin films (TiO_2 NR average length was about 2.5 µm with respect to few tens of nanometers in thin film devices), the forming voltage as well as V_{SET} and V_{RESET} are comparable. In analogy of what previously discussed for ZnO NW arrays, this observation suggests a much higher mobility of defects on the surface of NRs.

Afterward, a more detailed switching mechanism in Pt/TiO_2 NRs/FTO devices was proposed by Huang et al.[270] and is schematized in **Figure 21**a–d. In this case it was observed that the devices turned to a higher resistance state after the forming process, differently from what expected. Authors proposed that during forming the adsorption of O_2 molecules on the oxygen-deficient TiO_2 surface can be triggered by Joule heating. This process, which can be also facilitated by the high area provided by the nanorod geometry, increases the overall device resistance. As a consequence of the different porosity in the nanorod array that is higher on the surface and lower near the FTO electrode, a suboxide region is created near the bottom electrode when a positive bias at the Pt top electrode is applied during the forming process. This oxygen-deficient region acts as an oxygen vacancy reservoir that facilitates the creation of an oxygen vacancies conductive path during the SET process, while RESET occurs when the filament is interrupted due to Joule heating. It was proposed that not only the asymmetric oxidation of these nanostructures but also the metal patch distribution (that is different from the top and the bottom of the
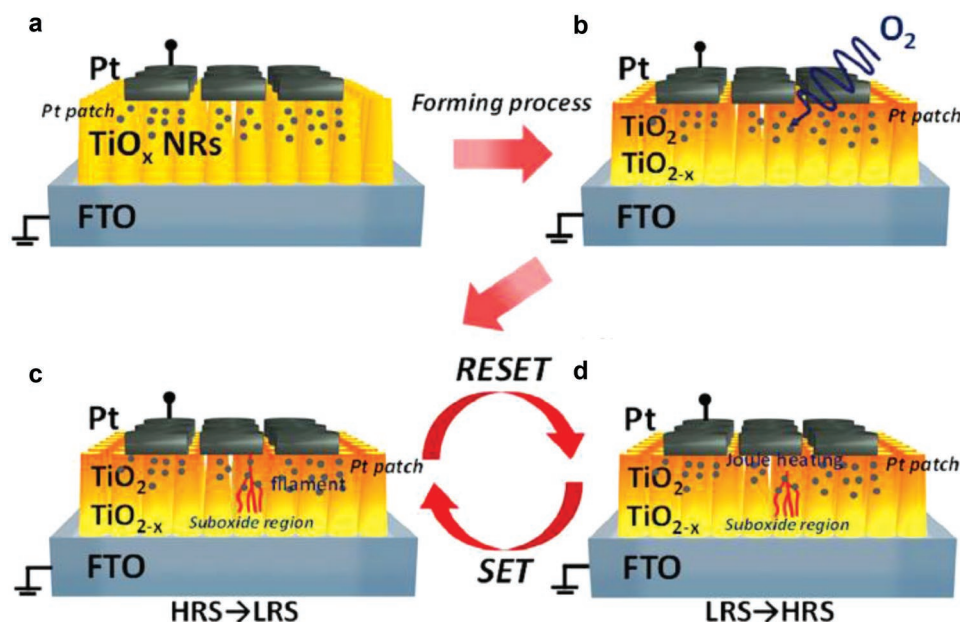
Figure 21. a) Schematic representation of resistive switching in TiO_2 NR arrays; a) pristine state, b) after forming, c) after the SET process, and d) after the RESET process. Grey dots in the TiO_2 region represent the penetration of the Pt top electrode in the NRs array due to the layer porosity. The Pt patch near the top electrode can assist the connection of filaments in the LRS. Reproduced under the terms of Creative Commons Attribution 4.0 International License.[270] Copyright 2017, the authors, published by Springer Nature.

NR array) can participate in the creation of the Schottky barrier that is responsible for the rectifying behavior. It is important to notice that devices realized by Zhang et al.[269] and Huang et al.[270] exhibited a self-rectifying behavior and thus are promising for the realization of crossbar arrays avoiding leakage currents.

The performances of TiO_2 NR array-based devices can be further improved by introducing a TiO_x seed layer on the FTO substrate before the hydrothermal growth of NRs, as reported by Xiao et al.[271] that realized $Al/TiO_2/TiO_x/FTO$ forming-free devices that exhibited high stability with an endurance of over 500 cycles and a retention of 3×10^4 s. Authors claimed that the insertion of this layer allows the growth of vertically aligned and uniform TiO_2 NRs that improved the stability of devices. In addition, NRs grow with a lower concentration of oxygen vacancies with a consequent reduction of programming currents, power consumption, and enabling multilevel memory performances. Authors proposed that the switching mechanism in such devices is linked to the presence of oxygen vacancies in nanorods that act as charge traps for the formation and rupture of electron transport channels. According to this model, when a positive bias voltage is applied to the Al top electrode, electrons start to fill oxygen vacancies charge traps and when all traps are filled the device switches to the LRS while, when an opposite polarity is applied, detrapping of oxygen vacancies turns the device back to the HRS. It is important to notice that the use of an Al top electrode can influence the resistive switching behavior because of the creation of an Al–Ti–O interfacial layer,[273,274] despite authors pointed out that resistive switching is dominated by TiO_2 NRs because the interface thickness ($\approx$3–5 nm) is negligible compared to the NR length ($\approx$3 μm).

6. Resistive Switching in Nanowire Random Networks

Differently from NW arrays, in which NWs are characterized by a high degree of order and are vertically aligned, NW networks exhibit a highly disordered structure. Resistive switching networks based on random ordered nanowires, dendritic, and fractal structures have attracted great attention because of the peculiar conduction properties that make these structures promising for resistive switching and neuromorphic applications.[275–283] In the following, resistive switching in stacked and planar devices based on NW networks is described.

6.1. Stacked Devices

Considering capacitor-like devices, resistive switching was observed in TiO_2 networks that were grown by hydrothermal technique on a Ti substrate, as reported by Shao et al.[274] After the growth process, a network of nanowires with anatase phase and a length of several micrometers was observed and Al/TiO_2 NW network/Ti devices were realized by depositing an Al top electrode. These devices, that also exhibited self-rectifying properties, exhibited bipolar resistive switching with an endurance of beyond 60 cycles, an HRS/LRS ratio of about 70 and a retention up to 10^4 s. The switching mechanism is in this case comparable to the previously discussed mechanism in single TiO_2 NWs[161] and NW arrays.[269–272] Similarly, resistive switching behavior was observed by Prakash et al.[284] in core–shell Ge/GeO_x nanowires and by Li et al.[285] in ITO nanowire networks. A SEM picture of an ITO NW interwoven network grown by using a self-assembled template of polystyrene spheres is
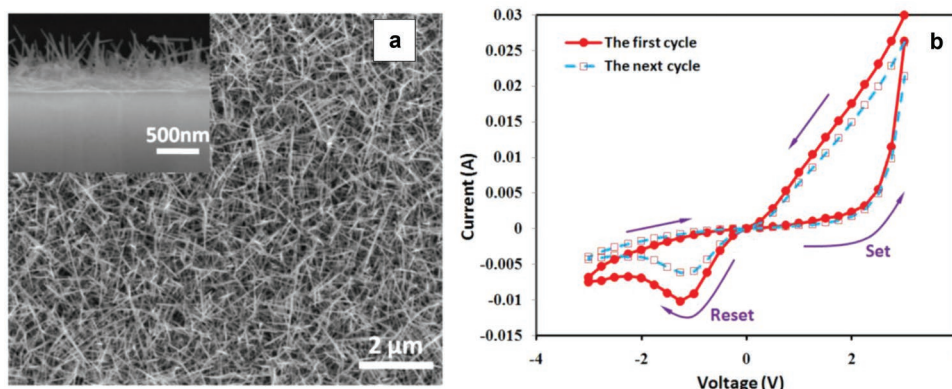
ADVANCED
SCIENCE NEWS
www.advancedsciencenews.com

ADVANCED
ELECTRONIC
MATERIALS
www.advelectronicmat.de

Figure 22. a) Top view SEM image of the ITO NW network after the growth process; inset shows a cross-sectional image; b) *I–V* characteristic of Ag/ITO NWs network/Al stacked device that exhibits bipolar resistive switching behavior. All panels reproduced under the terms of Creative Commons Attribution 4.0 International License.[285] Copyright 2016, the authors. published by American Institute of Physics.

shown in **Figure 22**a. These networks exhibited bipolar resistive switching (Figure 22b) with HRS and LRS values that tend to increase and to reduce the HRS/LRS window by increasing the number of cycles. The distinction of HRS and LRS becomes negligible after about 60 cycles. Interestingly, authors ascribed this behavior to the intrinsic nature of the network made of interwoven NWs. Indeed, every cycle resulted in some interwoven disconnection and thus an increased value of both LRS and HRS. After a certain amount of cycles only the reliable connections survived, and the NW network resistance tends to a constant value.

6.2. Planar Devices

Planar devices based on dispersed NWs represent a fascinating alternative for the realization of NW-based resistive switching devices. In 2011 Cagli et al.[148] observed for the first time resistive switching properties in a cross-point junction between two Ni–NiO core–shell NWs. In this case, the NiO shell layer has the role of the active switching layer while the inner Ni core is used as an electrode. These devices exhibited unipolar resistive switching that was ascribed to a thermochemical reduction/oxidation that gives rise to the formation/rupture of a conductive filament at the cross-point junction. A more detailed

analysis of Ni/NiO cross-point junctions was later reported by Oliver et al.[286] that pointed out that the filament geometry in the cross-point can be tuned by varying the electroforming process, allowing the creation of wide metallic or narrow semiconducting filaments as revealed by *I–V–T* measurements. The switching mechanism in Ni/NiO cross-point junctions was further elucidated by real time TEM investigation of filament creation/rupture by Ting et al.[287] that directly observed morphological changes at the cross-junction point as a consequence of the oxygen ions migration that is responsible for the evolution of the conductive filament. A schematization of the resistive switching mechanism in a cross-point junction is presented in **Figure 23**.

Exploiting the resistive switching properties of cross-point junctions, it is possible to explore resistive switching behavior in NW networks. Indeed, the NW network global properties arise from junctions between individual wires that determine the network connectivity.[275,277,280–283] Thus, the global resistive switching behavior of the network arises from resistive switching events located at the numerous wire interconnections. On those grounds, Bellew et al.[277] reported resistive switching in NW networks composed of Ni–NiO core shell NWs. Resistive switching devices were realized by simply drop casting NWs on a SiO$_2$ insulating substrate with subsequent realization of Ni electrodes (see **Figure 24**a). After a
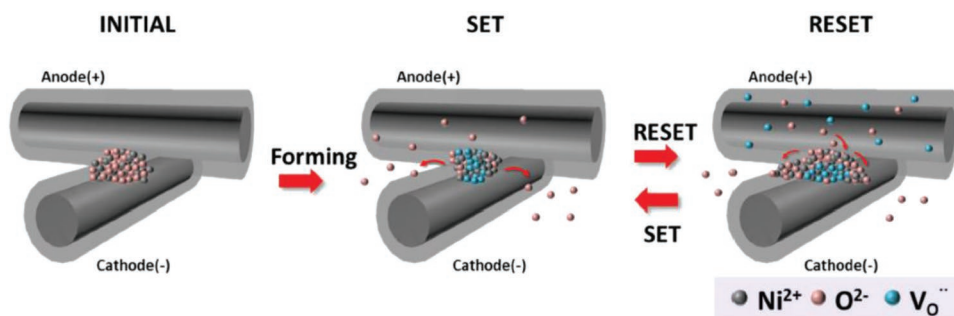

Figure 23. Resistive switching mechanism in a Ni/NiO cross-point junction. During electroforming, oxygen ions migrate outside the cross-junction and/or to the environment thus realizing a conductive filament of oxygen vacancies. During the subsequent RESET process, oxygen ions refill the crossbar center increasing the resistance. The formation/rupture of an oxygen vacancies filament at the cross-junction point is responsible for the unipolar resistive switching behavior. Adapted with permission.[287] Copyright 2017, Wiley-VCH.
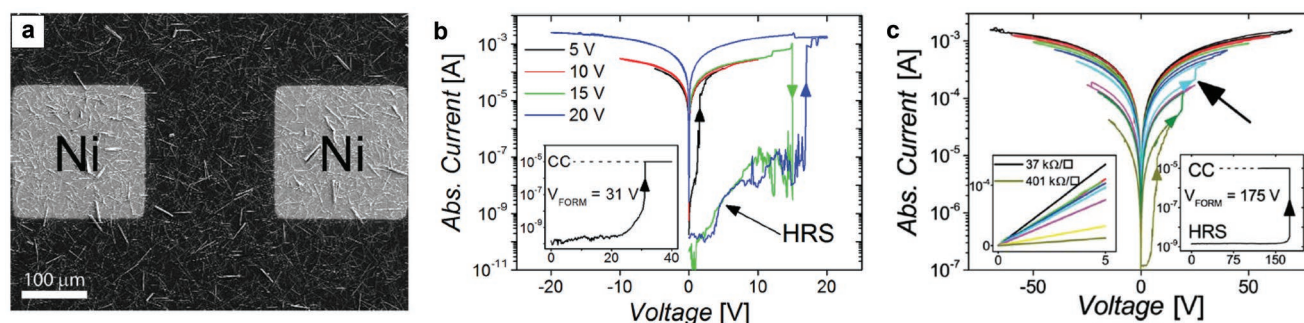
**ADVANCED
SCIENCE NEWS**
www.advancedsciencenews.com

**ADVANCED
ELECTRONIC
MATERIALS**
www.advelectronicmat.de

Figure 24. a) SEM image and b) I–V characteristics of a NW network with intermediate size (D/L_{NW} = 9.43) showing the coexistence of resistive switching and adaptive behavior; c) I–V characteristic of a very large network (D/L_{NW} = 47.17) exhibiting adaptive behaviour. Different network sizes were obtained by changing the electrode spacing, with NWs characterized by an average length of 10.6 µm. All panels reproduced with permission.[277] Copyright 2014, Royal Society of Chemistry.

forming process, a conductive path composed of some NWs and connecting junctions is formed between the two electrodes, reducing the overall resistance of the device. It is important to notice that each cross-point junction acts as a resistive switching element. The network dimensions, such as the electrode spacing (D) and the NW average length (L_{NW}), play a crucial role in the switching mechanism. Authors showed that considering small networks (D/L_{NW} < 2), although several wires contribute to the conduction mechanism after the forming process, a single junction dominates the resistive switching. This hypothesis was corroborated by the observation of roughly similar unipolar resistive switching characteristics in a single junction and in a small network, both characterized by comparable I_{RESET} current. More interestingly, it was observed that intermediate networks are able to evolve. In this case, when high voltages are applied, new junctions can be turned into the LRS thus increasing the overall conductivity, and a coexistence of resistive switching and adaptive behavior was observed. Indeed, as shown in Figure 24b, increasing voltage resulted in turning the device into the LRS by switching ON new junctions in the network. By considering these networks, the device can be turned again to the HRS when the voltage is sufficient to turn off the weakest junction in the prevailing conductive path. After turning ON the device again, the device exhibited adaptive characteristics with a further evolution of the LRS. Instead, increasing the network dimension (D/L_{NW} > 10) resulted in a dramatic decrease of the resistive switching probability. Indeed, as a consequence of the high level of connectivity, it was impossible to switch the devices to the HRS. Authors pointed out that, even if localized resistive switching phenomena can occur, these events have a small effect on the network conductivity because of redundancy within the network does not allow a reset of the device. Thus, large networks exhibited adaptive behavior with a progressive diminishing of resistance during voltage sweeps, until a stable configuration of the conductive path is reached. Thus, these NW networks exhibited a scale dependent behavior. However, it is necessary to take into account that an increase of the network dimension results in higher programmability voltages (up to 175 V are necessary to form very large networks as shown in the inset of Figure 24c).

In 2017, Du et al.[282] observed resistive switching in Ag–AgO$_x$ core–shell NW networks. In this case, Ag nanowires were spread out on a substrate and then a portion of them was UV irradiated for inducing the creation of an AgO$_x$ shell layer. Thus, a planar Ag/Ag–AgO$_x$ core–shell NW/Ag device was realized. These devices exhibited a resistive switching behavior due to the formation/rupture of a metallic filament in the shell layer at cross points. These metallic filaments are unstable, the device does not retain the state when the voltage returned to 0 V and is voltage polarity independent. Thus, the device is characterized by a volatile threshold switching behavior. In addition, it was observed that a device failure occurs after about 70 cycles, as a consequence of Ag accumulation at the cross-point junctions that makes the RESET process difficult. The observed fluctuations in threshold voltages were attributed to the different localized degree of oxidation and the numerous junctions with different localized Joule heating.

The memristive behavior of the networks can depend also on the different NW assembling, as shown by Puzyrev et al.[288] that evidenced different resistive switching properties in ZnO nanowire bundles and meshes contacted by Ag electrodes. In case of bundles, resistive switching was attributed to the modification of the Ag/ZnO Schottky barrier height as a consequence of a redistribution of Ag ions at the metal/semiconductor interface, while in case of meshes the switching mechanism was attributed to the formation of conductive bridges at the intersection of nanowires.

It has to be noticed that, differently from stacked devices based on NW networks that differ from NW arrays only for the NW degree of order and orientation, planar devices represent a totally different approach for the realization of resistive switching devices where the collective behavior gives rise to new features in the electrical properties.

7. Modulation of Resistive Switching Properties

In nanostructures with high surface-to-volume ratio, the surface states can play an important role in determining the electronic conduction mechanisms such as carrier mobility, carrier concentration, and the energy barrier height at interfaces. For these reasons, the memristive behavior of NW- and NR-based devices can be strongly modified and enhanced by using specific surface treatments to modify the surface structure and defectiveness

**ADVANCED
SCIENCE NEWS**
www.advancedsciencenews.com

**ADVANCED
ELECTRONIC
MATERIALS**
www.advelectronicmat.de

or by exploiting surface functionalizations, in order to modify surface states and achieve new features in the I–V hysteresis loop. Moreover, in metal–oxide nanostructures, resistive switching can be modulated or induced by illumination, since the large surface area enhances the light harvesting activity and the photoresponsive properties. By exploiting these characteristics, a new class of sensors based on NWs can be realized.

7.1. Surface Treatments

In 2011 Wu and Wang[173] examined the effect of different plasma pretreatments on resistive switching properties of single ZnO NWs, evidencing changes in the threshold voltages and resistivity in I–V characteristics. The authors showed that Ar plasma treatments resulted in lower threshold voltages and increased conductance, while higher threshold voltages were observed after oxygen plasma treatments. Indeed, by using these treatments, it is possible to modulate the oxygen vacancies concentration, thus influencing the NW resistivity, the Schottky barrier heights, and the switching parameters. The effects of plasma were further discussed by Lai et al. in their works[175,176] where authors suggested that a low cost Ar plasma treatment (100 W at 100 Pa, for 60/240 s) can enhance repeatability and decrease SET and RESET voltages in single isolated ZnO NWs grown by VLS method. It was shown that the effect of plasma on ZnO nanowires is both physical and chemical. From the physical point of view, the NW surface resulted to be damaged with increased roughness, as revealed by TEM analysis. Instead, from the chemical point of view, this treatment increases the quantity of oxygen vacancies on the surface, as reported by XPS and photoluminescence (PL) measurements. Even if a high quantity of vacancies decreases the HRS state and consequently the HRS/LRS ratio, the stochasticity of the switching events is reduced if more vacancies are involved in the filament formation, thus enhancing the reproducibility of plasma-treated devices. Moreover, it was shown that also data retention benefits from this treatment (data retention projection was reported to be over 10 years in case of plasma treated NWs with respect to less than one year in the untreated case).[176]

Another approach based on hydrogen annealing treatment of ZnO nanowires was proposed by Lee et al.[177] After the growth process, ZnO NWs were annealed at 350 °C for 30 min in a H_2/Ar mixture ambient. As a consequence of this treatment, an amorphous ZnO (a-ZnO) interfacial layer was formed in between a single crystalline nanowire and the Au electrode. This amorphous layer was proposed to have a key role during switching. Authors showed that, by controlling trapping and detrapping of electrons at this interface by applying voltage pulses, a multilevel memory based on single ZnO NW can be achieved. A similar approach based on hydrogen annealing was previously reported also by Sun et al.[249] in order to improve the resistive switching properties of ZnO NR arrays. Also in this case, the annealing was performed at 350 °C in H_2/Ar mixture, but for 15 min. As revealed by PL and AES, this treatment increases the concentration of vacancies on the surface, while improves the crystallinity at the bottom of the NR array. This resulted in a lower LRS and a higher HRS, thus incrementing the HRS/LRS ratio from 10 in bare NWs to $\approx 10^4$ after treatment.

7.2. Nanocomposites and Surface Functionalization

As an alternative, surface states of nanowires can be modified/controlled by realizing nanocomposites and heterointerfaces. By using this approach, Younis et al.[247] reported enhanced performances in ZnO NR arrays by introducing CeO_2 quantum dots (QDs). In this work, ZnO NR arrays were grown on a conductive FTO glass substrate by electrochemical deposition and, subsequently, CeO_2 quantum dots were dispersed on the NW array by using a simple drop technique. An Au electrode was then deposited realizing a capacitor-like resistive switching device. A schematic diagram summarizing the fabrication steps of devices based on CeO_2–ZnO nanocomposites is presented in **Figure 25**a. Comparing the resistive switching behavior with bare NR arrays, the addition of QDs strongly enhanced the electrical performances that exhibited higher stability and reliability (an endurance up to 200 cycles and retention of more than 10^4 s), with an increased HRS/LRS ratio of more than 10^2 (see Figure 25b). The enhanced performances were attributed to the CeO_2 QDs that act as quantum
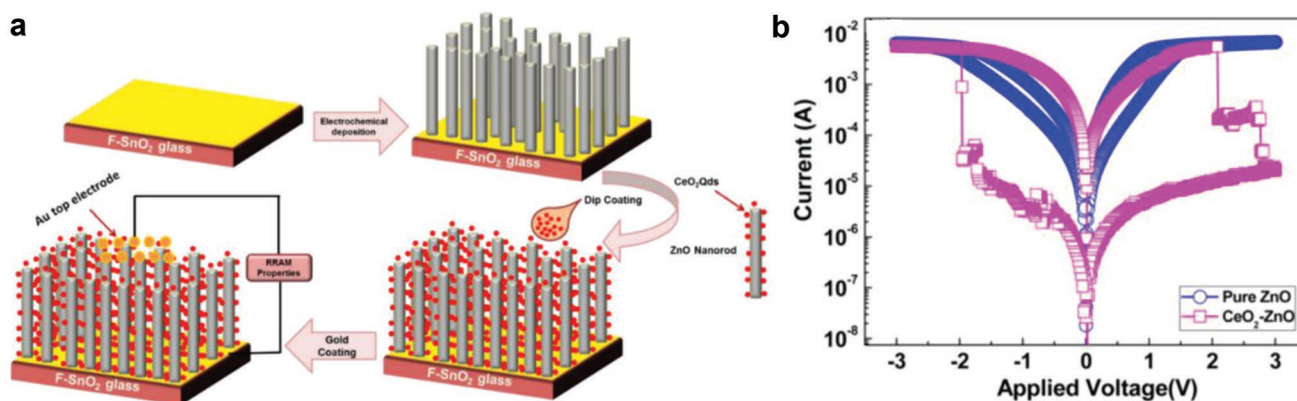

Figure 25. a) Schematic diagram for the realization of devices based on CeO_2–ZnO nanocomposites and b) comparison of the I–V characteristic in pure ZnO NR array and CeO_2-ZnO composites. All panels adapted with permission.[247] Copyright 2013, American Chemical Society.
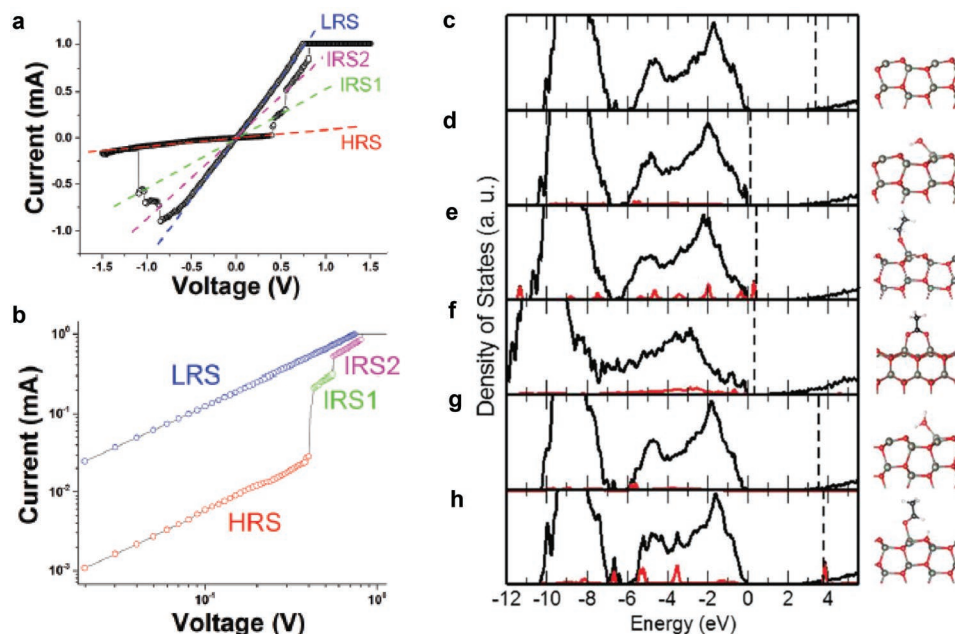
Figure 26. a) Electrical characterization of ZnO NW–PAA core–shell NW with a Cu top electrode and a Pt bottom electrode exhibiting multiple resistance states; b) logarithmic plot of the *I–V* characteristic; c–h) results of DFT theoretical calculation; DOS (black line), PDOS (red line), and ball and stick representation of c) clean n-doped ZnO(1100) surface, d) adsorption of OH⁻, e) ethanolate, f) acetate, g) H_2O, and (h) acetaldehyde. All panels reproduced with permission.[252] Copyright 2017, Royal Society of Chemistry.

well with discrete energy levels and form well-aligned shallow traps along the ZnO NR surface. During the HRS, electrons are trapped in QDs and the conductive path in between the electrodes is blocked. However, when electrons fill all the charge traps, a switch in resistance occurs and the device turns to the LRS, suggesting a purely electronic mechanism of switching. Modulation of the resistive switching characteristics were reported also in ZnO NW arrays by engineering interface states with α-Fe_2O_3 nanoparticles,[256] by interspersed $ZnOSnO_3$ nanocubes[289] or by adding a polymer coating.[250,252] Porro et al.[252] demonstrated that ZnO NWs conformally coated with polyacrylic acid layer (PAA) exhibit multiple resistive switching, introducing intermediate states (IRS1 and IRS2) in addition to HRS and LRS, as revealed by *I–V* characteristics in **Figure 26**a,b. The novel mechanism of switching was proposed to be based on redox reactions at the NW surface, as theoretically supported by DFT calculations. Different chemical species (such as hydroxyl, acetate, and alcoholate species) are present on the ZnO NW surface after the polymerization process. As a consequence of the presence of these species, the projected density of states (PDOS) of the system was modified and the Fermi level shifted from the conduction band close to the valence band (see Figure 26c–h). Thus, by applying a positive bias voltage to the Cu top electrode, electrons can be extracted from the deep surface states and redox reactions involving species at the surface can occur. Since each redox reaction occurs at a specific value of voltage applied to the device (as a consequence of specific redox potentials), intermediate states are introduced in the hysteresis loop that presents a step-wise characteristic. At the end, the device is turned to the LRS when the electromigration of Cu atoms is responsible for the formation of a conductive bridge in between the electrodes.

7.3. Light-Modulated Resistive Switching

In conventional resistive switching devices, the transition of the resistance state occurs when an electrical stimulus (such as voltage or current) is applied to the device. However, it was demonstrated that the transition between resistance states can be modulated or even induced by using different stimuli, such as illumination.[164,166,253,254,267,290–293] In semiconductor oxides, the electronic conductivity can be modified by photon irradiation. Enhanced photoconductivity properties compared to bulk materials or thin films can be observed in nanostructures, since a larger harvesting activity of photons and surface state densities are correlated with the high surface to volume ratio of these structures.[253,290]

In 2012, Park et al.[290] reported photostimulated resistive switching in ZnO NR arrays. In this case, authors pointed out that the illumination conditions (with a xenon light source, spectrum in the range 200–2500 nm) can strongly modify the *I–V* characteristic inducing resistive switching. Under dark conditions, resistive switching was not observed, since the formation of oxygen vacancies filaments is interfered by oxygen species that are adsorbed on the NR surface and cause a depletion region and band bending. Oxygen species act as oxygen sources inhibiting the oxygen vacancies filament formation. Under illumination, electron–hole pairs are generated, allowing holes to combine with oxygen ion species and causing their light-induced desorption from the NR surface. This results in a facilitated formation of oxygen vacancies assisted filaments when NWs are illuminated. A similar light-induced switching mechanism was proposed by Kathalingam et al.[291] in case of single isolated ZnO NR contacted by Au electrodes. Zhang et al.[179] pointed out that in single ZnO NWs the illumination with a UV light (λ = 254 nm) can enhance the carrier

**ADVANCED
SCIENCE NEWS**
www.advancedsciencenews.com

**ADVANCED
ELECTRONIC
MATERIALS**
www.advelectronicmat.de

concentration, leading to a temperature–current enhancement and a consequent decrease of the switching voltage due to the higher mobility of ionic species. An increase of resistive switching performances in terms of endurance has been reported also in ZnO NR arrays contacted by Ag and FTO electrodes by Russo et al.[294] Instead, an opposite trend was reported by Bera et al.[292] that observed a suppression of resistive switching characteristics as a consequence of UV illumination in ZnO NRs/Nb-doped SrTiO₃ heterojunctions. Moreover, Zhou et al.[263] showed that UV optical signals can be exploited for the realization of ZnO NRs-based optically modulated artificial synapses. Park et al.[253] proposed that light induced resistive switching properties can be exploited for the realization of position-controlled resistive switching devices, where the resistive switching behavior or simple resistive behavior depends on the device orientation with respect to the photon source. In this work, ZnO NR arrays with superhydrophobic properties were submerged in water. The superhydrophobic properties, due to the array roughness and a proper surface treatment, allowed the formation of an air layer on the ZnO NR arrays that prevented water to penetrate into the device. When the device was irradiated by a photon source, total internal reflection occurred when the light beam incidence exceeded the critical angle at the water/air interface ($\theta_c \approx 48°$), as depicted in **Figure 27**a. This can happen because light travels from water that has a higher refractive index ($n_{H2O} = 1.333$) to air that has a lower refractive index ($n_{air} = 1$). For this reason, the device simply acted as a resistor when the incident light beam exceeded the critical angle and light could not reach the ZnO NR array (Figure 27b), while resistive switching behavior was observed with incident light angle below the critical angle when light can reach the ZnO surface (Figure 27c). Despite numerous works reported the tuning of memristive behavior in ZnO NR and NW arrays by means of illumination, the physical mechanism responsible for the change of the switching behavior still needs to be clarified in order to elucidate the adsorption/desorption of chemical species from the NW surface when exposed to optical stimuli and to investigate the effect of illumination on the mobility of ionic species.

7.4. Memsensors

Since resistive switching properties of NW-based devices can be strongly modulated by external stimuli or by the surrounding

environment, as discussed in previous sections, these devices result to be particularly promising as sensors. Recently, it was shown that the memristive properties of suspended Si NWs realized by a top down approach can be strongly modulated by the presence of biomolecules, making possible the realization of highly sensitive biosensors.[295–299] By considering metal–oxide NWs, in 2017 Zhang et al.[178] exploited the resistive switching properties of ZnO NWs for the realization of gas sensors with high selectivity and improved recovery speed. Since the electronic transport mechanism differs in cases of the LRS and HRS, the two resistance states exhibited different sensing behavior. Indeed, different responses to oxidizing species (NO₂) and reducing species (NH₃) were observed depending on the device resistance state. High response to oxidizing gas was observed when the device was in the LRS, since NO₂ molecules adsorbed on the NW surface modulated the concentration of conduction electrons (**Figure 28**a,c). Oppositely, high response to reducing gas was detected in the HRS because NH₃ molecules on the surface can react with oxygen-rich regions at the anode, thus modulating the Schottky barrier height that dominated the conduction mechanism in the OFF state (Figure 28b,d). Thus, high selectivity of gas sensing was achieved depending on the internal resistance state of the device.

As suggested by Fan et al.,[159] single CuO NW devices can be used as electron irradiation sensors. Indeed, as previously discussed in Section 4.1.1, an e-beam forming method was applied to these devices in order to create an abundance of oxygen vacancies in part of the NW. An increament of the HRS/LRS ratio was reported by increasing the NW portion exposed to the e-beam during the forming process.

Memsensors can be realized also by coupling mechanical properties of single NWs with the resistive switching behavior. In 2013 Fan et al.[160] showed that CuO NW memristor properties can be modulated by mechanical deformation/force. In particular, it was shown that a displacement transducer can be realized by measuring the variation of the switching voltage as a function of the nanowire deformation. Even if the mechanism underlying such behavior is far from being understood, authors proposed that CuO NWs can have piezoelectric properties with the consequent generation of an extra voltage when the NW is under stress, thus reducing the switching voltage of the device. In a previous paper, Wu and Wang[173] reported that piezoelectric properties can be coupled to resistive
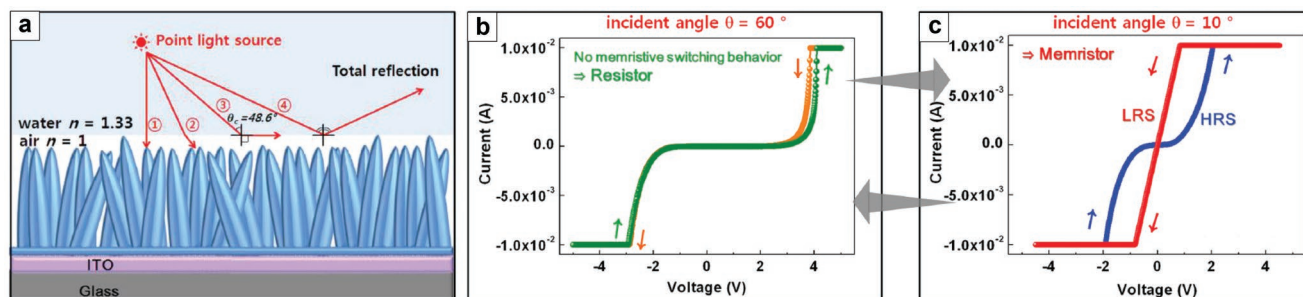

Figure 27. a) Schematic representation of the superhydrophobic ZnO NR array device when submerged in water and irradiated by a point light source; b) I–V characteristic of the device when light was totally reflected ($\theta = 60° > \theta_c$) showing no hysteresis (resistor); c) I–V characteristic of the device when light could reach the ZnO surface ($\theta = 10° < \theta_c$) showing a resistive switching behavior (memristor). All panels adapted with permission.[253] Copyright 2013, Wiley-VCH.
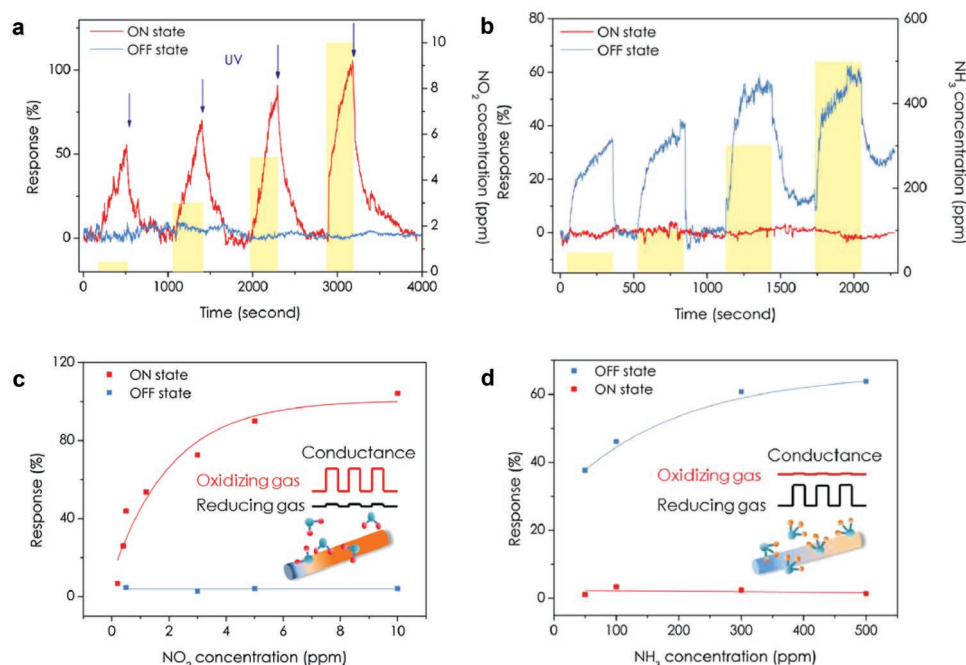
Figure 28. Response of the LRS and HRS of a ZnO NW based resistive switching device to different concentrations of a) NO$_2$ (oxidizing gas) and b) NH$_3$ (reducing gas); yellow bars refer to the gas concentration of each exposure; Response of the device as a function of c) NO$_2$ concentration and d) NH$_3$ concentration; insets reported the selective mechanism of gas sensing. The device response was defined as the absolute value of resistance change normalized by the initial resistance. All panels reproduced with permission.[178] Copyright 2017, Elsevier.

switching behavior, realizing a flexible device in which the voltage threshold can be modulated by an externally applied deformation. In this case, the piezoelectric potential induced by deformation modified the Schottky barrier height between ZnO NW and the Au electrode, resulting in a lower threshold voltage in case of tensile stress and a higher threshold voltage in case of compressive stress. These observations pave the way for the integration of resistive switching devices in nanoelectromechanical systems (NEMS).

8. Conclusions and Perspectives

Motivated by the ongoing miniaturization and scaling of electronic devices, memristive devices based on metal–oxide NWs synthetized with a bottom-up approach represent a promising alternative to conventional thin film memristors, as previously discussed also by Ielmini et al.[300] In this work, the state-of-the-art of memristive devices based on metal–oxide NWs was reviewed, evidencing a multitude of NW-based systems that exhibit different resistive switching mechanisms.

One of the most important aspects for controlling the resistive switching mechanisms in these devices is the synthesis process that determines the chemical/structural properties, defectivity, and doping of NWs. All these aspects have been shown to play a key role for determining not only the switching mechanism but also switching parameters such as programming voltages, resistance state values, device endurance, and retention.

At the single NW device level, understanding and dominating the resistive switching mechanism and neuromorphic functionalities still represents a challenge. In particular, these

memristive devices usually suffer from high operating voltages, and/or low endurance and retention compared to thin-film based memristive devices. An important aspect is that the device reliability is limited by NW melting due to the Joule overheating that was reported to be one of the main causes of device hard failure.[188,204,211,217,300] This means that proper solutions, such as current self-limitation,[226] are required for regulating electronic current densities in the nanosized NW cross-section in order to improve device performances.

From the material research point of view, the high localization of both electronic and ionic transport processes in NW systems facilitates direct investigation of the switching events, allowing correlation of device electrical responses with chemical/structural changes in the involved materials. Moreover, the peculiar planar structure allows to investigate resistive switching through multiprobe measurements and facilitates atmosphere-controlled measurements because of the high exposed surface. In these terms, NWs represent a fascinating platform for fundamental research in the field of memristors, where understanding ionic dynamics still represents a challenge for the development of neuromorphic functionalities.

However, one of the main challenges is the implementation of NW-based devices in high-density nanodevices, where manipulation and positioning of these nanostructures are required. In order to achieve high packing density integration, it is possible to consider array of NWs where each NW represents a memristive cell. However, the access to each single NW cell represents a challenge. Taking inspiration from thin-film based architectures, an alternative for integration of these nanostructures is to consider crossbar arrays realized by stacking ordered NWs, where each crossing junction between two NWs acts as

a memristive cell. The main drawback is that spatial manipulation of a large number of these nanostructures is required, strongly affecting the feasibility of this architecture.

In this scenario, memristive devices based on NW networks can drastically reduce the device fabrication complexity and represent a fascinating alternative to the conventional Von Neumann's computational architecture. Indeed, taking inspiration from biological neural networks, it has been shown that complex networks can be exploited for the realization of Touring's unorganized machines in which the global behavior arises from the randomly distributed interconnection of simple processing units.[276,301] The same concept can be applied to NW networks, where the collective behavior is determined by the switching dynamics of the randomly distributed NW cross-point junctions. NW networks can thus pave the way for the hardware implementation of reservoir computing, where the NW network system with random connectivity acts as a dynamic reservoir mapping the input signals to a higher dimensional space. It is important to underline that this computational paradigm allows to overcome the Von Neumann bottleneck, since biological inspired networks can store and process data simultaneously. In this framework, the realization of NW networks goes through a deep and challenging comprehension of resistive switching phenomena of single NW components and cross-point junctions.

Conflict of Interest

The authors declare no conflict of interest.

[1] L. Chua, *IEEE Trans. Circuit Theory* **1971**, *18*, 507.
[2] D. B. Strukov, G. S. Snider, D. R. Stewart, R. S. Williams, *Nature* **2008**, *453*, 80.
[3] L. Chua, *Appl. Phys. A* **2011**, *102*, 765.
[4] T. Calzecchi-Onesti, *Il Nuovo Cimento Series 3* **1884**, *16*, 58.
[5] R. Waser, M. Aono, *Nat. Mater.* **2007**, *6*, 833.
[6] Q. Xia, W. Robinett, M. W. Cumbie, N. Banerjee, T. J. Cardinali, J. J. Yang, W. Wu, X. Li, W. M. Tong, D. B. Strukov, G. S. Snider, G. Medeiros-Ribeiro, R. S. Williams, *Nano Lett.* **2009**, *9*, 3640.
[7] S. H. Jo, T. Chang, I. Ebong, B. B. Bhadviya, P. Mazumder, W. Lu, *Nano Lett.* **2010**, *10*, 1297.
[8] J. Borghetti, G. S. Snider, P. J. Kuekes, J. J. Yang, D. R. Stewart, R. S. Williams, *Nature* **2010**, *464*, 873.
[9] K.-H. Kim, S. Gaba, D. Wheeler, J. M. Cruz-Albrecht, T. Hussain, N. Srinivasa, W. Lu, *Nano Lett.* **2012**, *12*, 389.
[10] J. J. Yang, D. B. Strukov, D. R. Stewart, *Nat. Nanotechnol.* **2013**, *8*, 13.
[11] F. Alibart, E. Zamanidoost, D. B. Strukov, *Nat. Commun.* **2013**, *4*, 2072.
[12] C. Du, W. Ma, T. Chang, P. Sheridan, W. D. Lu, *Adv. Funct. Mater.* **2015**, *25*, 4290.
[13] M. Prezioso, F. Merrikh-Bayat, B. Hoskins, G. Adam, K. K. Likharev, D. B. Strukov, *Nature* **2015**, *521*, 61.
[14] S. Kim, C. Du, P. Sheridan, W. Ma, S. Choi, W. D. Lu, *Nano Lett.* **2015**, *15*, 2203.
[15] Z. Wang, S. Joshi, S. E. Savel'ev, H. Jiang, R. Midya, P. Lin, M. Hu, N. Ge, J. P. Strachan, Z. Li, Q. Wu, M. Barnell, G.-L. Li, H. L. Xin, R. S. Williams, Q. Xia, J. J. Yang, *Nat. Mater.* **2017**, *16*, 101.
[16] Z. Wang, S. Joshi, S. Savel'ev, W. Song, R. Midya, Y. Li, M. Rao, P. Yan, S. Asapu, Y. Zhuo, H. Jiang, P. Lin, C. Li, J. H. Yoon, N. K. Upadhyay, J. Zhang, M. Hu, J. P. Strachan, M. Barnell, Q. Wu, H. Wu, R. S. Williams, Q. Xia, J. J. Yang, *Nat. Electron.* **2018**, *1*, 137.
[17] X. Zhu, W. D. Lu, *ACS Nano* **2018**, *12*, 1242.
[18] M. A. Zidan, J. P. Strachan, W. D. Lu, *Nat. Electron.* **2018**, *1*, 22.
[19] D. Ielmini, H.-S. P. Wong, *Nat. Electron.* **2018**, *1*, 333.
[20] S. Ambrogio, P. Narayanan, H. Tsai, R. M. Shelby, I. Boybat, C. di Nolfo, S. Sidler, M. Giordano, M. Bodini, N. C. P. Farinha, B. Killeen, C. Cheng, Y. Jaoudi, G. W. Burr, *Nature* **2018**, *558*, 60.
[21] S. G. Kim, J. S. Han, H. Kim, S. Y. Kim, H. W. Jang, *Adv. Mater. Technol.* **2018**, *3*, 1800457.
[22] R. Waser, R. Dittmann, G. Staikov, K. Szot, *Adv. Mater.* **2009**, *21*, 2632.
[23] J. J. Yang, M. D. Pickett, X. Li, D. A. A. Ohlberg, D. R. Stewart, R. S. Williams, *Nat. Nanotechnol.* **2008**, *3*, 429.
[24] A. Sawa, *Mater. Today* **2008**, *11*, 28.
[25] H.-S. P. Wong, H.-Y. Lee, S. Yu, Y.-S. Chen, Y. Wu, P.-S. Chen, B. Lee, F. T. Chen, M.-J. Tsai, *Proc. IEEE* **2012**, *100*, 1951.
[26] D. Ielmini, *Semicond. Sci. Technol.* **2016**, *31*, 063002.
[27] I. Valov, W. D. Lu, *Nanoscale* **2016**, *8*, 13828.
[28] I. Valov, R. Waser, J. R. Jameson, M. N. Kozicki, *Nanotechnology* **2011**, *22*, 289502.
[29] M. Wuttig, N. Yamada, *Nat. Mater.* **2007**, *6*, 824.
[30] D. S. Jeong, R. Thomas, R. S. Katiyar, J. F. Scott, H. Kohlstedt, A. Petraru, C. S. Hwang, *Rep. Prog. Phys.* **2012**, *75*, 076502.
[31] V. K. Sangwan, D. Jariwala, I. S. Kim, K.-S. Chen, T. J. Marks, L. J. Lauhon, M. C. Hersam, *Nat. Nanotechnol.* **2015**, *10*, 403.
[32] S. Porro, E. Accornero, C. F. Pirri, C. Ricciardi, *Carbon* **2015**, *85*, 383.
[33] F. Hui, E. Grustan-Gutierrez, S. Long, Q. Liu, A. K. Ott, A. C. Ferrari, M. Lanza, *Adv. Electron. Mater.* **2017**, *3*, 1600195.
[34] V. K. Sangwan, H.-S. Lee, H. Bergeron, I. Balla, M. E. Beck, K.-S. Chen, M. C. Hersam, *Nature* **2018**, *554*, 500.
[35] Y. Shi, X. Liang, B. Yuan, V. Chen, H. Li, F. Hui, Z. Yu, F. Yuan, E. Pop, H.-S. P. Wong, M. Lanza, *Nat. Electron.* **2018**, *1*, 458.
[36] W. P. Lin, S. J. Liu, T. Gong, Q. Zhao, W. Huang, *Adv. Mater.* **2014**, *26*, 570.
[37] Y.-N. Zhong, T. Wang, X. Gao, J.-L. Xu, S.-D. Wang, *Adv. Funct. Mater.* **2018**, *28*, 1800854.
[38] S. I. Kim, J. H. Lee, Y. W. Chang, S. S. Hwang, K.-H. Yoo, *Appl. Phys. Lett.* **2008**, *93*, 033503.
[39] W. Lu, C. M. Lieber, *Nat. Mater.* **2007**, *6*, 841.
[40] H. J. Fan, P. Werner, M. Zacharias, *Small* **2006**, *2*, 700.
[41] A. L. Tiano, C. Koenigsmann, A. C. Santulli, S. S. Wong, *Chem. Commun.* **2010**, *46*, 8093.
[42] N. Wang, Y. Cai, R. Q. Zhang, *Mater. Sci. Eng., R* **2008**, *60*, 1.
[43] G. Cao, D. Liu, *Adv. Colloid Interface Sci.* **2008**, *136*, 45.

[44] N. Ramgir, N. Datta, M. Kaur, S. Kailasaganapathi, A. K. Debnath, D. K. Aswal, S. K. Gupta, *Colloids Surf. A* **2013**, *439*, 101.

[45] S. W. Schmitt, F. Schechtel, D. Amkreutz, M. Bashouti, S. K. Srivastava, B. Hoffmann, C. Dieker, E. Spiecker, B. Rech, S. H. Christiansen, *Nano Lett.* **2012**, *12*, 4050.

[46] K. Subannajui, F. Güder, M. Zacharias, *Nano Lett.* **2011**, *11*, 3513.

[47] C. R. K. Marrian, D. M. Tennant, *J. Vac. Sci. Technol., A* **2003**, *21*, S207.

[48] Z. R. Dai, Z. W. Pan, Z. L. Wang, *Adv. Funct. Mater.* **2003**, *13*, 9.

[49] D. Calestani, M. Zha, R. Mosca, A. Zappettini, M. C. Carotta, V. Di Natale, L. Zanotti, *Sens. Actuators, B* **2010**, *144*, 472.

[50] S. C. Lyu, Y. Zhang, C. J. Lee, H. Ruh, H. J. Lee, *Chem. Mater.* **2003**, *15*, 3294.

[51] H. Wan, H. E. Ruda, *J. Mater. Sci.: Mater. Electron.* **2010**, *21*, 1014.

[52] C. Wongchoosuk, K. Subannajui, A. Menzel, I. A. Burshtein, S. Tamir, Y. Lifshitz, M. Zacharias, *J. Phys. Chem. C* **2011**, *115*, 757.

[53] Z. Zhang, S. J. Wang, T. Yu, T. Wu, *J. Phys. Chem. C* **2007**, *111*, 17500.

[54] R. Yousefi, B. Kamaluddin, *J. Alloys Compd.* **2009**, *479*, L11.

[55] J. Li, Q. Zhang, H. Peng, H. O. Everitt, L. Qin, J. Liu, *J. Phys. Chem. C* **2009**, *113*, 3950.

[56] Y.-H. Kang, C.-G. Choi, Y.-S. Kim, J.-K. Kim, *Mater. Lett.* **2009**, *63*, 679.

[57] R. B. Saunders, S. Garry, D. Byrne, M. O. Henry, E. McGlynn, *Cryst. Growth Des.* **2012**, *12*, 5972.

[58] G. Meng, X. Fang, W. Dong, R. Tao, Y. Zhao, Z. Deng, S. Zhou, J. Shao, L. Li, *Appl. Surf. Sci.* **2010**, *256*, 6543.

[59] P. G. Li, W. H. Tang, X. Wang, *J. Alloys Compd.* **2009**, *479*, 634.

[60] K. Subannajui, C. Wongchoosuk, N. Ramgir, C. Wang, Y. Yang, A. Hartel, V. Cimalla, M. Zacharias, *J. Appl. Phys.* **2012**, *112*, 034311.

[61] N. S. Ramgir, K. Subannajui, Y. Yang, R. Grimm, R. Michiels, M. Zacharias, *J. Phys. Chem. C* **2010**, *114*, 10323.

[62] A. Menzel, K. Subannajui, R. Bakhda, Y. Wang, R. Thomann, M. Zacharias, *J. Phys. Chem. Lett.* **2012**, *3*, 2815.

[63] D. Calestani, M. Zha, G. Salviati, L. Lazzarini, L. Zanotti, E. Comini, G. Sberveglieri, *J. Cryst. Growth* **2005**, *275*, e2083.

[64] M. Mazzera, M. Zha, D. Calestani, A. Zappettini, L. Lazzarini, G. Salviati, L. Zanotti, *Nanotechnology* **2007**, *18*, 355707.

[65] C. Y. Zhi, X. D. Bai, E. G. Wang, *Appl. Phys. Lett.* **2004**, *85*, 1802.

[66] H. T. Ng, B. Chen, J. Li, J. Han, M. Meyyappan, J. Wu, S. X. Li, E. E. Haller, *Appl. Phys. Lett.* **2003**, *82*, 2023.

[67] Q. X. Zhao, M. Willander, R. E. Morjan, Q.-H. Hu, E. E. B. Campbell, *Appl. Phys. Lett.* **2003**, *83*, 165.

[68] H. Choi, *Semiconductor Nanostructures for Optoelectronic Devices*, Springer, Berlin Heidelberg **2012**.

[69] P. Yang, H. Yan, S. Mao, R. Russo, J. Johnson, R. Saykally, N. Morris, J. Pham, R. He, H.-J. Choi, *Adv. Funct. Mater.* **2002**, *12*, 323.

[70] K. Kolasinski, *Curr. Opin. Solid State Mater. Sci.* **2006**, *10*, 182.

[71] Y. Xia, P. Yang, Y. Sun, Y. Wu, B. Mayers, B. Gates, Y. Yin, F. Kim, H. Yan, *Adv. Mater.* **2003**, *15*, 353.

[72] Y. Zi, S. Suslov, C. Yang, *Nano Lett.* **2017**, *17*, 1167.

[73] M. Zha, D. Calestani, A. Zappettini, R. Mosca, M. Mazzera, L. Lazzarini, L. Zanotti, *Nanotechnology* **2008**, *19*, 325603.

[74] A. Bakin, A. Che Mofor, A. El-Shaer, A. Waag, *Superlattices Microstruct.* **2007**, *42*, 33.

[75] L. V. Podrezova, S. Porro, V. Cauda, M. Fontana, G. Cicero, *Appl. Phys. A* **2013**, *113*, 623.

[76] M. Laurenti, A. Verna, M. Fontana, M. Quaglio, S. Porro, *Appl. Phys. A* **2014**, *117*, 901.

[77] P. K. Giri, S. Dhara, R. Chakraborty, *Mater. Chem. Phys.* **2010**, *122*, 18.

[78] J.-J. Wu, S.-C. Liu, *Adv. Mater.* **2002**, *14*, 215.

[79] M. Willander, O. Nur, Q. X. Zhao, L. L. Yang, M. Lorenz, B. Q. Cao, J. Zúñiga Pérez, C. Czekalla, G. Zimmermann, M. Grundmann, A. Bakin, A. Behrends, M. Al-Suleiman, A. El-Shaer, A. Che Mofor, B. Postels, A. Waag, N. Boukos, A. Travlos, H. S. Kwack, J. Guinard, D. Le Si Dang, *Nanotechnology* **2009**, *20*, 332001.

[80] C. Czekalla, J. Guinard, C. Hanisch, B. Q. Cao, E. M. Kaidashev, N. Boukos, A. Travlos, J. Renard, B. Gayral, D. Le Si Dang, M. Lorenz, M. Grundmann, *Nanotechnology* **2008**, *19*, 115202.

[81] T. Nobis, E. M. Kaidashev, A. Rahm, M. Lorenz, M. Grundmann, *Phys. Rev. Lett.* **2004**, *93*, 103903.

[82] A. O. Ankiewicz, M. C. Carmo, N. A. Sobolev, W. Gehlhoff, E. M. Kaidashev, A. Rahm, M. Lorenz, M. Grundmann, *J. Appl. Phys.* **2007**, *101*, 024324.

[83] T. Nobis, E. M. Kaidashev, A. Rahm, M. Lorenz, J. Lenzner, M. Grundmann, *Nano Lett.* **2004**, *4*, 797.

[84] R. Sui, P. Charpentier, *Chem. Rev.* **2012**, *112*, 3057.

[85] S. Jung, E. Oh, K. Lee, Y. Yang, C. G. Park, W. Park, S. Jeong, *Cryst. Growth Des.* **2008**, *8*, 265.

[86] L. Mai, L. Xu, C. Han, X. Xu, Y. Luo, S. Zhao, Y. Zhao, *Nano Lett.* **2010**, *10*, 4750.

[87] K. Takahashi, S. J. Limmer, Y. Wang, G. Cao, *Jpn. J. Appl. Phys.* **2005**, *44*, 662.

[88] C.-C. Hu, K.-H. Chang, M.-C. Lin, Y.-T. Wu, *Nano Lett.* **2006**, *6*, 2690.

[89] M. Zheng, L. Zhang, G. Li, W. Shen, *Chem. Phys. Lett.* **2002**, *363*, 123.

[90] D. Conti, A. Lamberti, S. Porro, P. Rivolo, A. Chiolerio, C. F. Pirri, C. Ricciardi, *Nanotechnology* **2016**, *27*, 485208.

[91] T. Pauporté, G. Bataille, L. Joulaud, F. J. Vermersch, *J. Phys. Chem. C* **2010**, *114*, 194.

[92] D. O. Miles, P. J. Cameron, D. Mattia, *J. Mater. Chem. A* **2015**, *3*, 17569.

[93] S. J. Limmer, S. Seraji, M. J. Forbess, Y. Wu, T. P. Chou, C. Nguyen, G. Z. Cao, *Adv. Mater.* **2001**, *13*, 1269.

[94] S. J. Limmer, G. Cao, *Adv. Mater.* **2003**, *15*, 427.

[95] Y. C. Wang, I. C. Leu, M. H. Hon, *J. Mater. Chem.* **2002**, *12*, 2439.

[96] Z. Miao, D. Xu, J. Ouyang, G. Guo, X. Zhao, Y. Tang, *Nano Lett.* **2002**, *2*, 717.

[97] D. Pan, Z. Shuyuan, Y. Chen, J. G. Hou, *J. Mater. Res.* **2002**, *17*, 1981.

[98] Q. Lu, F. Gao, S. Komarneni, T. E. Mallouk, *J. Am. Chem. Soc.* **2004**, *126*, 8650.

[99] K. Takahashi, Y. Wang, K. Lee, G. Cao, *Appl. Phys. A* **2006**, *82*, 27.

[100] L.-W. Ji, S.-M. Peng, J.-S. Wu, W.-S. Shih, C.-Z. Wu, I.-T. Tang, *J. Phys. Chem. Solids* **2009**, *70*, 1359.

[101] D.-Y. Son, K.-H. Bae, H.-S. Kim, N.-G. Park, *J. Phys. Chem. C* **2015**, *119*, 10321.

[102] K. H. Kim, K. Utashiro, Y. Abe, M. Kawamura, *Int. J. Electrochem. Sci.* **2014**, *9*, 2080.

[103] Y. Tao, M. Fu, A. Zhao, D. He, Y. Wang, *J. Alloys Compd.* **2010**, *489*, 99.

[104] M. Laurenti, V. Cauda, R. Gazia, M. Fontana, V. F. Rivera, S. Bianco, G. Canavese, *Eur. J. Inorg. Chem.* **2013**, *2013*, 2520.

[105] A. Phuruangrat, D. J. Ham, S. J. Hong, S. Thongtem, J. S. Lee, *J. Mater. Chem.* **2010**, *20*, 1683.

[106] X. Feng, K. Shankar, O. K. Varghese, M. Paulose, T. J. Latempa, C. A. Grimes, *Nano Lett.* **2008**, *8*, 3781.

[107] Y. Mao, S. S. Wong, *J. Am. Chem. Soc.* **2006**, *128*, 8217.

[108] J.-K. Oh, J.-K. Lee, H.-S. Kim, S.-B. Han, K.-W. Park, *Chem. Mater.* **2010**, *22*, 1114.

[109] J.-K. Oh, J.-K. Lee, S. J. Kim, K.-W. Park, *J. Ind. Eng. Chem.* **2009**, *15*, 270.

[110] S. Hormoz, S. Ramanathan, *Solid-State Electron.* **2010**, *54*, 654.

**ADVANCED
SCIENCE NEWS**
www.advancedsciencenews.com

**ADVANCED
ELECTRONIC
MATERIALS**
www.advelectronicmat.de

[111] S. A. Corr, M. Grossman, J. D. Furman, B. C. Melot, A. K. Cheetham, K. R. Heier, R. Seshadri, *Chem. Mater.* **2008**, *20*, 6396.

[112] A. C. Santulli, W. Xu, J. B. Parise, L. Wu, M. C. Aronson, F. Zhang, C.-Y. Nam, C. T. Black, A. L. Tiano, S. S. Wong, *Phys. Chem. Chem. Phys.* **2009**, *11*, 3718.

[113] L. I. Vera-Robles, A. Campero, *J. Phys. Chem. C* **2008**, *112*, 19930.

[114] C. Xiong, A. E. Aliev, B. Gnade, K. J. Balkus, *ACS Nano* **2008**, *2*, 293.

[115] B. Sipos, M. Duchamp, A. Magrez, L. Forró, N. Barišić, A. Kis, J. W. Seo, F. Bieri, F. Krumeich, R. Nesper, G. R. Patzke, *J. Appl. Phys.* **2009**, *105*, 074317.

[116] M. Ye, H. Zhong, W. Zheng, R. Li, Y. Li, *Langmuir* **2007**, *23*, 9064.

[117] Z. Guo, M. Li, J. Liu, *Nanotechnology* **2008**, *19*, 245611.

[118] S. K. Han, D.-S. Kang, S.-K. Hong, M.-J. Kim, J.-H. Song, J.-H. Song, H. Kim, D. Kim, J. W. Lee, J. Y. Lee, in *2010 3rd Int. Nanoelectron. Conf.*, IEEE, Hong Kong, China **2010**, pp. 1098–1099.

[119] B. H. Kim, J. W. Kwon, *Sci. Rep.* **2015**, *4*, 4379.

[120] A. Manekkathodi, M.-Y. Lu, C. W. Wang, L.-J. Chen, *Adv. Mater.* **2010**, *22*, 4059.

[121] Z. J. Chew, L. Li, *Mater. Lett.* **2012**, *76*, 226.

[122] O. F. Farhat, M. M. Halim, M. J. Abdullah, M. K. M. Ali, N. K. Allam, *Beilstein J. Nanotechnol.* **2015**, *6*, 720.

[123] V. Cauda, R. Gazia, S. Porro, S. Stassi, G. Canavese, I. Roppolo, A. Chiolerio, *Handbook of Nanomaterials Properties*, Springer, Berlin Heidelberg **2014**.

[124] Y. Dong, H. Yang, R. Rao, A. Zhang, *J. Nanosci. Nanotechnol.* **2009**, *9*, 4774.

[125] C.-J. Jia, L.-D. Sun, Z.-G. Yan, L.-P. You, F. Luo, X.-D. Han, Y.-C. Pang, Z. Zhang, C.-H. Yan, *Angew. Chem.* **2005**, *117*, 4402.

[126] J. Wan, Y. Yao, G. Tang, *Appl. Phys. A* **2007**, *89*, 529.

[127] L. Gao, L. Fei, H. Zheng, *Mater. Lett.* **2007**, *61*, 1785.

[128] D. Zheng, S. Sun, W. Fan, H. Yu, C. Fan, G. Cao, Z. Yin, X. Song, *J. Phys. Chem. B* **2005**, *109*, 16439.

[129] S. Hu, X. Wang, *J. Am. Chem. Soc.* **2008**, *130*, 8126.

[130] A. Phuruangrat, D. J. Ham, S. Thongtem, J. S. Lee, *Electrochem. Commun.* **2009**, *11*, 1740.

[131] X. Xie, W. Shen, *Nanoscale* **2009**, *1*, 50.

[132] W. E. Teo, S. Ramakrishna, *Nanotechnology* **2006**, *17*, R89.

[133] J. Wu, J. L. Coffer, *J. Phys. Chem. C* **2007**, *111*, 16088.

[134] P. S. Archana, R. Jose, C. Vijila, S. Ramakrishna, *J. Phys. Chem. C* **2009**, *113*, 21538.

[135] Y. Feng, W. Hou, X. Zhang, P. Lv, Y. Li, W. Feng, *J. Phys. Chem. C* **2011**, *115*, 3956.

[136] N. A. M. Barakat, M. S. Khil, F. A. Sheikh, H. Y. Kim, *J. Phys. Chem. C* **2008**, *112*, 12225.

[137] N. A. M. Barakat, K.-D. Woo, S. G. Ansari, J.-A. Ko, M. A. Kanjwal, H. Y. Kim, *Appl. Phys. A* **2009**, *95*, 769.

[138] H. Wang, H. Tang, J. He, Q. Wang, *Mater. Res. Bull.* **2009**, *44*, 1676.

[139] W. Zheng, X. Lu, W. Wang, Z. Li, H. Zhang, Y. Wang, Z. Wang, C. Wang, *Sens. Actuators, B* **2009**, *142*, 61.

[140] I.-D. Kim, A. Rothschild, B. H. Lee, D. Y. Kim, S. M. Jo, H. L. Tuller, *Nano Lett.* **2006**, *6*, 2009.

[141] E. Formo, M. S. Yavuz, E. P. Lee, L. Lane, Y. Xia, *J. Mater. Chem.* **2009**, *19*, 3878.

[142] Y. Li, S. Zhan, *J. Dispersion Sci. Technol.* **2009**, *30*, 246.

[143] A. F. Lotus, E. T. Bender, E. A. Evans, R. D. Ramsier, D. H. Reneker, G. G. Chase, *J. Appl. Phys.* **2008**, *103*, 024910.

[144] M. Lanza, H.-S. P. Wong, E. Pop, D. Ielmini, D. Strukov, B. C. Regan, L. Larcher, M. A. Villena, J. J. Yang, L. Goux, A. Belmonte, Y. Yang, F. M. Puglisi, J. Kang, B. Magyari-Köpe, E. Yalon, A. Kenyon, M. Buckwell, A. Mehonic, A. Shluger, H. Li, T.-H. Hou, B. Hudec, D. Akinwande, R. Ge, S. Ambrogio, J. B. Roldan, E. Miranda, J. Suñe, K. L. Pey, X. Wu, N. Raghavan, E. Wu, W. D. Lu, G. Navarro, W. Zhang, H. Wu, R. Li, A. Holleitner,

[145] U. Wurstbauer, M. C. Lemme, M. Liu, S. Long, Q. Liu, H. Lv, A. Padovani, P. Pavan, I. Valov, X. Jing, T. Han, K. Zhu, S. Chen, F. Hui, Y. Shi, *Adv. Electron. Mater.* **2018**, *1800143*, 1800143.

[145] G. Milano, L. D'Ortenzi, K. Bejtka, L. Mandrile, A. M. Giovannozzi, L. Boarino, C. F. Pirri, C. Ricciardi, S. Porro, *J. Phys. Chem. C* **2018**, *122*, 8011.

[146] M. M. Rojo, O. C. Calero, A. F. Lopeandia, J. Rodriguez-Viejo, M. Martín-Gonzalez, *Nanoscale* **2013**, *5*, 11526.

[147] C. M. Hangarter, N. V. Myung, *Chem. Mater.* **2005**, *17*, 1320.

[148] C. Cagli, F. Nardi, B. Harteneck, Z. Tan, Y. Zhang, D. Ielmini, *Small* **2011**, *7*, 2899.

[149] Y. Huang, X. Duan, Q. Wei, C. M. Lieber, *Science* **2001**, *291*, 630.

[150] D. L. Fan, F. Q. Zhu, R. C. Cammarata, C. L. Chien, *Appl. Phys. Lett.* **2004**, *85*, 4175.

[151] R. Agarwal, K. Ladavac, Y. Roichman, G. Yu, C. M. Lieber, D. G. Grier, *Opt. Express* **2005**, *13*, 8906.

[152] J. Suehiro, N. Nakagawa, S. Hidaka, M. Ueda, K. Imasaka, M. Higashihata, T. Okada, M. Hara, *Nanotechnology* **2006**, *17*, 2567.

[153] S. J. Papadakis, Z. Gu, D. H. Gracias, *Appl. Phys. Lett.* **2006**, *88*, 233118.

[154] D. Whang, S. Jin, Y. Wu, C. M. Lieber, *Nano Lett.* **2003**, *3*, 1255.

[155] J. J. Yang, J. Borghetti, D. Murphy, D. R. Stewart, R. S. Williams, *Adv. Mater.* **2009**, *21*, 3754.

[156] A. Wedig, M. Luebben, D.-Y. Cho, M. Moors, K. Skaja, V. Rana, T. Hasegawa, K. K. Adepalli, B. Yildiz, R. Waser, I. Valov, *Nat. Nanotechnol.* **2016**, *11*, 67.

[157] D. Ielmini, R. Bruchhaus, R. Waser, *Phase Transitions* **2011**, *84*, 570.

[158] Y.-T. Huang, S.-Y. Yu, C.-L. Hsin, C.-W. Huang, C.-F. Kang, F.-H. Chu, J.-Y. Chen, J.-C. Hu, L.-T. Chen, J.-H. He, W.-W. Wu, *Anal. Chem.* **2013**, *85*, 3955.

[159] Z. Fan, X. Fan, A. Li, L. Dong, in *2012 12th IEEE Int. Conf. Nanotechnol.*, IEEE, Birmingham, UK **2012**, pp. 1–4.

[160] Z. Fan, X. Fan, A. Li, L. Dong, *Nanoscale* **2013**, *5*, 12310.

[161] C. O'Kelly, J. A. Fairfield, J. J. Boland, *ACS Nano* **2014**, *8*, 11724.

[162] E. Gale, *Semicond. Sci. Technol.* **2014**, *29*, 104004.

[163] G. Sassine, S. La Barbera, N. Najjari, M. Minvielle, C. Dubourdieu, F. Alibart, *J. Vac. Sci. Technol., B: Nanotechnol. Microelectron.: Mater., Process., Meas., Phenom.* **2016**, *34*, 012202.

[164] L. Lin, L. Liu, K. Musselman, G. Zou, W. W. Duley, Y. N. Zhou, *Adv. Funct. Mater.* **2016**, *26*, 5979.

[165] D. S. Hong, Y. S. Chen, J. R. Sun, B. G. Shen, *Adv. Electron. Mater.* **2016**, *2*, 1500359.

[166] C. J. O'Kelly, J. A. Fairfield, D. McCloskey, H. G. Manning, J. F. Donegan, J. J. Boland, *Adv. Electron. Mater.* **2016**, *2*, 1500458.

[167] X. He, Y. Yin, J. Guo, H. Yuan, Y. Peng, Y. Zhou, D. Zhao, K. Hai, W. Zhou, D. Tang, *Nanoscale Res. Lett.* **2013**, *8*, 50.

[168] Y. Zhou, Y. Yin, Y. Peng, W. Zhou, H. Yuan, Z. Qin, B. Liu, Y. Zhang, D. Tang, *Mater. Res. Express* **2014**, *1*, 025025.

[169] Y. Zhou, Y. Peng, Y. Yin, F. Zhou, C. Liu, J. Ling, L. Lei, W. Zhou, D. Tang, *Sci. Rep.* **2016**, *6*, 32712.

[170] L. Lei, Y. Yin, C. Liu, Y. Zhou, Y. Peng, F. Zhou, J. Ling, W. Zhou, D. Tang, *Solid State Ionics* **2017**, *308*, 107.

[171] Y.-D. Chiang, W.-Y. Chang, C.-Y. Ho, C.-Y. Chen, C.-H. Ho, S.-J. Lin, T.-B. Wu, J.-H. He, *IEEE Trans. Electron Devices* **2011**, *58*, 1735.

[172] J. Song, Y. Zhang, C. Xu, W. Wu, Z. L. Wang, *Nano Lett.* **2011**, *11*, 2829.

[173] W. Wu, Z. L. Wang, *Nano Lett.* **2011**, *11*, 2779.

[174] K. R. G. Karthik, R. Ramanujam Prabhakar, L. Hai, S. K. Batabyal, Y. Z. Huang, S. G. Mhaisalkar, *Appl. Phys. Lett.* **2013**, *103*, 123114.

[175] Y. Lai, P. Xin, S. Cheng, J. Yu, Q. Zheng, *Appl. Phys. Lett.* **2015**, *106*, 031603.

[176] Y. Lai, W. Qiu, Z. Zeng, S. Cheng, J. Yu, Q. Zheng, *Nanomaterials* **2016**, *6*, 16.

[177] S. Lee, J. Park, M. Lee, J. J. Boland, *AIP Adv.* **2016**, *6*, 125010.

[178] R. Zhang, W. Pang, Z. Feng, X. Chen, Y. Chen, Q. Zhang, H. Zhang, C. Sun, J. J. Yang, D. Zhang, *Sens. Actuators, B* **2017**, *238*, 357.

[179] R. Zhang, W. Pang, Q. Zhang, Y. Chen, X. Chen, Z. Feng, J. Yang, D. Zhang, *Nanotechnology* **2016**, *27*, 315203.

[180] F. M. Simanjuntak, D. Panda, K.-H. Wei, T.-Y. Tseng, *Nanoscale Res. Lett.* **2016**, *11*, 368.

[181] M. Laurenti, S. Porro, C. F. Pirri, C. Ricciardi, A. Chiolerio, *Crit. Rev. Solid State Mater. Sci.* **2017**, *42*, 153.

[182] D. Conti, M. Laurenti, S. Porro, C. Giovinazzo, S. Bianco, V. Fra, A. Chiolerio, C. F. Pirri, G. Milano, C. Ricciardi, *Nanotechnology* **2019**, *30*, 065707.

[183] C.-W. Huang, J.-Y. Chen, C.-H. Chiu, W.-W. Wu, *Nano Lett.* **2014**, *14*, 2759.

[184] Z. Fan, J. G. Lu, *J. Nanosci. Nanotechnol.* **2005**, *5*, 1561.

[185] T. Moriyama, T. Yamasaki, T. Ohno, S. Kishida, K. Kinoshita, *J. Appl. Phys.* **2016**, *120*, 215302.

[186] G. Milano, S. Porro, M. Y. Ali, K. Bejtka, S. Bianco, F. Beccaria, A. Chiolerio, C. F. Pirri, C. Ricciardi, *J. Phys. Chem. C* **2018**, *122*, 866.

[187] C. H. Kim, H. B. Moon, S. S. Min, Y. H. Jang, J. H. Cho, *Solid State Commun.* **2009**, *149*, 1611.

[188] K.-D. Liang, C.-H. Huang, C.-C. Lai, J.-S. Huang, H.-W. Tsai, Y.-C. Wang, Y.-C. Shih, M.-T. Chang, S.-C. Lo, Y.-L. Chueh, *ACS Appl. Mater. Interfaces* **2014**, *6*, 16537.

[189] Y. Huang, Y. Luo, Z. Shen, G. Yuan, H. Zeng, *Nanoscale Res. Lett.* **2014**, *9*, 381.

[190] J. Tang, Z. Huo, S. Brittman, H. Gao, P. Yang, *Nat. Nanotechnol.* **2011**, *6*, 568.

[191] X. Lu, T. Zhai, X. Zhang, Y. Shen, L. Yuan, B. Hu, L. Gong, J. Chen, Y. Gao, J. Zhou, Y. Tong, Z. L. Wang, *Adv. Mater.* **2012**, *24*, 938.

[192] L.-F. Cui, Y. Yang, C. Hsu, Y. Cui, *Nano Lett.* **2009**, *9*, 3370.

[193] L. J. Lauhon, M. S. Gudiksen, D. Wang, C. M. Lieber, *Nature* **2002**, *420*, 57.

[194] K. Oka, T. Yanagida, K. Nagashima, H. Tanaka, T. Kawai, *J. Am. Chem. Soc.* **2009**, *131*, 3434.

[195] K. Oka, T. Yanagida, K. Nagashima, T. Kawai, J. Kim, B. H. Park, *J. Am. Chem. Soc.* **2010**, *132*, 6634.

[196] K. Nagashima, T. Yanagida, K. Oka, M. Taniguchi, T. Kawai, J. S. Kim, B. H. Park, *Nano Lett.* **2010**, *10*, 1359.

[197] K. Nagashima, T. Yanagida, K. Oka, M. Kanai, A. Klamchuen, J.-S. Kim, B. H. Park, T. Kawai, *Nano Lett.* **2011**, *11*, 2114.

[198] K. Nagashima, T. Yanagida, M. Kanai, K. Oka, A. Klamchuen, S. Rahong, G. Meng, M. Horprathum, B. Xu, F. Zhuge, Y. He, T. Kawai, *Jpn. J. Appl. Phys.* **2012**, *51*, 11PE09.

[199] K. Nagashima, T. Yanagida, K. Oka, M. Kanai, A. Klamchuen, S. Rahong, G. Meng, M. Horprathum, B. Xu, F. Zhuge, Y. He, B. H. Park, T. Kawai, *Nano Lett.* **2012**, *12*, 5684.

[200] S. Tappertzhofen, I. Valov, T. Tsuruoka, T. Hasegawa, R. Waser, M. Aono, *ACS Nano* **2013**, *7*, 6396.

[201] M. Lübben, S. Wiefels, R. Waser, I. Valov, *Adv. Electron. Mater.* **2017**, *1700458*, 1700458.

[202] T. Heisig, C. Baeumer, U. N. Gries, M. P. Mueller, C. La Torre, M. Luebben, N. Raab, H. Du, S. Menzel, D. N. Mueller, C.-L. Jia, J. Mayer, R. Waser, I. Valov, R. A. De Souza, R. Dittmann, *Adv. Mater.* **2018**, *30*, 1800957.

[203] I. Valov, T. Tsuruoka, *J. Phys. D: Appl. Phys.* **2018**, *0*, 413001.

[204] L. He, Z.-M. Liao, H.-C. Wu, X.-X. Tian, D.-S. Xu, G. L. W. Cross, G. S. Duesberg, I. V. Shvets, D.-P. Yu, *Nano Lett.* **2011**, *11*, 4601.

[205] C.-W. Hsu, L.-J. Chou, *Nano Lett.* **2012**, *12*, 4247.

[206] C.-H. Huang, W.-C. Chang, J.-S. Huang, S.-M. Lin, Y.-L. Chueh, *Nanoscale* **2017**, *9*, 6920.

[207] S. Porro, A. Jasmin, K. Bejtka, D. Conti, D. Perrone, S. Guastella, C. F. Pirri, A. Chiolerio, C. Ricciardi, *J. Vac. Sci. Technol., A* **2016**, *34*, 01A147.

[208] S. Porro, K. Bejtka, A. Jasmin, M. Fontana, G. Milano, A. Chiolerio, C. F. Pirri, C. Ricciardi, *Nanotechnology* **2018**, *29*, 495201.

[209] C. Giovinazzo, C. Ricciardi, C. F. Pirri, A. Chiolerio, S. Porro, *Appl. Phys. A* **2018**, *124*, 686.

[210] S. M. George, *Chem. Rev.* **2010**, *110*, 111.

[211] T.-K. Huang, J.-Y. Chen, Y.-H. Ting, W.-W. Wu, *Adv. Electron. Mater.* **2018**, *4*, 1800256.

[212] B. Cheng, Z. Ouyang, C. Chen, Y. Xiao, S. Lei, *Sci. Rep.* **2013**, *3*, 3249.

[213] E. D. Herderick, K. M. Reddy, R. N. Sample, T. I. Draskovic, N. P. Padture, *Appl. Phys. Lett.* **2009**, *95*, 203505.

[214] K. Park, J.-S. Lee, *Sci. Rep.* **2016**, *6*, 23069.

[215] Y.-C. Huang, P.-Y. Chen, T.-S. Chin, R.-S. Liu, C.-Y. Huang, C.-H. Lai, *Appl. Phys. Lett.* **2012**, *101*, 153106.

[216] I. Valov, M. N. Kozicki, *J. Phys. D: Appl. Phys.* **2013**, *46*, 074005.

[217] Y. Yang, X. Zhang, M. Gao, F. Zeng, W. Zhou, S. Xie, F. Pan, *Nanoscale* **2011**, *3*, 1917.

[218] F. Raffone, F. Risplendi, G. Cicero, *Nano Lett.* **2016**, *16*, 2543.

[219] H. Dong, X. Zhang, D. Zhao, Z. Niu, Q. Zeng, J. Li, L. Cai, Y. Wang, W. Zhou, M. Gao, S. Xie, *Nanoscale* **2012**, *4*, 2571.

[220] J. Qi, J. Huang, D. Paul, J. Ren, S. Chu, J. Liu, *Nanoscale* **2013**, *5*, 2651.

[221] S. Park, S. Jung, M. Siddik, M. Jo, J. Park, S. Kim, W. Lee, J. Shin, D. Lee, G. Choi, J. Woo, E. Cha, B. H. Lee, H. Hwang, *Phys. Status Solidi RRL* **2012**, *6*, 454.

[222] S. Gao, F. Zeng, F. Li, M. Wang, H. Mao, G. Wang, C. Song, F. Pan, *Nanoscale* **2015**, *7*, 6031.

[223] L. Zou, W. Hu, J. Fu, N. Qin, S. Li, D. Bao, *AIP Adv.* **2014**, *4*, 037106.

[224] Y. Yang, P. Gao, S. Gaba, T. Chang, X. Pan, W. Lu, *Nat. Commun.* **2012**, *3*, 732.

[225] B. Wang, T. Ren, S. Chen, B. Zhang, R. Zhang, J. Qi, S. Chu, J. Huang, J. Liu, *J. Mater. Chem. C* **2015**, *3*, 11881.

[226] G. Milano, M. Luebben, Z. Ma, R. Dunin-Borkowski, L. Boarino, C. F. Pirri, R. Waser, C. Ricciardi, I. Valov, *Nat. Commun.* **2018**, *9*, 5151.

[227] Y. Yang, P. Gao, L. Li, X. Pan, S. Tappertzhofen, S. Choi, R. Waser, I. Valov, W. D. Lu, *Nat. Commun.* **2014**, *5*, 4232.

[228] F. Raffone, G. Cicero, *Solid State Ionics* **2017**, *299*, 93.

[229] Y. Dong, G. Yu, M. C. McAlpine, W. Lu, C. M. Lieber, *Nano Lett.* **2008**, *8*, 386.

[230] P. F. Flowers, M. J. Catenacci, B. J. Wiley, *Nanoscale Horiz.* **2016**, *1*, 313.

[231] M. J. Catenacci, P. F. Flowers, C. Cao, J. B. Andrews, A. D. Franklin, B. J. Wiley, *J. Electron. Mater.* **2017**, *46*, 4596.

[232] H. G. Manning, S. Biswas, J. D. Holmes, J. J. Boland, *ACS Appl. Mater. Interfaces* **2017**, *9*, 38959.

[233] S. Raoux, G. W. Burr, M. J. Breitwisch, C. T. Rettner, Y.-C. Chen, R. M. Shelby, M. Salinga, D. Krebs, S.-H. Chen, H.-L. Lung, C. H. Lam, *IBM J. Res. Dev.* **2008**, *52*, 465.

[234] M. Wuttig, *Nat. Mater.* **2005**, *4*, 265.

[235] W. Wetnic, M. Wuttig, *Mater. Today* **2008**, *11*, 20.

[236] S. H. Lee, D. K. Ko, Y. Jung, R. Agarwal, *Appl. Phys. Lett.* **2006**, *89*, 223116.

[237] Y. Jung, S.-H. Lee, D.-K. Ko, R. Agarwal, *J. Am. Chem. Soc.* **2006**, *128*, 14026.

[238] S.-H. Lee, Y. Jung, R. Agarwal, *Nat. Nanotechnol.* **2007**, *2*, 626.

[239] S.-H. Bae, S. Lee, H. Koo, L. Lin, B. H. Jo, C. Park, Z. L. Wang, *Adv. Mater.* **2013**, *25*, 5098.

[240] S. Brivio, G. Tallarida, D. Perego, S. Franz, D. Deleruyelle, C. Muller, S. Spiga, *Appl. Phys. Lett.* **2012**, *101*, 223510.

[241] S. Brivio, D. Perego, G. Tallarida, M. Bestetti, S. Franz, S. Spiga, *Appl. Phys. Lett.* **2013**, *103*, 153506.

[242] Y.-C. Huang, P.-Y. Chen, K.-F. Huang, T.-C. Chuang, H.-H. Lin, T.-S. Chin, R.-S. Liu, Y.-W. Lan, C.-D. Chen, C.-H. Lai, *NPG Asia Mater.* **2014**, *6*, e85.

**ADVANCED
SCIENCE NEWS**

www.advancedsciencenews.com

**ADVANCED
ELECTRONIC
MATERIALS**

www.advelectronicmat.de

[243] W. Y. Chang, C. A. Lin, J. H. He, T. B. Wu, *Appl. Phys. Lett.* **2010**, *96*, 242109.

[244] Z.-L. Tseng, P.-C. Kao, M.-F. Shih, H.-H. Huang, J.-Y. Wang, S.-Y. Chu, *Appl. Phys. Lett.* **2010**, *97*, 212103.

[245] C.-H. Huang, J.-S. Huang, S.-M. Lin, W.-Y. Chang, J.-H. He, Y.-L. Chueh, *ACS Nano* **2012**, *6*, 8407.

[246] P. Y. Huang, J. C. Meyer, D. a. Muller, *MRS Bull.* **2012**, *37*, 1214.

[247] A. Younis, D. Chu, X. Lin, J. Yi, F. Dang, S. Li, *ACS Appl. Mater. Interfaces* **2013**, *5*, 2249.

[248] E. J. Yoo, I. K. Shin, T. S. Yoon, Y. J. Choi, C. J. Kang, *J. Nanosci. Nanotechnol.* **2014**, *14*, 9459.

[249] Y. Sun, X. Yan, X. Zheng, Y. Liu, Y. Zhao, Y. Shen, Q. Liao, Y. Zhang, *ACS Appl. Mater. Interfaces* **2015**, *7*, 7382.

[250] A. Jasmin, S. Porro, C. F. Pirri, C. Ricciardi, A. Chiolerio, in *2015 IEEE 15th Int. Conf. Nanotechnol.*, IEEE, Rome, Italy **2015**, pp. 496–498.

[251] G. Anoop, V. Panwar, T. Y. Kim, J. Y. Jo, *Adv. Electron. Mater.* **2017**, *3*, 1600418.

[252] S. Porro, F. Risplendi, G. Cicero, K. Bejtka, G. Milano, P. Rivolo, A. Jasmin, A. Chiolerio, C. F. Pirri, C. Ricciardi, *J. Mater. Chem. C* **2017**, *5*, 10517.

[253] J. Park, S. Lee, J. Lee, K. Yong, *Adv. Mater.* **2013**, *25*, 6423.

[254] W. X. Zhao, B. Sun, Y. H. Liu, L. J. Wei, H. W. Li, P. Chen, *AIP Adv.* **2014**, *4*, 077127.

[255] S. Park, J. H. Lee, H.-D. Kim, S. M. Hong, H.-M. An, T. G. Kim, *Phys. Status Solidi RRL* **2013**, *7*, 493.

[256] D. Sarkar, A. K. Singh, *J. Phys. Chem. C* **2017**, *121*, 12953.

[257] F. M. Simanjuntak, P. Singh, S. Chandrasekaran, F. J. Lumbantoruan, C.-C. Yang, C.-J. Huang, C.-C. Lin, T.-Y. Tseng, *Semicond. Sci. Technol.* **2017**, *32*, 124003.

[258] L. Li, Y. Zhang, Z. Chew, *Nano-Micro Lett.* **2013**, *5*, 159.

[259] Z. J. Chew, L. Li, *Mater. Lett.* **2013**, *91*, 298.

[260] G.-H. Shen, A. R. Tandio, M.-Y. Lin, G.-F. Lin, K.-H. Chen, F. C.-N. Hong, *Thin Solid Films* **2016**, *618*, 90.

[261] Z. L. Wang, *J. Phys.: Condens. Matter* **2004**, *16*, R829.

[262] Y. Zhang, M. K. Ram, E. K. Stefanakos, D. Y. Goswami, *J. Nanomater.* **2012**, *2012*, 20.

[263] W. Zhou, R. Yang, H.-K. He, H.-M. Huang, J. Xiong, X. Guo, *Appl. Phys. Lett.* **2018**, *113*, 061107.

[264] L. Dugaiczyk, T.-T. Ngo-Duc, J. Gacusan, K. Singh, J. Yang, S. Santhanam, J.-W. Han, J. E. Koehne, N. P. Kobayashi, M. Meyyappan, M. M. Oye, *Chem. Phys. Lett.* **2013**, *575*, 112.

[265] W.-Y. Chang, Y. C. Lai, T. B. Wu, S. F. Wang, F. Chen, M. J. Tsai, *Appl. Phys. Lett.* **2008**, *92*, 022110.

[266] J. Xiao, W. L. Ong, Z. Guo, G. W. Ho, K. Zeng, *ACS Appl. Mater. Interfaces* **2015**, *7*, 11412.

[267] K. Bandopadhyay, K. N. Prajapati, J. Mitra, *Nanotechnology* **2018**, *29*, 105701.

[268] S. Lee, J. Lee, J. Park, Y. Choi, K. Yong, *Adv. Mater.* **2012**, *24*, 2418.

[269] F. Zhang, X. Gan, X. Li, L. Wu, X. Gao, R. Zheng, Y. He, X. Liu, R. Yang, *Electrochem. Solid-State Lett.* **2011**, *14*, H422.

[270] C.-H. Huang, T.-S. Chou, J.-S. Huang, S.-M. Lin, Y.-L. Chueh, *Sci. Rep.* **2017**, *7*, 2066.

[271] M. Xiao, K. P. Musselman, W. W. Duley, Y. N. Zhou, *ACS Appl. Mater. Interfaces* **2017**, *9*, 4808.

[272] V. Senthilkumar, A. Kathalingam, V. Kannan, K. Senthil, J.-K. Rhee, *Sens. Actuators, A* **2013**, *194*, 135.

[273] X. L. Shao, L. W. Zhou, K. J. Yoon, H. Jiang, J. S. Zhao, K. L. Zhang, S. Yoo, C. S. Hwang, *Nanoscale* **2015**, *7*, 11063.

[274] M. Xiao, K. P. Musselman, W. W. Duley, N. Y. Zhou, *Nano-Micro Lett.* **2017**, *9*, 15.

[275] P. N. Nirmalraj, A. T. Bellew, A. P. Bell, J. A. Fairfield, E. K. McCarthy, C. O'Kelly, L. F. C. Pereira, S. Sorel, D. Morosan, J. N. Coleman, M. S. Ferreira, J. J. Boland, *Nano Lett.* **2012**, *12*, 5966.

[276] A. Z. Stieg, A. V. Avizienis, H. O. Sillin, C. Martin-Olmos, M. Aono, J. K. Gimzewski, *Adv. Mater.* **2012**, *24*, 286.

[277] A. T. Bellew, A. P. Bell, E. K. McCarthy, J. A. Fairfield, J. J. Boland, *Nanoscale* **2014**, *6*, 9632.

[278] A. Z. Stieg, A. V. Avizienis, H. O. Sillin, C. Martin-Olmos, M. L. Lam, M. Aono, J. K. Gimzewski, *Jpn. J. Appl. Phys.* **2013**, *53*, 01AA02.

[279] C. Gomes da Rocha, H. G. Manning, C. O'Callaghan, C. Ritter, A. T. Bellew, J. J. Boland, M. S. Ferreira, *Nanoscale* **2015**, *7*, 13011.

[280] A. T. Bellew, H. G. Manning, C. Gomes da Rocha, M. S. Ferreira, J. J. Boland, *ACS Nano* **2015**, *9*, 11422.

[281] J. A. Fairfield, C. G. Rocha, C. O'Callaghan, M. S. Ferreira, J. J. Boland, *Nanoscale* **2016**, *8*, 18516.

[282] H. Du, T. Wan, B. Qu, F. Cao, Q. Lin, N. Chen, X. Lin, D. Chu, *ACS Appl. Mater. Interfaces* **2017**, *9*, 20762.

[283] H. G. Manning, F. Niosi, C. G. da Rocha, A. T. Bellew, C. O'Callaghan, S. Biswas, P. F. Flowers, B. J. Wiley, J. D. Holmes, M. S. Ferreira, J. J. Boland, *Nat. Commun.* **2018**, *9*, 3219.

[284] A. Prakash, S. Maikap, S. Rahaman, S. Majumdar, S. Manna, S. K. Ray, *Nanoscale Res. Lett.* **2013**, *8*, 220.

[285] Q. Li, Z. Gong, S. Wang, J. Wang, Y. Zhang, F. Yun, *AIP Adv.* **2016**, *6*, 025222.

[286] S. M. Oliver, J. A. Fairfield, A. T. Bellew, S. Lee, J. G. Champlain, L. B. Ruppalt, J. J. Boland, P. M. Vora, *Appl. Phys. Lett.* **2016**, *109*, 203101.

[287] Y.-H. Ting, J.-Y. Chen, C.-W. Huang, T.-K. Huang, C.-Y. Hsieh, W.-W. Wu, *Small* **2018**, *14*, 1703153.

[288] Y. S. Puzyrev, X. Shen, C. X. Zhang, J. Hachtel, B. K. Ni, B. K. Choi, E.-X. Zhang, O. Ovchinnikov, R. D. Schrimpf, D. M. Fleetwood, S. T. Pantelides, *Appl. Phys. Lett.* **2017**, *111*, 153504.

[289] G. U. Siddiqui, M. M. Rehman, K. H. Choi, *J. Mater. Chem. C* **2017**, *5*, 5528.

[290] J. Park, S. Lee, K. Yong, *Nanotechnology* **2012**, *23*, 385707.

[291] A. Kathalingam, H. S. Kim, S. D. Kim, H. C. Park, *Opt. Mater. (Amsterdam, Neth.)* **2015**, *48*, 190.

[292] A. Bera, H. Peng, J. Lourembam, Y. Shen, X. W. Sun, T. Wu, *Adv. Funct. Mater.* **2013**, *23*, 4977.

[293] J. Park, H. Song, E. K. Lee, J. H. Oh, K. Yong, *J. Electrochem. Soc.* **2015**, *162*, H713.

[294] P. Russo, M. Xiao, R. Liang, N. Y. Zhou, *Adv. Funct. Mater.* **2018**, *28*, 1706230.

[295] S. Carrara, D. Sacchetto, M. A. Doucey, C. Baj-Rossi, G. De Micheli, Y. Leblebici, *Sens. Actuators, B* **2012**, *171–172*, 449.

[296] F. Puppo, M. A. Doucey, M. Di Ventra, G. De Micheli, S. Carrara, *Proc. IEEE Int. Symp. Circuits Syst.* IEEE, Melbourne VIC, Australia **2014**, 2257.

[297] I. Tzouvadaki, P. Jolly, X. Lu, S. Ingebrandt, G. de Micheli, P. Estrela, S. Carrara, *Nano Lett.* **2016**, *16*, 4472.

[298] I. Tzouvadaki, N. Madaboosi, I. Taurino, V. Chu, J. P. Conde, G. De Micheli, S. Carrara, *J. Mater. Chem. B* **2016**, *4*, 2153.

[299] M.-A. Doucey, S. Carrara, *Trends Biotechnol.* **2019**, *37*, 86.

[300] D. Ielmini, C. Cagli, F. Nardi, Y. Zhang, *J. Phys. D: Appl. Phys.* **2013**, *46*, 074006.

[301] A. Z. Stieg, A. V. Avizienis, H. O. Sillin, C. Martin-Olmos, M.-L. Lam, M. Aono, J. K. Gimzewski, *Jpn. J. Appl. Phys.* **2014**, *53*, 01AA02.

[302] K. Nagashima, T. Yanagida, K. Oka, M. Kanai, A. Klamchuen, J.-S. Kim, B. H. Park, T. Kawai, *Nano Lett.* **2011**, *11*, 2114.

1800909 (34 of 34)